**Universidad San Pablo – CEU** **Fraunhofer IIS**

**Escuela Politécnica Superior**

Ingeniería de Telecomunicación



PROYECTO FINAL DE CARRERA

# ALGORITHMS TO CALCULATE GPS POSITION USING THE PHASE OF CARRIER SIGNALS

Autor: Elena Alonso Yebra

Director: Lucila Patiño Studencki

Codirector: Carlos Óscar Sánchez Sorzano

# Agradecimientos

Son muchas las personas gracias a las cuáles este proyecto ha sido una realidad, así que pido disculpas de antemano si dejo a alguien en el tintero - o cartón de la impresora.

En primer lugar, agradezco a mi familia su apoyo, cariño y confianza que siempre me han brindado. Sin duda, sin ellos este proyecto y esta carrera únicamente hubiesen sido un sueño rezagado bajo la almohada. A mis amigos y compañeros les dedico también este agradecimiento, por su ilusión y aliento, por estar siempre ahí, por vuestros consejos, ayudas y comprensión. De todos vosotros, familia y amigos, he aprendido tanto o más que con cualquier clase magistral.

Agradezco a la Universidad San Pablo CEU y en forma muy especial a nuestros profesores, por su apoyo y capacidad para guiar nuestras ideas en nuestra formación como ingenieros.

Quiero expresar también mi más sincero agradecimiento al Dr. Carlos Oscar Sánchez Sorzano, a Lucila Patiño Studencki y al centro Fraunhofer IIS (Nuremberg, Alemania) por su importante aporte, disponibilidad y paciencia en el desarrollo de este proyecto.

# Contents

# Resumen

En el Sistema Global de Posicionamiento - más conocido por sus siglas GPS, procedentes del inglés '*Global Positioning System*' - los equipos destinados a uso civil ofrecen precisiones cuya exactitud depende, en su mayor parte, de la calidad en la medida de la distancia existente entre el receptor y cada uno de los satélites. Este parámetro se obtiene mediante el seguimiento de los códigos transmitidos en las señales procedentes de los satélites y, en general, se suele denominar 'pseudo-rango' o medida de código.

Los pseudo-rangos no son representaciones fieles de las distancias reales entre el receptor y los satélites ya que existen fuentes de error degradando la calidad de dichas medidas. Por ejemplo, la propia atmósfera altera las trayectorias que describen las señales satelitales provocando curvaturas que prolongan los trayectos, este efecto se ve reflejado en las medidas de distancia. Por otro lado, las derivas de los relojes, tanto del receptor como de cada uno de los satélites, y el propio ruido generado en los equipos receptores son causas también de errores en las medidas resultantes que afectan, a su vez, a los resultados de posicionamiento obtenidos. Por consiguiente, las medidas de código son relativamente 'ruidosas'.

En el proceso de 'adquisión' de la señal GPS, el receptor no sólo realiza un seguimiento de los códigos contenidos en las frecuencias emitidas por los satélites sino que también monitoriza la fase con la que dichas frecuencias son interceptadas. Las medidas de fase ofrecen precisiones milimétricas siendo mucho menos ruidosas que los 'pseudo-rangos'; además, de ellas también se puede extraer información sobre las distancias existentes entre el receptor y los satélites. En contraposición, dichas medidas de fase se ven afectadas por ambigüedades que deben ser estimadas si se desea obtener medidas absolutas de distancia a los satélites. Como ejemplo ilustrativo, se podría relacionar las

medidas de código con una cinta que únicamente posee marcas métricas y las fases con una cinta que sólo presenta marcas milimétricas.

Los algoritmos convencionales que los receptores GPS emplean para estimar su posición procesan únicamente medidas de código, esto es, los 'pseudo-rangos'. Desde las primeras investigaciones realizadas en 1982 por Ron Hatch [3.7], varios métodos han sido propuestos para incorporar también las medidas de fase en el proceso de posicionamiento. Esta técnicas de integración de medidas GPS se denominan algoritmos CSC (del inglés *carrier smoothing code*) y se aplican ya sea directamente sobre los 'pseudo-rangos' [4.2] [4.13] [4.10] [4.6] [4.4] [4.3] o indirectamente durante el cómputo de la posición del receptor empleando, en algunos casos, filtros Kalman [4.19] [4.18] [4.14] [4.11].

Este proyecto nace con el objetivo de estudiar dichas técnicas CSC que combinan las medidas ruidosas de código con las medidas más precisas pero ambiguas derivadas de las fases de portadora para obtener así mejores precisiones en el cálculo de la posición del receptor. Con este fin, se ha realizado un proceso exhaustivo de documentación para posteriormente implementar varias técnicas CSC y evaluar, de este modo, sus efectos sobre el cálculo de las posiciones.

El desarrollo del proyecto se ha llevado a cabo en el seno del *Fraunhofer IIS* con sede en *Nuremberg* (Alemania). En dicho centro se está diseñando un simulador GPS que procesa la 'solución de navegación', esto es, la posición, velocidad y hora local de un receptor GPS, valiéndose de medidas tomadas de las señales satelitales que éste intercepta. Con el presente proyecto se han realizado mejoras incorporando nuevas funcionalidades tales como los algoritmos CSC anteriormente mencionados.

Realizar simulaciones en un entorno GPS requiere de herramientas que faciliten el procesado de álgebra matricial, señales digitales y teoría de control; por ello se ha hecho uso de un lenguaje de programación de alto nivel como es MATLAB.

Los resultados experimentales de estos estudios ofrecen mejoras apreciables de la precisión con la que las posiciones del receptor GPS son estimadas. Concretamente, se ha conseguido estabilizar y reducir el error en estas estimaciones por debajo de los 2 metros.

# Abstract

The accuracy of positioning services for civil use provided by the Global Positioning System (GPS) equipments depends to a great extend on the quality of the measured satellite-to-user distances. These measurements are obtained by tracking the codes embedded on signals broadcast by GPS satellites; they are generally referred to as pseudo-ranges or code observations.

Pseudo-ranges do not exactly represent the actual distances between satellite and user since several sources of errors degrade the quality of these measurements. For example, the radio signals broadcast by GPS satellites suffer refractions and reflections as they cross the atmosphere causing bending of the signal paths; this effect affects the measurement of satellite-to-user distances. Furthermore, satellite and receiver clock deviations and the noise generated on the receiver equipment itself are also causes of erros in measurements. Therefore, code measurements, i.e. the pseudo-ranges, are relatively ‘noisy’.

Besides code measurements, the phase of the gathered carrier frequency is also sampled within GPS receivers. This data is also considered as a very fine and precise measurement of satellite-to-user distance. Therefore, since the first statements posed by Ron Hatch in 1982, several techniques have been studied and performed; these try to integrate the GPS pseudo-ranges together with phase data in order to achieve better accuracies while computing positions within the GPS receivers. The present study was focused on these integration approaches that blend together GPS code and carrier measurements. The aim was initiated to assess if better positioning outcomes could be obtained when performances are adjusted by these integration approaches. These integration techniques are referred to as *carrier smoothing code (CSC)* algorithms and they are applied either directly on pseudo-ranges or while computing receiver position.

The most widely adopted strategy to combine these GPS measurements is a recursive filter that “smoothes out” the noise on pseudo-ranges with the aid of carrier-phases. This algorithm was firstly described by Ron Hatch in 1982 [3.7] and improvements have also been posed during the last decade [4.2] [4.13] [4.10] [4.6] [4.4] [4.3]. However, these filtering schemes are relatively susceptible to information losses or alterations in code measurements. A number of strategies have thus been posed to improve these aspects providing higher robustness and unbiased filtering based on Kalman filters [4.19] [4.18] [4.14] [4.11].

During the first years of the 21st century, an ensemble of GPS simulation packages was developed in the Satellite Navigation Department at Fraunhofer IIS Nürnberg (Germany). Those investigations were aimed at simulating a GPS navigation processor that computes the “navigation solution” (that is, the receiver’s position, velocity and time) with the aid of real GPS collected by gathering satellites signals within GPS receivers. In the present study, enlargements of this simulation packages have been developed in order to perform different CSC algorithms. The aim was to theoretically study and analyse different CSC schemes in order to implement some of them and compare test results in terms of positioning accuracy.

Because GPS simulation requires a broad spectrum of tools covering matrix algebra, digital signal processing, control theory, and navigation algorithms, a high-level programming language was considered. In that way, the simulation packages implemented while performing these studies have been developed and tested with MATLAB R2006a. Test results have shown that the implemented CSC schemes can reduce the error in position estimates below 2 metres.

# The goal of this Master's Thesis

The present study was focused on the integration of GPS code and carrier measurements by means of *carrier smoothing code (CSC)* algorithms. The aim was initiated to assess if better positioning outcomes could be obtained when performances are adjusted by these CSC approaches.

The goal of this work is the design of different CSC algorithms that combines the advantages of both code- and carrier-based measurements to obtain better accuracies in the estimation of position.

The analysis of possible algorithms should be done by using a high-level programming language like MATLAB, from The Mathwoks.

# Chapter 1

# Introduction

*"I'm astounded by people who want to 'know' the universe when it's hard enough to find your way around Chinatown."*

Woody Allen

Using today's state of the art satellite navigation systems, you can pinpoint your location anywhere on Earth with an accuracy of less than fifteen meters. Currently, the most used system available to the general public is the *NAVSTAR Global Positioning System* (GPS), which has been fully functional since mid-1994. GPS handsets can provide positioning (latitude, longitude, and altitude) and timing services to civilian users on a continuous worldwide basis. This technology has become a mainstay of many transportation systems, reinforcing navigation for aviation, ground, and maritime operations. Life-saving missions carried out by disaster relief and emergency services depend upon GPS for location and timing capabilities. Everyday activities such as banking and mobile phone operations are facilitated by the accurate timing provided by GPS. Perhaps someday navigation systems will find extremely useful applications, such as replacing seeing-eye dogs and guiding motor vehicles.

Figure 1 **GPS Applications – Mount Everest height measurement.** The current accepted Everest's height (8848 meters) was arrived at in 1954 by an Indian Surveyor named B.L. Gulatee. In 1998, the *American Everest Expedition* used GPS equipments to achieve more accurate measurements. Recent investigations have revealed a new height at 8844.43 meters.

Though the overall performance of GPS can claim to excel in significant aspects, such as availability to users, reliability or cost, *position accuracy* is also a relevant facet in some areas such as military, aviation or land surveying applications; even scientific investigations use the precision of GPS measurements (an example of GPS application is shown in Figure 1).

Conventional stand-alone GPS equipments depend on *code measurements*, referred to as *pseudo-ranges,* to derive a proper positioning solution. This measurement type is yielded while the receiver tracks the *ranging codes* embedded on GPS satellite broadcast signals. In fact, a pseudo-range is considered as a relatively "corrupted" approximation of the distance between the GPS receiver and a satellite in view (which is called *range* in GPS terminology – see Figure 2).

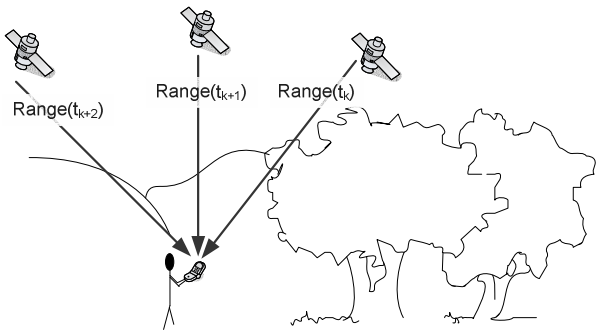


Figure 2 **Satellite-to-user ranges in GPS terminology**

Error sources affecting reliability of code measurements degrade the accuracy of positioning solutions. In fact, the most important causes of inaccuracies are the noise generated within the receiver electronics, atmospheric phenomena and possible drifts of satellites and receiver oscillators. Even the multipath effects bring down the efficiency of the obtained pseudo-ranges. The combined effect of all these error sources affects the accuracy of positioning results.

Besides pseudo-ranges, the relative phase between the received carrier and a reference oscillator within GPS equipments is also tracked. This measurement can be considered as a very fine and precise *range* measurement but, with all, there is no information about the absolute phase, that is, the most significant whole cycles (see Figure 3). In fact, the resolution of these carrier-based measurements offers higher positioning accuracies when combined with pseudo-ranges. As an analogy to illustrate this fact, carrier-phases can be considered as the millimetre marks in a tape measure while code pseudo-ranges would correspond to the metre marks.

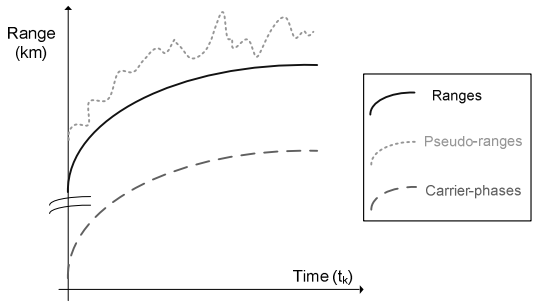


Figure 3 **Pseudo-ranges and carrier-phase measurements in GPS terminology**

The present study was focused on the integration of these two types of GPS observables (code and carrier-based) to enhance positioning accuracies. This work was aimed at researching different filtering schemes that blend together these quantities in such a way that many of the errors affecting positioning results are eliminated or, at least, minimized. Specifically, a group of techniques have been considered in order to reduce or "*smooth*" the noise on pseudo-ranges with the aid of the gathered carrier-phases. The performance of several schemes was compared in order to find proper methods to incorporate GPS carrier phases into the navigation solution process. These methods are referred to as *carrier smoothing code pseudo-ranges techniques*. They are applied either directly on pseudo-ranges or while computing receiver position. Analysis of the derived positioning accuracies is also exposed.

During the first years of the 21st century, an ensemble of GPS simulation packages using the popular and versatile MATLAB programming language were developed in the Satellite Navigation Department at *Fraunhofer IIS Nürnberg* (Germany). Those investigations were aimed at simulating a GPS navigation processor that computes the "*navigation solution*" (that is, the position, velocity and time) with the aid of data collected by gathering satellites signals within GPS receivers.

In the present study, extensions of this simulation packages have been developed under the supervision of Lucila Patiño Studencki. The research and development was done in early 2007 and attempted to implement positioning algorithms that combine GPS pseudo-range and carrier-phase measurements, that is, code and carrier-based observables (see the following Figure 4).

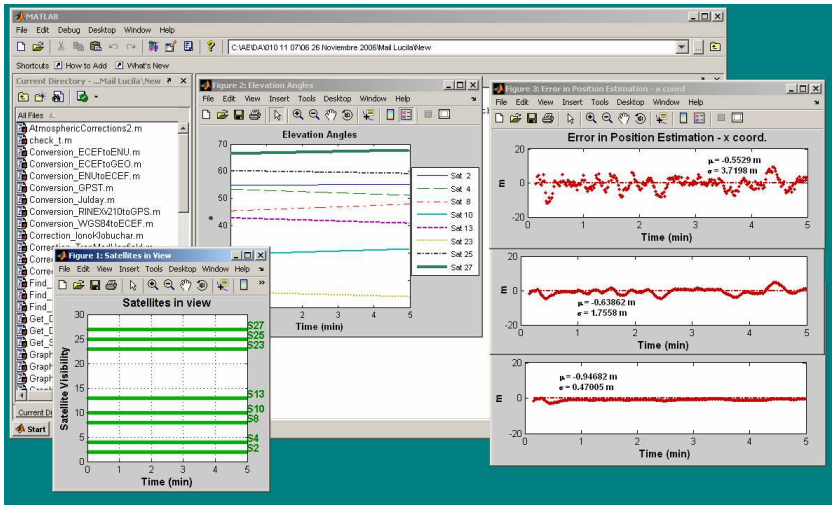


Figure 4 **Image of GPS Matlab Simulator 2007**

An ensemble of GPS real data, captured under the *Receiver Independent Exchange Format* (RINEX) Version 2.10, were considered to achieve more realistic outcomes. The implemented MATLAB Tool aims at reading GPS data from RINEX files and deriving a *navigation solution* by applying convenient corrections on measurements and estimating satellite locations.

This report is structured as follows. Chapter 1 consists of a brief introduction to the main objects in these studies. In Chapter 2, basic GPS positioning concepts are introduced and the main aspects in terms of processing the navigation solution (i.e. the receiver's position) are highlighted. Chapter 3 is focused on GPS measurements mathematical models and sources of errors affecting empirical data. Chapter 4 brings proposals to combine GPS measurement types in order to reduce the errors affecting these quantities; in this context, the concept of "*smoothing*" in range and position domains is exposed. Finally Chapter 5 overviews test results and the achieved improvements in terms of position accuracy.

# Chapter 2

# Navigation – GPS Positioning

*"I must down to the seas again,*
*to the lonely sea and the sky,*
*And all I ask is a tall ship*
*and a star to steer her by …"*

John Masefield - *Sea Fever*

The word *navigate* is derived from the Latin roots *navis,* meaning boat, and *agire,* meaning to guide or direct. Navigational techniques have been applied over the ages in many different civilizations; all involve locating one's position compared to known locations, such as the stars.

On the age of the ancient sailors, the sun and the stars were useful references to allocate the ships on their journeys by means of navigational techniques. As early as 1519, on the voyage organized by Magellan to circumnavigate the globe, the crew was equipped with "*sea charts, a terrestrial globe, wooden and metal theodolites*[1]*, wooden and wood-and-bronze quadrants, compasses, magnetic needles, hourglasses and timepieces*" (according to "*The American Practical Navigator*" written by Nathaniel Bowditch in 1802). With these instruments, and great personal skills, sailors could estimate the ship's speed, direction, and even latitude.

The technology of the twentieth century placed artificial stars in the sky, the well-known satellites. They "shine" all the time radiating signals that provide far more information than the sailors of old ever got from the stars. In this way, accurate

[1] *Theodolites* are instruments for measuring both horizontal and vertical angles, as used in triangulation methods.

estimates of position, velocity, and even local time are freely available to all instantaneously thanks to global satellite navigation systems such as NAVSTAR Global Positioning System (GPS).

GPS represents the fulfilment of several technologies, which matured and came together in the second half of the 20th century. In particular, *stable space-borne platforms*, *ultra-stable atomic frequency standards*, *spread spectrum signalling*, and *microelectronics* are the key developments in the achievement and success of GPS. These technologies have been integrated and applied to implement an ancient idea of positioning: ***trilateration***, a way of location by measuring distances from known reference points.

This chapter deals with the general principles of GPS, a brief introduction to this satellite navigation system is exposed together with the essential processes of GPS positioning. In the following figure, a conceptual view of this satellite network is shown.

Figure 5 **NAVSTAR GPS satellite network –** image courtesy of cnice.mec.es

## 2.1 The Global Positioning System - GPS

Our ancestors did also manage to keep from getting lost. As a result, monumental landmarks were erected and detailed maps were laboriously drafted. Also, sailors learned how to read the stars in the sky at night. Today, things are much easier; we are living in an "Age of Technology" and pocket-sized equipments that provide user location service are available for less than 100 euros. Nowadays, not more than a GPS handset and a "line of sight" towards the sky are needed for location.

According to the GPS general public education website [2.5], created by the U.S. Government, the Global Positioning System (GPS) is "*a U.S. space-based radionavigation system that provides reliable positioning, navigation, and timing services to civilian users on a continuous worldwide basis – freely available to all*". The United States Department of Defence (DoD) developed and implemented this satellite network as a military navigation system, but soon it was available for civilian users as a common good (Ronald Reagan, 1983).

GPS is vast and expensive but the basic concepts are quite intuitive. It is made up of three parts (called segments): a constellation of *MEO*[2] satellites orbiting the Earth; a group of ground control and monitoring stations; and the GPS receivers owned by users.

GPS satellites broadcast precise microwave signals from space that are subsequently picked up and identified by the receivers. Each receiver then processes the information embedded on those gathered signals in order to provide a three-dimensional location (latitude, longitude, and altitude) plus local time.

In this section, each of the GPS segments is briefly commented. Positioning techniques and the structure of the broadcast GPS signals are mentioned in sections 2.2 and 2.3.

[2] The *Medium Earth Orbit (MEO)* is the region of space around the Earth above low Earth orbit (LEO - 2,000 kilometres) and below geostationary orbit (GEO -35,786 kilometres).

### 2.1.1 GPS space segment: satellites

The GPS satellite constellation was originally designed for 24 satellites, each 8 distributed along three circular orbital planes, but it was finally modified to 6 planes with 4 satellites each. The orbits are arranged so that, at any time, at least 6 satellites are always within a user-to-satellite line of sight from almost everywhere on Earth's surface (see Figure 6).

Each of these solar-powered satellites circles the globe at an altitude of approximately 20,200 kilometres (orbital radius of 26,600 km), making two complete rotations every *sidereal day*[3].

Nowadays, there are 31 actively broadcasting satellites in the GPS constellation (September 2007). The additional satellites improve the precision of GPS receiver calculations by providing redundant measurements.

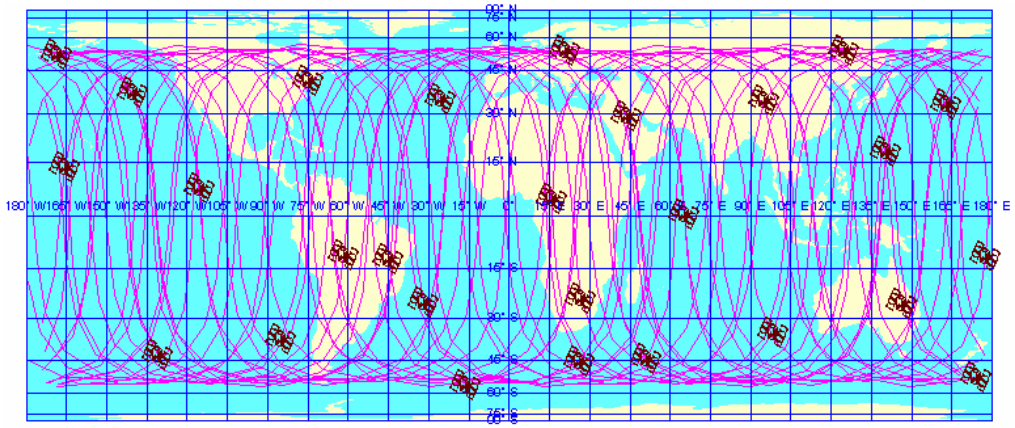

Figure 6 **NAVSTAR GPS satellites and orbits for 27 operational satellites** on September 29, 1998, satellite positions at 00:00:00 9/29/98 with 24 hours (2 orbits) of ground tracks to 00:00:00 9/30/98 – image courtesy of University of Colorado at Boulder – Department of Geography

[3] The *sidereal day* is defined to be the length of time for the vernal equinox to return to your celestial meridian. The *solar day* is defined to be the length of time for the Sun to return to your celestial meridian (*1 sidereal day = 23.9344696 hours).*

### 2.1.2 GPS control segment: ground stations

The flight paths of GPS satellites are tracked by a group of ground stations belonging to the *US Air Force* and the *National Geospatial-Intelligence Agency (NGA)*. The job of this segment is the maintenance of satellites in their proper orbits through occasional command maneuvers, and the adjustments of clocks on board, achieving a precision within a few nanoseconds.

Six worldwide *monitor stations* check the exact altitude, position, speed, and overall health of the orbiting satellites. In addition, a *"Master Control Station"* uses this collected information to predict the behaviour of each satellite's orbit and clock. The predicted data is up-linked to the satellites for transmission back to users. Figure 7 shows the locations of these ground stations.

As mentioned before, the control segment ensures that GPS satellite orbits and clocks remain within acceptable limits. Checks are performed by each station twice a day (as the satellites complete their journeys around the earth). In that way, a group of ground antennas are used to track the satellites and upload the corrections to each satellite.

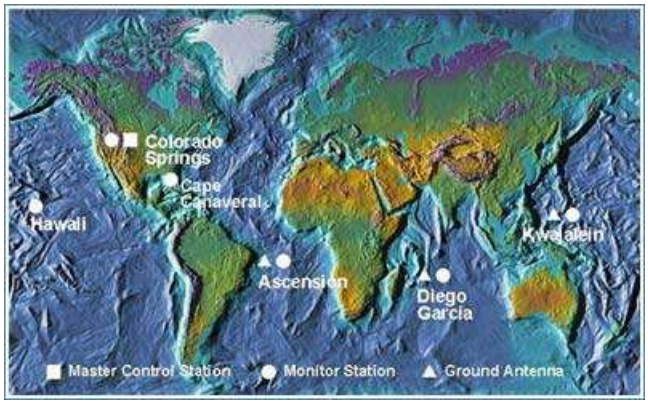


Figure 7 **Map of the GPS Control Segment –** image courtesy of Federal Aviation Administration

### 2.1.3 GPS user segment: receivers

When people talk about “a GPS”, they usually mean a GPS receiver. Individuals may purchase GPS handsets that are readily available through commercial retailers. The job of this kind of equipments is to allocate four or more of the GPS satellites “in view”, figure out the distance to each, and use this information to deduce its own location. This operation is based on a simple mathematical principle called trilateration that uses measurements of distances to satellites (i.e. the known locations) in order to derive an estimation of position.

The present study was focused on the algorithms implemented at receiver site and used to allocate GPS users, i.e. to estimate the receiver’s position. Therefore, the main topic in this report is the GPS receiver. The principal concepts about how this type of equipments works are commented together with the data broadcast by satellites and processed at receiver site in order to allocate both satellites (the reference points) and receiver (the user’s equipment).

In the following figure, a general view of the three mentioned GPS segments is shown.

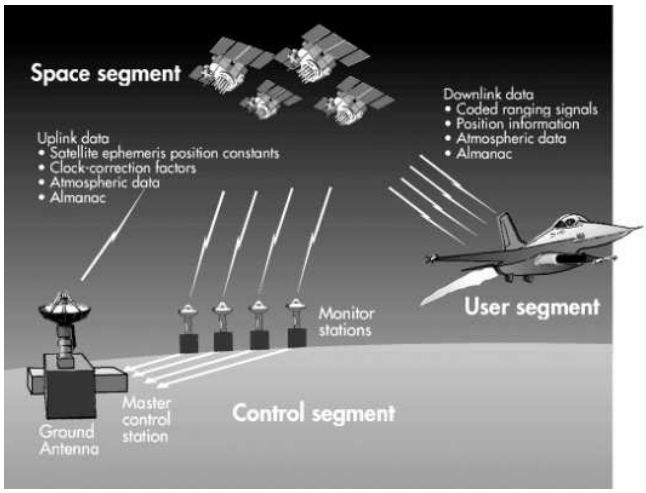


Figure 8 **General view of the three GPS segments: Space, Control and Users.**

## 2.2 GPS positioning: how a GPS receiver works

In order to allocate themselves, GPS receivers estimate the positions of several reference points (i.e. the satellites) that, together with distances in between, are processed to estimate the required position by means of "*trilateration*" methods.

In GPS terminology, distances to satellites are known as *ranges*. These quantities are estimated within receiver equipments by determining the "one-way signal transit time" from satellite to receiver in a process known as time-of-arrival (TOA) ranging.

Both trilateration and TOA methods are briefly introduced in the following sections.

### 2.2.1 Trilateration

GPS receivers compute their positions in two or three dimensional space frames by using this mathematical process. In fact, *triangulation* sounds more familiar; both are methods one can use to determine relative positions of objects using the geometry of triangles. Angle measurements, together with at least one known distance and two reference points, are used to allocate a subject in terms of triangulation. However, to derive a position in terms of *trilateration*, the distances between reference points and the object to be localized are required.

Generally, at least three reference points are used to accurately and uniquely determine the relative position of an object in a two-dimensional plane (2D) by means of *trilateration*. GPS positioning is a three-dimensional process (3D), in that case *trilateration* can be a little tricky; therefore a brief introduction of 2D methods is shown before 3D procedures.

## 2-D Trilateration

The concept of 2D trilateration is easy to understand through an example.

Consider a car driving through an unfamiliar country. A road sign indicates that the car is 500 km from a city. In fact, this is not of much help because the car could be anywhere on a circle around this city with a radius of 500 km. A shepherd the driver stops says that there is another city 450 km away. Now the driver is in a better position to find his location - he is at one of the two intersecting points of the two circles surrounding each of the located cities. If he could also get the distance between his car and another place he can pinpoint his position very precisely, as the three resultant circles can intersect each other at just one point. This is the principle behind 2D trilateration. Figure 9 below illustrates this example.

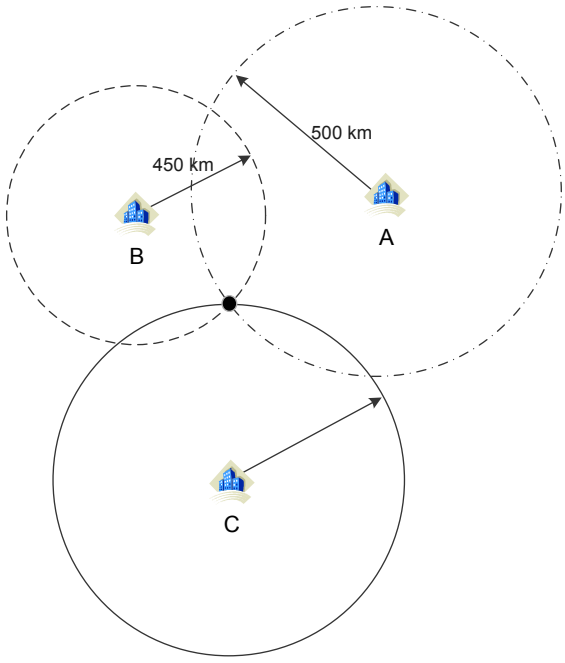


Figure 9 **GPS Positioning – 2D Trilateration**

### 3-D Trilateration

The fundamental concepts are the same for 2D and 3D trilateration, but it is a little trickier to visualize. Considering that the radii from the previous 2D trilateration example go in all directions, a series of spheres (instead of circunferences) is thus formed around the predefined points (see Figure 10). Therefore, the location of an object has to be defined with reference to the intersecting point of these three resultant spheres.

The first two spheres intersect in a perfect circunference. Then, the sphere linked to a third reference point would intersect this circunference at just two points. Additionally, one of the two intersection points can be ruled out assuming the Earth as the fourth required sphere (see Figure 10).

GPS receivers however take into account four or more satellites to improve accuracy and provide extra information such as altitude of the object and local time. The reference frame considered for the computation of the receiver's position will be the earth-centered, earth-fixed (ECEF) frame.

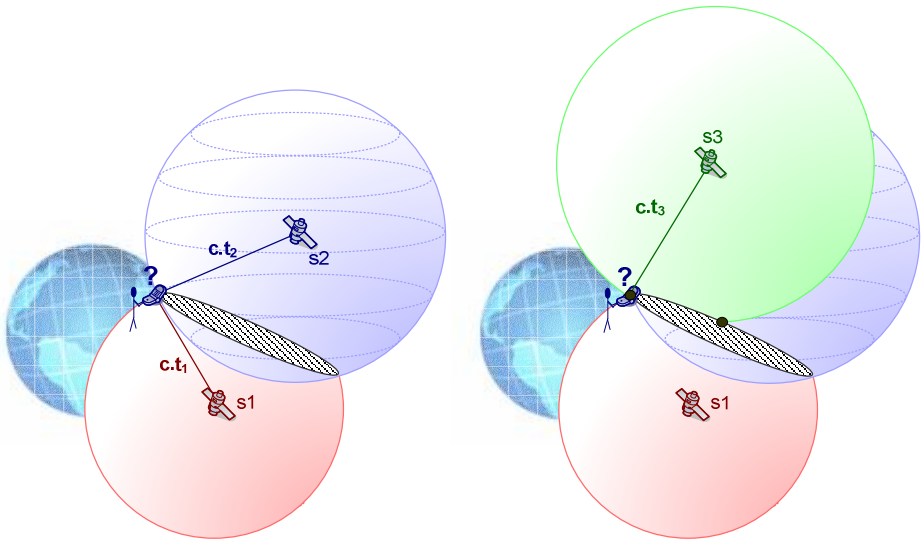


Figure 10 **GPS Positioning – 3D Trilateration**

### 2.2.2 Ranging using time-of-arrival (TOA) measurements

Together with trilateration methods, GPS receivers utilize a concept referred to as *time-of-arrival (TOA) ranging* in order to determine satellite-to-user distances (i.e. the *ranges*). In this context, the time it takes for a signal transmitted by a satellite to reach a receiver is measured and multiplied by the speed at which this signal propagates to obtain an estimation of the distance in between. Consequently, by measuring propagation times of signals broadcast from multiple emitters at known locations, the receiver can determine its position by means of trilateration methods.

For example, consider the case of a mariner equipped with a GPS handset trying to determine his/her position from a group of satellites in view. Assume that the satellites contain accurate clocks on board and the mariner's handset has an approximate knowledge of the satellite positions on their orbits. Furthermore, satellite broadcast signals are assumed to be emitted precisely on specified time marks and clocks aboard are considered to be perfectly synchronized to the receiver's clock. In this scenario, the GPS handset notes the elapsed time from each time mark until the signal is intercepted; this time measure is thus the propagation time it took for the signal to leave satellite and travel to the receiver's antenna. Signals broadcast by GPS satellites are radio waves, considering that all forms of electromagnetic radiation travel at the speed of light, the mariner could estimate the distance to the satellite (i.e. the range) by multiplying the measured propagation time (i.e. the TOA measurement) by this quantity.

It is worth highlighting that a perfect synchronization between clocks in receiver and emitter sites is required in order to derive appropriate one-way range measurements by means of TOA processes; otherwise, the effects of possible clock offsets need to be taken into consideration to perform a correct measurement of the satellite-to-user distance.

In some literature, the GPS signal propagation time is referred to as *signal transmit time.* This quantity varies between 70 and 90 ms approximately. For example, if the satellite signal took 75 ms to reach the mariner's GPS receiver, the distance to the satellite is therefore about 22484,434 km.

**Common clock offsets and compensations**

In the example above, the clock within the mariner's GPS handset was assumed to be precisely synchronized with those aboard satellites. However, this might not be the case. For example, consider that the clock on mariner's equipment is advanced by 1 ms with respect to the satellites time base (that is, it believes that the time mark is occurring 1 ms earlier). Hence, the measured propagation time intervals will be larger by 1 ms due to this time deviation (see Figure 11 to observe the effects on position certainty).

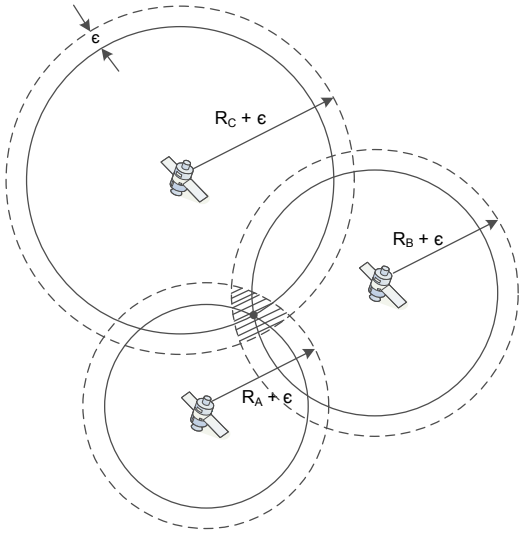


Figure 11 **Effect of receiver clock offset (ε) on position certainty**

The 1ms time deviation shown in Figure 11 affects equally all satellite measurements (the same incorrect time base is being applied) and equates to a distance error of 299.792 km. GPS receivers consider this common clock offset as an unknown together with the three position coordinates of receiver. Therefore, measurements taken from a fourth satellite are required to solve for this fourth parameter.

**Effects of independent measurement errors on position certainty**

Even in the above hypothetical scenario, the TOA measurements would not be perfect due to errors in signal path caused by atmospheric effects and other interfering phenomena. Unlike the receiver's clock deviation, these errors would be generally independent and not common to all measurements; they would affect each measurement in a unique manner and, as a result, inaccurate distance computations will be yielded. An illustrative example of the effects on position certainty caused by these independent measurement errors is shown in the following figure.

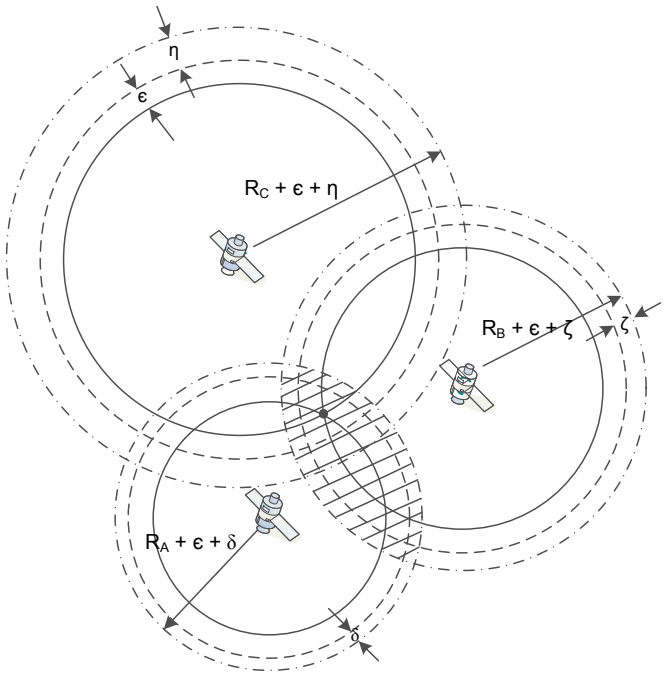


Figure 12 **Effect of independent measurement errors on position certainty**

## 2.3 GPS satellite signals

In order to estimate its location on Earth's surface by means of trilateration methods, the GPS receiver needs the *positions* of the *satellites* visible in the sky [4] and the respective *measurements of distances* in between.

The data contained on the high-frequency signals radiated by the GPS satellites represent the essential information required to estimate both satellites locations and distances in between. These "navigational" signals are centred on two L-band frequencies of the electromagnetic spectrum: *L1* (at 1575.42MHz) and *L2* (at 1227.60MHz) and carry the "navigational information" in the form of two ranging codes and a navigation message.

The primary function of the *ranging codes* is to permit the signal transit time from satellite to receiver to be determined (i.e. the TOA measurement); in fact, these sequences act as the "time marks" required to derive the elapsed time since the signal was transmitted. In addition, the *navigation message* consists of a group of orbital, system status and atmospheric parameters necessary to perform real-time navigation processes; in fact, the GPS receiver uses part of these parameters to allocate satellites.

In the next sections, the main characteristics of the signals broadcast by GPS satellites are mentioned emphasizing the most important elements that permit user's location to be determined within the GPS receiver.

[4] The more sophisticated the GPS equipment, the more its number of tracked channels, so that signals from a larger number of satellites are taken into account for the computations and, therefore, improved accuracy can be achieved.

### 2.3.1 Carrier waves

As the name implies, carrier waves provide the means by which the ranging codes and the navigation message are transmitted to Earth, and, consequently, to the user. As mentioned before, GPS satellites continuously emit electromagnetic radiations centered on two radio frequencies located on the L-band[5] and referred to as *L1* (at 1575.42MHz) and *L2* (at 1227.60MHz). These signals are generated on board satellites regarding to highly stable atomic clocks - usually caesium or rubidium. As a matter of fact, GPS satellites transmit on more than two L-band frequencies[6] but these are associated with classified payloads aboard satellites that do not concern these studies.

The radio waves broadcast by GPS satellites are right-hand circularly polarised and capable of transmission through the atmosphere over great distances. Though signals at these microwave frequencies are highly directional and hence, easily blocked or reflected by solid objects and water surfaces, clouds are penetrated without difficulty. Nevertheless, dense or wet foliage can block the transmissions.

Carrier waves do not contain any information. Furthermore, all GPS satellites broadcast the same frequencies, though the gathered ones are slightly different because of the Doppler effect. In order to provide these carriers the navigational information required at receiver site, they must be "modified" (i.e. *modulated*). GPS uses two different kinds of binary codes in order to modulate the radiated L-band signals; these are referred to as the ranging codes and the navigation message.

[5] The *L band* is a portion of the microwave band of the electromagnetic spectrum ranging roughly from 1 to 2 GHz.
[6] L3 at 1381.05 MHz, L4 at 1379.913 MHz and L5 at 1176.45 MHz – according to http://en.wikipedia.org.

### 2.3.2 Ranging Codes

These binary sequences of 0s and 1s allow the receiver to instantaneously determine the signal transit time (i.e. TOA measurement) and, consequently, obtain the satellite-to-user distance when multiplying by the speed of electromagnetic radiation.

The GPS ranging codes have characteristics of random sequences, but are in fact generated by mathematical algorithms and therefore referred to as *"pseudo-random-noise" codes (or PRN codes)***.** This type of codes possesss two important caracteristics that facilitate the acquisition and tracking of the GPS signals at receiver site. First of all, the *cross-correlation function* of two different ranging codes is nearly zero no matter the shift in between; this *orthogonality* allows all satellites to broadcast simultaneously at the same frequency without interferences in between. Secondly, an individual ranging sequence will correlate with an exact replica of itself only when the two codes are aligned, that is, the *autocorrelation* function *is nearly zero* except for zero-shift (where it shows a sharp peak). This autocorrelation property allows the receiver to estimate the elapsed time since the signal was radiated by satellite's antenna.

Two kinds of ranging codes are transmitted on the broadcast L-band frequencies: the *civil C/A code*, known as "clear/access" or "coarse/acquisition" code, and the *private P code*, aimed at *DoD*[7] authorized users and named as "precise" because of its higher precision and restricted availability.

**C/A codes**

An individual C/A code is a unique binary sequence of 1023 chips (or bits) assigned to each GPS satellite. This sequence is generated at a rate of 1023000 bits per second that is a frequency of 1.023 MHz. Hence, the entire C/A code sequence repeats every millisecond and the "code wavelength", i.e. the length of a bit, is approximately 300 m considering that the radio waves transmitted by the GPS satellites propagate

[7] Deparment of Defense - USA

approximately at the speed of light in vacuum (the entire sequence is about 300 km long).

**P codes**

The P code is a far more complex binary sequence that consists of an extremely long unique PRN segment of about $10^{14}$ chips. These codes are approximately 266.4 days long with chipping rates located on the frequency 10.23 MHz. The wavelength of this code is therefore approximately 30 m (i.e. ten times the resolution of the C/A code[8]). Instead of assigning each satellite a unique code (as in the case of C/A sequences) the P code is allocated such that each satellite transmits a one week portion of the 266.4 day long sequence (according to reference [3.5], restarting on Saturday midnight).

When *Anti-Spoofing* (AS)[9] capabilities are activated, the P code is broadcast as an encrypted sequence referred to as *P(Y)-code*. In order to acquire or "reconstruct" the signals broadcast by satellites and measure then distances in between, the GPS receiver needs to know how to generate the ranging codes transmitted on satellite signals, that is, need to know how to decrypt the encrypted P code. Since the access to the signals containing this high precision P(Y)-code is only restricted to DoD authorized users, civil users obtain range measurements from tracking only the 'less-precise' C/A-codes embedded on the gathered signals.

[8] The smaller length of the P code chip result in greater precision in the derived range measurements compared with that obtained from C/A codes

[9] *Anti-Spoofing* (AS) it the process of encrypting the P code by addition (modulo 2) of the code itself and a secret encryption sequence so that P code cannot be replicated by hostile forces, i.e. avoiding 'spoofing'. When encrypted, P code is referred to as P(Y) code.

### 2.3.3 Navigation message

In order for a GPS equipment to derive real-time positions of satellites and receiver, a group of parameters are transmitted on both L-band frequencies. These are named as the *navigation message* and contain the information regarding to predicted satellite ephemeris, predicted satellite clock correction model coefficients, GPS system status information and an ionosphere model.
Ground control stations uplink this information into each satellite for subsequent transmission to all users. Satellite messages are in binary form but, unlike ranging codes, the sequences are not random like. The data is emitted at a rate of one bit every 20 repetitions of the C/A code, that is 50 bits per second (50 bps). The entire sequence length consists of 1500 bits.

### 2.3.4 Signal broadcasting

The signal radiated by each GPS satellite antenna is a combination of the three components mentioned before: carrier waves, ranging codes and navigation message. In fact, all these components are generated in 'synchrony', that is, they are derived by multiplying or dividing the output of the highly stable atomic clocks onboard satellites. These clocks generate a pure sine wave at a frequency $f_0$ = 10.23 MHz referred to as the *fundamental frequency*.

As mentioned in reference [3.5], the output of clocks aboard satellites is offset by a small amount in order to compensate for relativistic effects. The actual clock output is then 10.22999999543 MHz. Just as a matter of interest, tiny instabilities in those orbiting clocks contribute at least a few meters of error to a single receiver GPS measurement; in order to keep the error within acceptable limits, ground stations monitor continuously the satellite broadcast signals and perform daily uploads on the broadcast navigational parameters.

The fundamental frequency is multiplied by integer factors to generate the carrier frequencies L1 and L2 (154 and 120 respectively[10]), as shown in the following figure.

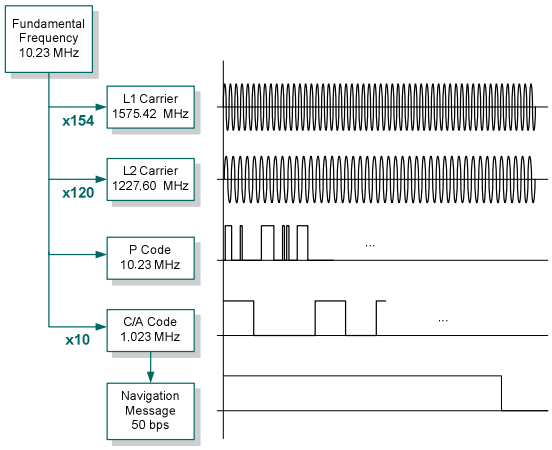


Figure 13 **Components of a GPS signal –** carrier waves, ranging codes and navigation message.

Each of the ranging codes are also generated from the satellite clock (as shown in figure above). These sequences are combined with the navigation data using *modulo-2 additions*, that is, whenever the data bit of the navigation message is equal to 1 the next twenty C/A code repetitions will be inverted. Conversely, when the data bit is 0 the consecutive ranging code sequences will remain unaffected (see Figure 14).

The composite binary signal is then impressed upon the carrier in a *BPSK* (*binary phase shift keying*) modulation process consisting of applying a *carrier signal shift of 180º* [11] when code transits from 0 to 1, or from 1 to 0. In fact, the composite signal derived from the P code is used to modulate both the L1 and L2 carriers, and the one derived from the C/A code is only used to modulate the L1 carrier. An illustrative example of this process is shown in the Figure 14.

[10] $f_{L1} = f_0$ x 154 = 1575.42 MHz equivalent wavelength $\lambda_{L1} = c/f_{L1} \approx 19$ cm
$f_{L2} = f_0$ x 120 = 1227.60 MHz equivalent wavelength $\lambda_{L2} = c/f_{L2} \approx 24$ cm

[11] A *carrier signal shift of 180º* implies that the carrier is multiplied by -1.

It is worth mentioning that the phase shifting of the carrier results in a ‘spreading’ of power around the carrier frequencies due to the ranging codes (i.e. pseudo-random sequences) modulating these waves.

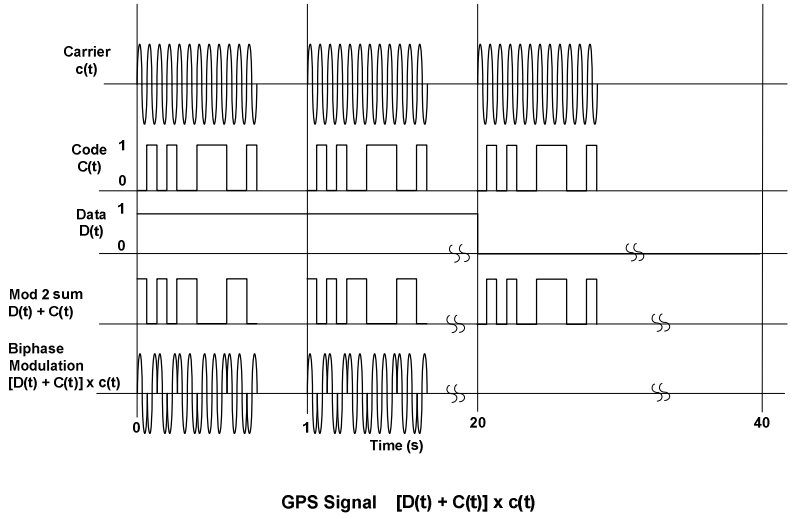


Figure 14 **Structure of a GPS signal.** Each signal comprises three components: an RF carrier, a binary pseudo-random sequence and the binary Navigation Message.

As already discussed, L1 carrier frequency transmits both public C/A codes and restricted P sequences. This is accomplished by generating two carrier signals on L1; one as generated by the clock (*in-phase component*) and the other is obtained by shifting it in phase by 90º (*quadrature component*). Specifically, the in-phase component is modulated by a P code, and quadrature one is modulated by a C/A code. L2 signal carries solely P codes. Hence, the resultant three BPSK-modulated signals are then broadcast by each GPS satellite.

The GPS receiver can obtain the measurements of satellite-to-user distances by tracking the C/A code or the P code (if it is possible) embedded on the gathered signal. However, the C/A code resolution is ‘coarser’, and the derived measurements are subject to greater ‘noise’. According to reference [3.5], the absence of a C/A code on L2 is intentional in order to limit the accuracy of the GPS system for civil users, as the access

restriction to the encrypted P(Y) code. Hence, only authorized users (i.e. DoD users, military users) can access to preciser satellite-to-user distances and therefore obtain finer positioning results. As a result, the distinction between the ranging codes and the associated policies for their use results in the availability of two GPS positioning services: the *Precise Positioning Service* based on dual frequency P code measurements, and the *Standard Positioning Service* based on single frequency C/A code measurements.

Just as a matter of interest, dual-frequency measurements are an important challenge to overcome drawbacks caused by ionosphere phenomena on GPS positioning accuracy. According to reference [3.6], receiver manufacturers have devised and implemented standards in civil applications with P code encryption notwithstanding. Anyway, a price is paid for the lack of knowledge of the P code structure in the form of lowered signal-to-noise ratios. Nevertheless, an approximate ionosphere model is provided within the navigation message.

# Chapter 3

# Measurements, Models and Errors

*"Some talk of millimetres, and some of kilograms,*
*And some of decilitres, to measure beer and drams;*
*But I'm a British Workman, too old to go to school,*
*So by pounds I'll eat, and by quarts I'll drink, and I'll work by my three foot rule.*
*A party of astronomers went measuring the Earth,*
*And forty million metres they took to be its girth;*
*Five hundred million inches, though, go through from Pole to Pole;*
*So lets stick to inches, feet and yards, and the good old three foot rule."*

William Rankine - *The Three-Foot Rule*

At its simplest, GPS civil users under the *Standard Positioning Service* (SPS)[12] provides positioning accuracy of tens of meters. The performance is dynamic and changes with time and place. In fact, accuracy of position estimates depends not only upon the number of satellites in view and their spatial distribution, but also upon the nature of the errors in the derived measurements, that is, the reliability of the available measurements.

As it has been shown on chapter 2, the basic operation of a GPS receiver is focused on the acquisition and maintenance of captured radio frequency signals transmitted by the satellites spread out in the sky. From these processes a group of measurements or observations are derived. *Firstly*, tracking the ranging codes embedded on the transmitted GPS signals yields estimates of instantaneous user-to-satellites distances, referred to as *ranges* (see chapter 2 – section 2.3.2). These measurements, however, are all affected by common offsets and are thus named as *pseudo-ranges*. *Secondly*, the

[12] *SPS* - Common civilian positioning accuracy obtained by using the single frequency C/A code. Under selective availability conditions, guaranteed to be no worse than 100 meters 95% of the time.

phase of the received carrier wave might also be tracked by bringing it face to face with a local generated sine wave of the same frequency. Several researches (see references [3.6], [3.7], [3.8]) have shown that the resultant *phase observation* contains precise information about how satellite-to-user ranges change with time. Both code and carrier-based measurements can be used subsequently to extract information of *ranges*, the basic quantity used while processing the navigation solution (position, velocity and time determination - PVT).

In this chapter, the generation of these measurements is firstly exposed by explaining the main hardware operations within the GPS receiver electronics. Secondly, in order to develop an appropriate parameter model for GPS measurement data processing, simple physical and mathematical models for these two kinds of measurements are posed in connection with the receiver-to-satellite geometric *ranges*. Additionally, as a requirement of this process, error sources affecting these data and convenient models to characterize them are also commented.

Figure 15 **Applications of precise GPS measurements**. **Research into Earth processes** via high-precision geodesy using GPS – A permanent GPS station collects remote measurements of surface deformation associated with volcanic processes (island of Monserrat, Soufrière Hills volcano) – image courtesy of UNAVCO (University NAVSTAR Consotium 1998).

## 3.1 GPS hardware tracking

The satellite broadcast GPS signals must be acquired and tracked in order to derive the required *navigation parameters* and *distance measurements* aimed at computing receiver's location. In this section, the overall GPS hardware tracking operation will be briefly expounded.

First of all, the satellite signals are gathered by the GPS receiver's omnidirectional antenna. Tracking processes begin with the determination of which satellites are currently being observed. The receiver can ascertain which GPS satellites are above the horizon with the aid of a recent *almanac*[13] and a rough idea of the user location. If almanac information is not available, or only a very poor estimate of PVT is at hand, the receiver will carry out a "sky search" attempting to randomly detect and lock onto a signal.

After the identification of which satellites are in view, the receiver attempts to *acquire* or "reconstruct" the incoming carrier wave and extract the embedded data (these are the *ranging codes* and *navigation message*, see chapter 2 sections 2.3.2 and 2.3.3). In this process, the receiver needs to know how to generate the ranging codes transmitted on satellites signals; these are pseudo-random sequences that modulate (together with the navigation message) the carriers broadcast by GPS satellites. As a result of this modulation, signal power is spread over a wider spectral region and it is received below the background noise (these schemes are referred to as *spread spectrum techniques*). Hence, carrier signal must be made "visible" at the receiver in order to carry out the signal acquisition. With that purpose *code-correlating* techniques are performed within the GPS receivers. It is worth highlighting that, in order to maintain the captured radio frequency signals, every noise source as well as any possible error due to Doppler effect, ionosphere or synchronization is taken into account on the GPS tracking process.

[13] *Almanac data* is used by GPS receivers to predict which satellites are nearby when trying to gather signals. It consists of a set of parameters related to each of the GPS satellites and used to calculate their approximate locations in orbits. Hence, using almanac data saves time by letting the receiver skip looking for satellites that are below the horizon.

### 3.1.1 Code and Carrier Tracking Loops

In order to track the carrier frequency, a *'carrier-tracking loop'* is used while a '*code-tracking loop*' operates in order to track the ranging codes (C/A and/or P code - if it is possible). According to reference [3.5], these two tracking loops work together in an iterative manner, aiding each other in order to *acquire* and *track* the satellite signals.

The receiver's ***carrier tracking loop*** is on the trail of the changes in the received carrier frequency. This process is performed essentially by the local generation of a sinusoidal signal at frequency L1 (or L2 depending on receiver's features) which mainly differs from the incoming carrier due to the Doppler offset. In order to *maintain lock on the carrier*, this feedback control loop must adjust the frequency of the receiver-generated carrier until it "matches" the incoming frequency. The amount of offset applied in this alignment is named as the *"beat frequency"* which can be processed to give a periodic *carrier beat phase measurement*. This kind of measurement is useful for some applications such as "phase smoothing" of code measurements (or pseudo-ranges), because the noise on them is lower than the one affecting pseudo-ranges. The derivative of the carrier beat phase corresponds to the Doppler measurement, which is used to determine the receiver's velocity.

As mentioned before, the carrier signal must be 'made visible' above the background noise, in order for the carrier tracking loop *to acquire the incoming satellite signal*. This task is performed by another feedback control loop referred to as ***code tracking loop*** or ***delay-lock loop***. Additionally, a GPS observable is derived from this process; referred to as code-phase or *pseudo-range measurement*. This quantity is basic while processing the navigation solution since it contains information about the satellite-to-user distance.

In the code tracking loop, the code modulations embedded on the broadcast GPS signal are removed by mixing a "tuned" code replica with the incoming signal. The code replica is generated within the receiver electronics. Then, this feedback control loop

tunes or *alignes*[14] the locally generated code with the one embedded on the picked up signal. In fact, the replica is continuously adjusted by sliding it in time and computing the *correlation function* with the gathered signal. GPS receivers applying this technique are referred to as *code-correlation receivers*. Thanks to this procedure the ranging code modulations are removed and the signal power is boosted well above the background noise collapsing in the original very narrow carrier frequency band. However, this technique requires knowledge of the ranging codes generating algorithms. As mentioned in chapter 2 section 2.3.2, under the policy of Anti-Spoofing, the transmitted P code is encrypted (i.e. secret) and hence cannot be used in this code-correlating technique. According to reference [3.5], GPS instrument manufacturers use a technique referred to as "squaring" to perform P code phase measurements on L2. Nevertheless, the most important advantage of the code-correlating approach is the resultant higher signal-to-noise ratio (and thus better quality in the derived measurements) than any other signal processing technique.

As soon as the incoming signal and the replica ranging code are aligned and mixed, the "0"s and "1"s of these two binary sequences are cancelled, leaving the incoming carrier signal modulated only by the navigation message. This process is summarised in the figure below. Navigation data can be obtained by mixing the resultant signal with a locally generated sine wave at the same frequency; as mentioned before, this process is achieved in the *carrier tracking loop*.

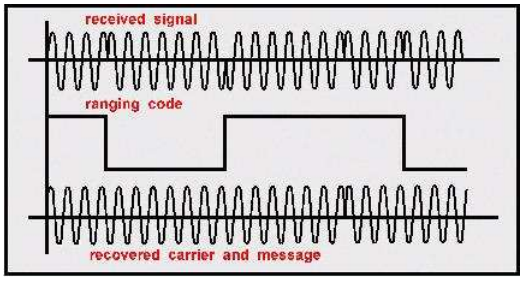


Figure 16 **Recovery of the GPS ranging codes -** image courtesy of SNAP-Lab

[14] An *alignment* of the gathered signal with the receiver-generated C/A code is required because of the different time scales affecting both signals (caused by the lack of synchronization between the receiver clock to the general GPS time and the travel time of the signal from satellite to receiver's antenna) – see section 3.2.

Therefore code and carrier tracking loops are designed to aid each other in order to acquire and track GPS satellite signals. In addition, the measurements used to compute the "*navigation solution*" (i.e. position, velocity and local time) are also derived on these receiver's operations; these are referred to as code and carrier observations.

## 3.2 Code observations: pseudo-ranges

As mentioned in sections before, the ranging codes transmitted on the GPS satellite signals act as accurate "time marks" that permit the receiver to estimate the elapsed time that took any portion of the signal to travel from the satellite to the receiver. Considering that GPS signals are electromagnetic radiation propagating in straight lines at the speed of light, a rough measurement of satellite-to-user distance (i.e. a *range*) can be achieved from the measured propagation time. This measurement is referred to as *pseudo-range* and is essential while computing the position of the GPS receiver.

In fact, an individual GPS pseudo-range is obtained while tracking the phase of the C/A code or P code embedded on the gathered signal. The code phase is measured as the time shift required to align a replica of the ranging code, generated at receiver site, with the incoming one, embedded on the received signal (see section 3.1.1). The range measurement is yielded when the above time measurement is multiplied by the speed at which the signal propagates (i.e. translation into metric units). An illustrative example of this idea is shown in the following figure.

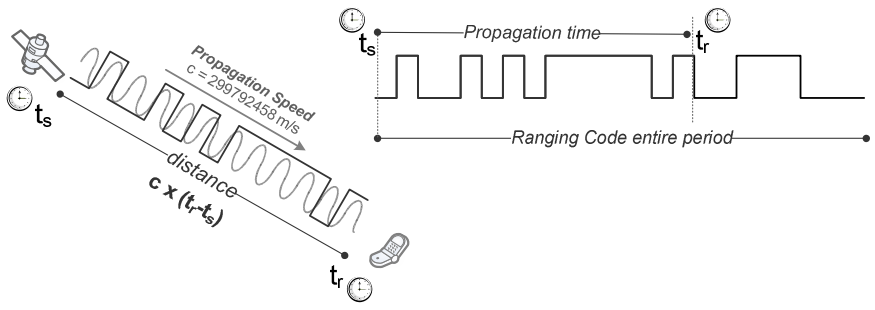


Figure 17 **The GPS code-range measurement**

### 3.2.1 Measuring the phase of the ranging codes

Each chip of the GPS ranging codes is generated at precise known instants of time in accordance with clocks on board the satellites. At receiver site, these time snapshots are used as 'time-tags' that facilitate the estimation of the time interval it took the signal to travel from satellite to receiver, that is, the *signal transit time* or the *propagation time*. But how does the GPS receiver generate this time measurement?

Let's assume that all satellite clocks are synchronized to the same time scale, referred to the general GPS time (GPST). Consider that the ground receiver's clock maintains also the same synchronization (there is thus no clock offset with respect to GPST). If one of the satellites starts transmitting a C/A code sequence on the L1 carrier and, at the same instant of time, receiver begins generating a C/A code replica corresponding to that particular satellite, the replica would match the code arriving from the respective satellite. However, this is not the case since the propagation time causes a lag on the received code with respect to the local generated replica. This delay is roughly estimated within the code tracking loop as the *time shift* applied on the replica to align it with the incoming code, that is, the time shift that shows the sharp peak[15] in the correlation function between both replica and incoming code sequences – as shown in the following figure.

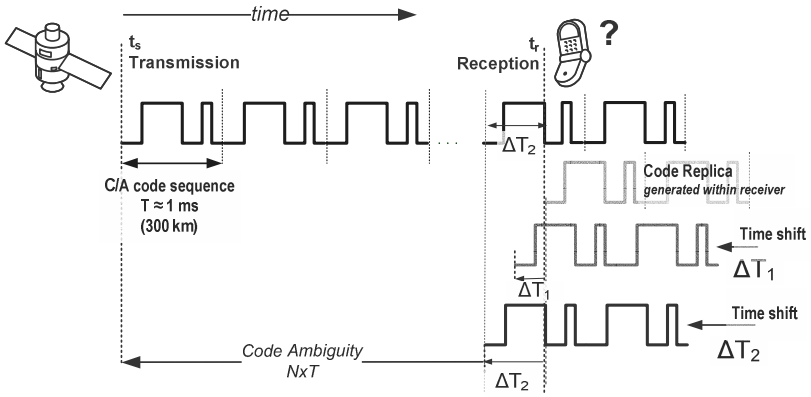


Figure 18 **Use of the replica code to determine the satellite-to-user signal transit time.**

[15] This effect is due to the auto-correlation properties of ranging codes, mentioned in section 2.3.2

### C/A code pseudo-range ambiguity

In terms of C/A codes, the time shift applied on the code's replica in order to align it with the incoming signal does not entirely correspond to the transit time that took the signal to travel from satellite to receiver – see previous Figure 18. Distances to satellites are about 20.000 km when overhead, and about 26.000 km when rising or setting and signal transit times approximately vary between 70 ms and 90 ms. A C/A code sequence repeats each millisecond, and the code correlation process essentially provides a measurement of 'pseudo-transit time' modulo 1 ms, that is, the measurement of signal transit time derived from tracking the phase of a C/A code is ambiguous in whole milliseconds (as shown in Figure 18 by means of the term *NxT*, being *T* the C/A code period *T=1ms*). It is worth pointing out that the one week P code portion transmitted by each satellite provides unambiguous pseudo-ranges; however, the access to this code is only restricted to DoD authorize users.

According to reference [3.3], the GPS receiver can easily overcome the drawbacks caused by the C/A code ambiguity if it has a rough idea of its location within hundreds of kilometres (considering that the entire C/A sequence is about 300 km long). The code measurements processed on these studies do not seem to be ambiguous; it is supposed that the C/A code ambiguity estimation was performed previously while deriving the measurements. The following figure shows an example of pseudo-range measurements used while performing these studies.

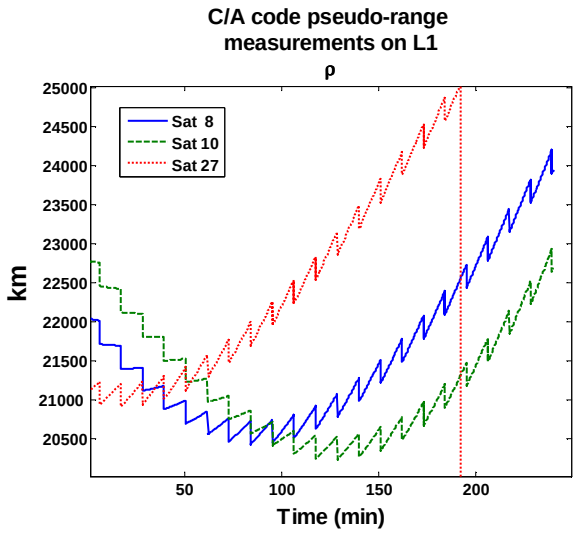


Figure 19 **Example of code measurements (pseudo-ranges) taken by a stationary receiver** that observed three satellites during a time period of 4 hours on July 19, 2007 from 9:00 to 13:00**.**

**Obtaining measurements of distances and ranging**

Once the absolute signal transit time is derived, this time measurement is multiplied by the speed of electromagnetic radiation yielding a rough measurement of satellite-to-receiver distance, referred to as *range*. Hence, as mentioned in chapter 2, measuring simultaneous ranges to three satellites, the receiver will be able to compute its position as the intersection of three imaginary spheres of known radii, i.e. the measured ranges, and centred at each satellite whose positions are computed by processing some parameters taken from the navigation message - as illustrated in the following figure.

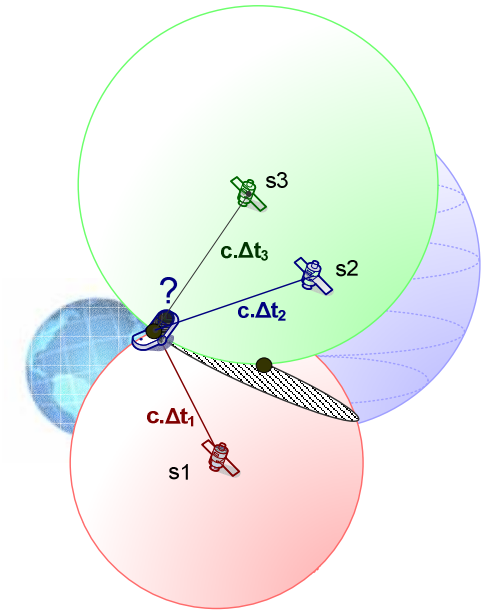


Figure 20 **Ranging with code measurements.**

Nevertheless, the real situation has some drawbacks. The receivers are generally equipped with quartz crystal oscillators that do not keep the same time as the more stable atomic clocks onboard satellites. In fact, both clocks (onboard satellites and within the GPS receiver) deviate from the general GPS time scale; these offsets must be taken into consideration while processing the derived range measurements. Satellites clocks can be approximately synchronized to GPST using the clock correction model broadcast in the navigation message. Consequently each range measurement is "contaminated" by the receiver clock error, for that reason it is referred to as *pseudo-*

*range* instead of range. Hence, a minimum of four satellites must be tracked in order to determine the receiver's coordinates and clock error.

**Precision of the C/A code pseudo-ranges**

As it was introduced in the section 2.3.2, an individual C/A code is a unique binary sequence of 1023 chips (or bits) that is repeated each millisecond. The uncertainty in matching the replicas with the incoming code is thus limited to only 1023 code chips per millisecond. According to reference [4.9], the alighment is generally possible to within about 1-2% of the chipping rate or the chip length. The chipping rate of the C/A codes is 1023 Mbps and the chip length is about 300 m. Hence, a C/A code phase measurement precision is on the order of 3-5 metres. P code direct adquisition requires, by design, higher complexity due to the length of this code; these studies are not focused on this area, readers can look up literature quoted on references [3.3][3.4][2.1].

Though metre precision can be possible, pseudo-ranges are affected by several error sources that degrade the accuracy of these measurements. These error sources will be mentioned in subsequent sections.

### 3.2.2 GPS pseudo-ranges: observation equations

Once the definition of pseudo-range has been introduced, physical and mathematical patterns need to be described in order to develop an appropriate parameter model for processing this kind of GPS measurements. First of all, the physical model for an individual pseudo-range is posed. Then, a mathematical model is derived incorporating only those terms that will be parameterised while processing the pseudo-ranges. The following development is principally taken from references [3.3], [3.4] and [3.6].

In the following sections, measurements from a GPS satellite are analyzed in a generic way, making no reference to the satellite identification number or carrier frequency (L1 or L2) to keep the notation simple. Subscript *s* is used to identify a term associated with a satellite, and subscript *r* to identify a term associated with the GPS receiver.

**Pseudo-range in terms of 'signal transit time'**

Consider an estimate of the transit time ΔT associated with a specific code transition of a signal from a satellite received at time *t* per GPST. Let $t_s(t-\tau)$ be the corresponding transmission time, stamped in the broadcast signal and $t_r(t)$ be the arrival time, measured by clock within receiver. Hence, the measured pseudo-range $\rho(t)$ can be written as

$$\rho(t) = c\Delta T = c[t_r(t) - t_s(t-\tau)] \quad (3.2\text{-}1)$$

where $\tau$ is the real signal transit time from satellite to receiver. The terms $t$ and $t-\tau$ corresponds to the transmission and reception times in the general GPS time (GPST). As mentioned before, the instant of time $t-\tau$ is known in advance because it corresponds to a time stamp printed on the signal and translated to the GPST scale (i.e. corrected by using the satellite clock model broadcast on the navigation message). However, $t$ and $\tau$ are unknown.

**Clock errors, offsets or biases**

Oscillators in satellites and receivers are used to generate timed signals such as the P code and the C/A codes. It is common therefore, to consider them *clocks*. As it has been introduced before, GPS satellite and receiver clocks keep time independently; this lack of synchronization affects measurements derived within receivers.

In developing the observation equations for GPS code and carrier measurements it is useful to assume that every clock, or oscillator, can be compared directly with a "perfect" oscillator having a known and constant frequency in the reference time scale referred to as GPS Time (GPST). Then, the errors caused by the variations of frequency on real satellite and receiver oscillators are named as *clock errors, offsets or biases*. Times derived from the real receiver and satellite oscillators are therefore affected by these clock errors and relations to the general GPST frame can be thus specified by the following equations

$$(3.2\text{-}2) \quad t_r(t) = t + b_r(t) \qquad\qquad t_s(t-\tau) = (t-\tau) + b_s(t-\tau)$$

where $b_r$ is the receiver clock offset and $b_s$ is the residual modelling error in translating the signal transmission time stamp to GPST. Both $b_r$ and $b_s$ reflect the time advances affecting satellite and receiver clocks regarding to GPST (as shown in the following figure).

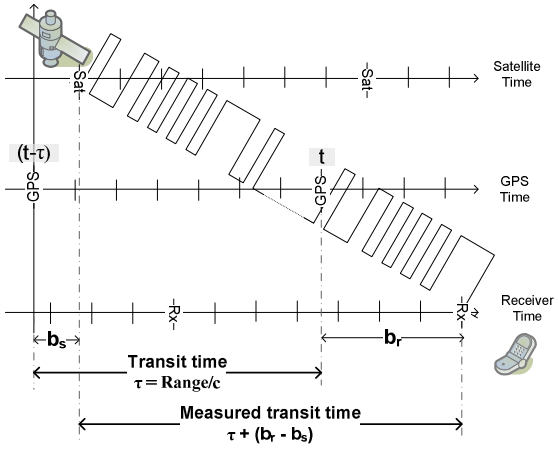


Figure 21 **Effects of clocks errors on the measured transit time –** $b_s$ satellite clock error; $b_r$ receiver clock error.

**Pseudo-range in terms of 'clock errors'**

Considering the "time advance" affecting receiver and satellite clocks as shown in eq. (3.2-2), the pseudo-range equation (3.2-1) can be rewritten as

$$\rho(t) = c[t + b_r(t)] - c[t - \tau + b_s(t-\tau)] \Rightarrow \rho(t) = c\tau + c[b_r(t) - b_s(t-\tau)] \quad (3.2\text{-}3)$$

where the terms $b_r$ and $b_s$ are the receiver and satellite clocks advances, respectively; and $c\tau$ corresponds to the satellite-to-user distance covered by the gathered signal, as it can be observed in the following figure.

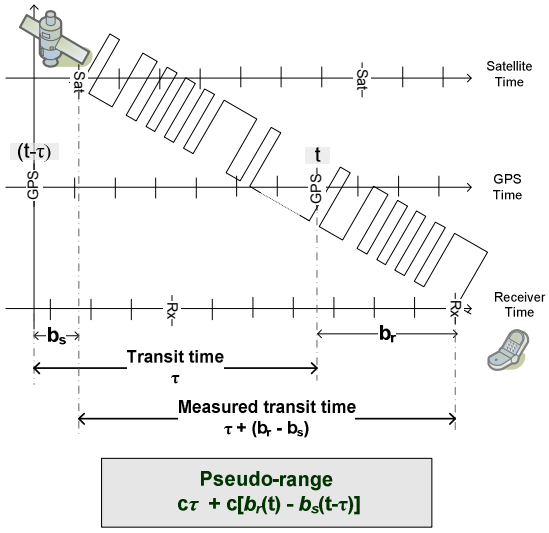


Figure 22 **Theoretical concept of pseudo-range measurements.** The receiver and satellite clocks are unsynchronized. Hence, the measured transit time ΔT is the difference between signal reception time (according to receiver clock) and emission time (stamped on signal in accordance with satellite time scale).

The transit time component τ in equation (3.2-3) is made up of two parts. The main one refers to the time it takes for the signal to travel through the real geometric range or distance between the satellite at the time of transmission $t$-$\tau$ and the receiver at the time of reception $t$. This can be determined from the position vectors of the satellite and the receiver at these time snapshots, if they are expressed in the same reference system. The satellite and receiver position information contained in the geometric range *Range(t,t-τ)* is essential for GPS positioning.

The second part of the transit time term accounts for the "extra time" taken for the signal to travel through the Earth's atmosphere. In fact, the GPS signals are affected by the medium through which they travel. All but the final 5% of the signal travel can be regarded as in a vacuum or free space, through which the electromagnetic signals travel with a constant speed c = 299792458 m/s. Close to the surface of the earth, at a height of about 1000 km, the signals enter an atmosphere of charged particles, called the *ionosphere* that *acts as a refractive and dispersive medium* in the case of the GPS frequencies. Later, at a height of about 40 km, the signals encounter an electrically neutral gaseous *refractive* atmosphere known as the *troposphere*. The atmosphere changes therefore the propagation velocity (speed and direction) of radio signals. This effect can be modelled as a time delay or an increase in the range measurement and is incorporated in the observation equation as a code correction term $\rho_{atm}$.

(3.2-4) $$c\tau = Range(t, t-\tau) + \rho_{atm}(t)$$

The term $\rho_{atm}$ can be broken down into two components taking into consideration the two most important atmospheric layers generating delays or advances in the GPS signals, according to GPS literature, these are the ionosphere and the troposphere. Both terms will be discussed in the next section (Measured pseudo-ranges).

Combining equations (3.2-3) and (3.2-4), a ***physical model*** for an individual pseudo-range can be derived in units of meters

(3.2-5) $$\rho(t) = Range(t, t-\tau) + c[b_r(t) - b_s(t-\tau)] + \rho_{atm}(t)$$

**Measured pseudo-ranges**

The measured pseudo-range differs from the above physical model (3.2-5) in some aspects that must be taken into consideration.

*Firslty*, the derived pseudo-ranges will have *random noise* and signal interferences such as *multipath*, both affecting the measurement process. To denote these and other uncompensated modelling and measurement errors, an additional term $\rho_{\text{noise}}$ is considered

$$\rho(t) = Range(t, t-\tau) + c[b_r(t) - b_s(t-\tau)] + \rho_{atm}(t) + \rho_{noise}(t) \quad \text{(3.2-6)}$$

*Secondly*, atmosphere effects will be modelled separately into an ionosphere term and a troposphere term. On the one hand, the carrier and its modulating signal (i.e. the ranging codes and navigation message) propagate at different speeds through ionosphere. Specifically, the code phase is delayed while the carrier phase is advanced by the same amount. This means that code observables are measured longer than they should be. On the other hand, the path delay for both code and carrier is the same while crossing the troposphere; in fact, both signals suffer a delay because of the refractive characteristics of this atmospheric layer. Therefore, atmosphere effects will be modelled as two positive terms denoting the code transmission delays associated with ionosphere ($I$) and troposphere ($T$).

$$\rho_{atm}(t) = I(t) + T(t) \quad \text{(3.2-7)}$$

The above code pseudo-range mathematical model (3.2-6) is rewritten taking into consideration the terms mentioned in this section and dropping references to the measurement epoch $t$ in order to simplify the mathematical expressions

$$\rho = Range + c(b_r - b_s) + I + T + \rho_{noise} \quad \textbf{(3.2-8)}$$

Equation (3.2-8) represents a ***general observation equation (or mathematical model) for an individual code measurement or pseudo-range***. Ideally, it would be perfect to achieve a measurement of *range*, the true distance to the satellite. What it is obtained instead is a pseudo-range ρ which is a distance measurement "corrupted" by several errors (atmosphere effects, measurement noise, clock offsets). ***How accurate an estimate of position it is yielded from these measurements would depend upon the GPS receiver's ability to compensate for or eliminate the errors affecting these quantities.***

It is worth highlighting that atmosphere effects and the noise term $\rho_{noise}$ depend on the receiver's reliability, satellites layout and period of the day (or night). However, these quantities vary slightly between closed observation epochs. The change with time in observed pseudo-ranges is therefore equal to the change in any of the following quantities: geometric range between satellite and receiver, difference between satellite and receiver clock errors, troposphere and ionosphere delays, or measurement noise and signal disturbances.

In the following section, an example of the pseudo-range measurements used in these studies is shown. Figure 23 above shows the *pseudo-range* measurements from three observed satellites taken by a permanent GPS station located on *E.T.S.I of Topography, Geodesy and Cartography* in *Polytechnic University* of Madrid. Observations were collected on July 19, 2007 during approximately 4 hours (9:00 – 13:00) and are available on RINEX [16] 2.10 files. Additionally, antenna's elevation angles were computed so that a graphic of satellites' layout in the sky can be shown. The three observed satellites stayed in view for almost the whole observation time. In fact, they started setting about the same time (after the first 50 min) - this is also noticeable since the elevation angles started decreasing. One of them (satellite 27) came overhead and stayed in view for almost the whole observation time till it disappeared beyond the horizon. The other two satellites remained visible higher in the sky, i.e. shorter distances

[16] *RINEX* - Receiver Independent Exchange Format

or ranges in between. As the GPS receiver is fixed in a known location (stationary antenna), variation in the pseudo-range measurements shown in this figure is mainly due to changes in geometric ranges resulting from the satellite motion and rotation of the Earth. It is worth highlighting that the GPS receiver's basic quartz crystal oscillator tends to drift, that is, it deviates from the general GPS system time. According to reference [3.3], some receiver manufacturers attempt to limit these deviations by letting the clock drift until it reaches a certain threshold (typically, 1 ms), and then reset it with a 'jump' to return the bias to zero. The common discontinuities that are observed on all *pseudo-range* measurements shown in Figure 23 are therefore the consequence of these clock readjustments.

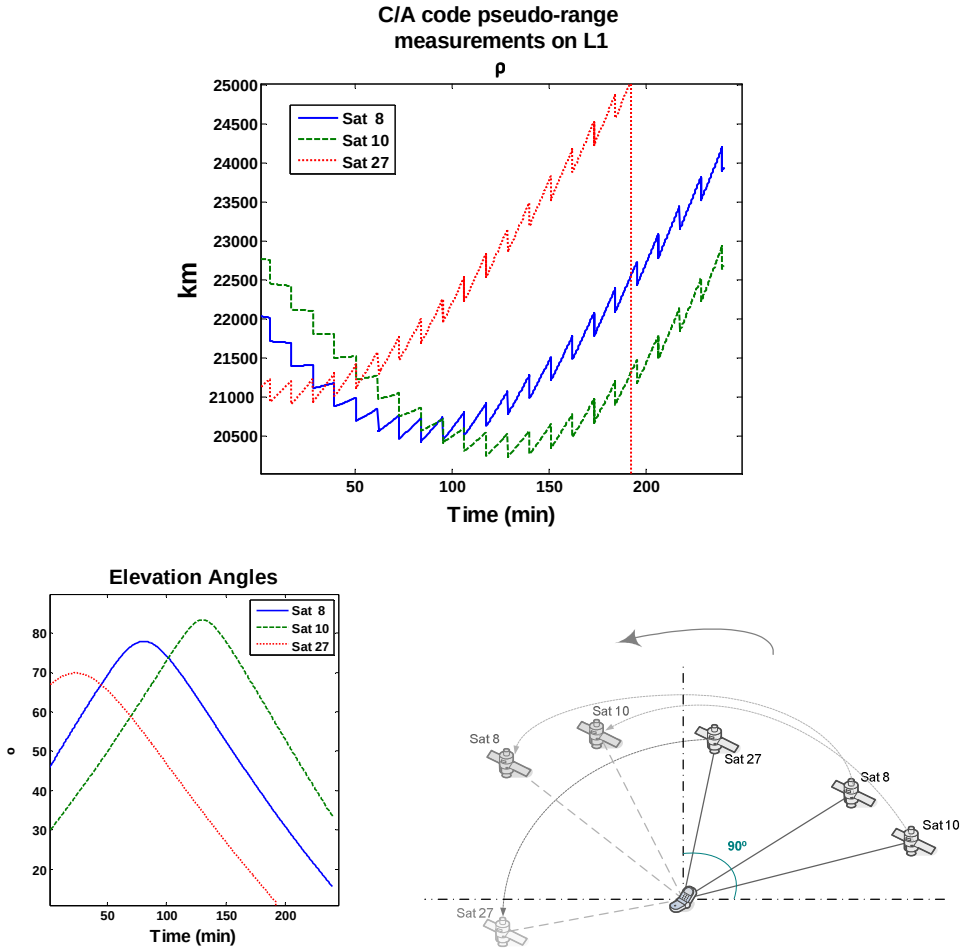


Figure 23 **Example of code measurements (pseudo-ranges) taken by a stationary receiver** that observed three satellites during a time period of 4 hours on July 19, 2007 from 9:00 to 13:00**.** Antenna's elevation angles are shown together with satellites' layout in the sky.

## 3.3 Carrier observations: Carrier phases

An individual code pseudo-range is obtained by tracking the "phase" of the received ranging code; a more precise measurement can be derived by tracing the phase of the carrier received from a satellite. Carrier centimetre-level wavelengths ($\lambda_{L1} \approx 19$ cm, $\lambda_{L2} \approx 24$ cm) are very short compared with codes chip lengths (specifically, C/A and P code chip lengths are about 300 and 30 m, respectively). Therefore, if resolutions might be considered between 1-2% of the wavelength, the phase of the received signal can be measured with precisions in the range of millimetres. This aspect implies an important advantage in comparison with the metre-level C/A code precisions.

In this section it will be shown that GPS carrier-phase measurements can also be defined as a function of satellite-to-user distances. Therefore, information about ranges to satellites can be extracted from these signals.

Firstly, as in the case of code pseudo-ranges, a theoretical and physical definition of GPS carrier phase measurements will be commented. Secondly, mathematical models are also described in order to develop an appropriate parameter schema that permits these carrier-based measurements to be properly processed.

### 3.3.1 Carrier beat phase measurements

An individual carrier phase measurement is defined as the difference between the phase of the reference sine wave generated within receiver and the phase of the reconstructed carrier after the ranging codes are removed from the gathered one (see section 3.1).

Actually, GPS receivers "difference" the Doppler shifted carrier arriving from satellite by the locally generated reference signal, this process results in a *carrier beat frequency* on which carrier phases are taken by periodic sampling. As mentioned by C. Rizos in [3.5], these raw phase measurements are generally the by-product of all GPS receivers

but they cannot be directly used as range observations since they are ambiguous. An analogy can be considered for better understanding, carrier phase might be thought as a tape measure than only has “millimetre” marks. You can keep track of the covered distance with this tape achieving the accuracy of one millimetre, as long as you monitor the tape measure continuously in order to keep track of the covered full centimetres, metres and even kilometres. Furthermore, if you want to know the absolute distance and keep track of it in an accurate way, you need to determine the initial unknown number of full kilometres between your GPS handset and the respective satellite, this quantity is known as *integer ambiguity* in GPS terms.

Consider the illustrative example shown in Figure 24 below, if the phase is taken as a fractional carrier wavelength, referred to as Fr(Φ), and a cycle or whole wavelength is approximately 19 cm in the case of L1, it is obvious that the most significant whole cycles to satellite are missed in each of these phase measurements.

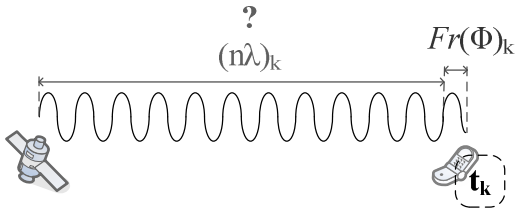


Figure 24 **Theoretical concept of a carrier beat phase measurement** at k-th epoch, $Fr(\Phi)_k$

An ideal case of “error-free measurement” is firstly considered. In the scenario shown above in Figure 24, satellite and receiver clocks are perfectly synchronized and no relative motion in between is affecting measurement processes. A *carrier beat phase measurement*, derived at any observation epoch $t_k$, would be therefore a fraction of a cycle (or a fraction of a wavelength Fr(Φ) when talking in metric units). Hence, the distance between the specific satellite and the receiver would be an unknown number of whole wavelengths $n\lambda$ plus the measured fractional wavelength $Fr(\Phi)_k$.

It is observed how the resultant carrier measurement Fr(Φ) contains no information regarding the number of whole satellite-to-user entire cycles *n*, i.e. the *integer ambiguity*. Therefore, the above mentioned carrier beat phase observation cannot be directly used as a *range* measurement because of the inherent unknown quantity *n*.

If relative motion between satellite and user is considered, the ambiguity term *n* might continuously change and hence, it would depend on both receiver channel tracking the satellite and time.

**Integrated carrier beat phase**

Actually, GPS equipments keep track of the elapsed full cycles as the carrier beat phase is sampled within (*phase-lock loops* capabilities). An *integrated carrier beat phase* observation is thus derived taking into consideration the measured partial wavelength Fr(Φ) and the counted number of full carrier wavelengths, elapsed since lock on. If the receiver or satellite in the above Figure 24 moves so that the distance between them grows by two wavelengths or cycles, the corresponding integrated carrier beat phase measurement would be the number of counted full cycles since the first measurement epoch (i.e. $Int(\Phi)_{0,k}=2$), plus the fractional measured cycle at that observation epoch $Fr(\Phi)_k$ . An illustrative example is shown in the following figure.

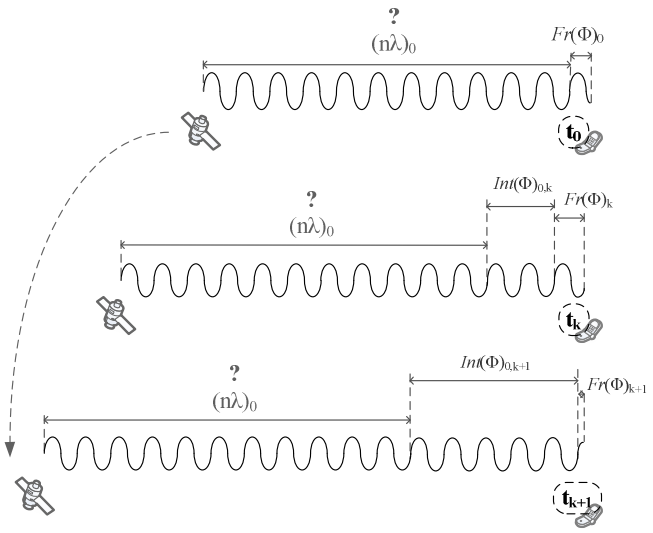


Figure 25 **Theoretical concept of the integrated carrier beat phase measurement**. GPS equipments measure carrier phases by taking into consideration the elapsed whole cycles between consecutive epochs plus the measured fractional cycle at each epoch of observation.

**Ranging with integrated carrier beat phase measurements**

As stated by C. Rizos in reference [3.5], a GPS carrier phase observation from a specific satellite can be defined at any measurement epoch $t_k$ as

(3.3-1) $\phi_k = Fr(\phi)_k + Int(\phi)_{0,k} + C_0$ in cycles

(3.3-2) $\Phi_k = \lambda\phi_k = Fr(\Phi)_k + \lambda Int(\phi)_{0,k} + \lambda C_0$ in units of length

where $Fr(\phi)_k$ is the fractional cycle[17] . The term $Int(\phi)_{0,k}$ corresponds to the current reading on a zero-crossing counter that only registers the number of whole cycles since lock-on. The cycle counter has an initial value of $C_0$ (usually zero). $Fr(\Phi)_k$ is the measured fractional cycle translated into metric units, i.e. the measured fractional wavelength. In this section, subscripts *k* identify the epoch of measurement.

The ideal relation between the measured phase and the satellite-to-user geometric distance (or *range*) at any epoch $t_k$ can be defined as

(3.3-3) $\frac{f_0}{c} Range_k = \phi_k + n_0$ in cycles

(3.3-4) $Range_k = \Phi_k + \lambda n_0$ in units of length

where $n_0$ is the number of unknown satellite-to-user entire cycles on the first observation epoch that is the *integer ambiguity term*. The geometric satellite-to-user range is scaled into units of cycles by $f_0/c$, where $f_0$ is the carrier frequency and *c* the speed of light in vacuum.

[17] In metric units, a whole cycle corresponds approximately to 19 cm ( L1 carrier) and 24 cm (L2 carrier)

If no loss of lock happened between observation epochs, the term $n_0$ on (3.3-3) and (3.3-4) remains fixed for a particular satellite-to-receiver ensemble of carrier measurements.

In order to convert the above measured phase into range measurement, the initial unknown number of satellite-to-user cycles $n_0$ has to be determined. Unlike the receiver clock error, time and algorithm complexity trade-offs are higher when trying to solve for this ambiguities. There are techniques focused on the resolution of these unknown quantities, all involve important challenges in terms of algorithm design and software implementation. The mathematical process for determining the value of the ambiguities is referred to as *ambiguity resolution* or *initialization*. According to Guy L. Thompson in reference [3.4], tremendous progress has been made in this environment during the last decades.

### 3.3.2 Carrier-phase observation equations

Let's have a look on a convenient mathematical model for the above mentioned carrier-phase measurements. In this section, observation equations for an individual GPS carrier-phase observation will be developed. The posed model is valid for measurements made on either L1 or L2 frequency.

In the absence of clock offsets and measurement errors, the "beat phase", formed as an observation within the GPS receiver, is defined as the difference between the phase of the local receiver oscillator and the phase of the gathered signal at the instant of observation *t*

$$\phi_b(t) = \phi_{lo}(t) - \phi_r(t) \qquad \text{in units of cycles} \tag{3.3-5}$$

where $\phi_b(t)$ is the carrier beat phase at reception time *t*, $\phi_{lo}(t)$ corresponds to the local receiver oscillator's phase at time *t* and $\phi_r(t)$ is the phase of the received signal from a certain satellite at time *t*.

Assuming constant running oscillator frequencies, the phase of the received signal at any instant can be related to the phase at satellite at the time of transmission in terms of the signal transit time τ (see Figure 26).

$$\phi_b(t) = \phi_{lo}(t) - \phi_r(t) = \phi_{lo}(t) - \phi_s(t-\tau) \tag{3.3-6}$$

*The carrier phase measurement is thus an indirect measurement of the signal transit time τ.*

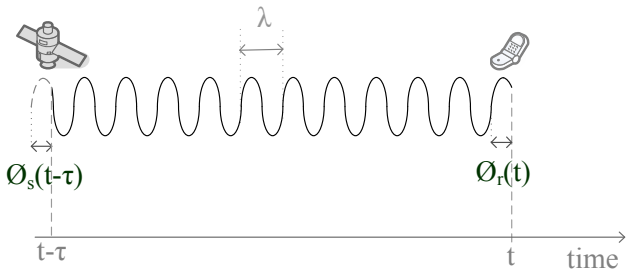


Figure 26 **Example of carrier-phases in satellite and receiver oscillators** assuming constant frequencies

In developing the observation equations it is useful to consider that every clock (essentially, an oscillator) can be compared with an "ideal" oscillator having a constant frequency $f_0$ in the reference time scale GPST. As time goes by, the phase of this oscillator $\theta(t)$ behaves in accordance with

$$\begin{aligned} \theta(t) &= \theta(t_0) + \int_{t_0}^{t} f(t)dt \\ \theta(t) &= \theta(t_0) + f_0(t - t_0) \end{aligned} \tag{3.3-7}$$

where $f(t)$ is the time-dependent frequency of the oscillator and $t_0$ corresponds to some arbitrary epoch. As mentioned before, in equation (3.3-7) the frequency of the ideal reference oscillator $f(t)$ has been assumed to be constant $f_0$.

As it was mentioned in sections before, clocks aboard GPS satellites and receivers are not perfect and the frequencies they generate are usually affected by slight variations. Therefore, the phase of a real GPS satellite or receiver oscillator obeys the relation

$$\text{(3.3-8)} \qquad \phi(t) = \theta(t) + f_0 b(t) \qquad \text{being} \qquad b(t) = \frac{1}{f_0}[\phi(t) - \theta(t)]$$

where $f_0 b(t)$ is the oscillator phase error $\phi(t) - \theta(t)$ - regarding to the phase of the "ideal" oscillator $\theta(t)$. The term $b(t)$ will be denoted as the *clock error*. The phase of the local clock within GPS receiver can thus be written as

$$\text{(3.3-9)} \quad \phi_{lo}(t) = \theta(t) + f_0 b_r(t)$$

where $f_0 b_r(t)$ is the clock phase error corresponding to the GPS receiver.

An expression relating phase and satellite clock phase error at transmission time, can be derived considering the equations stated above

$$\text{(3.3-10)} \quad \phi_s(t-\tau) = \theta(t-\tau) + f_0 b_s(t-\tau) = \theta(t) + f_0 b_s(t-\tau) - f_0 \tau$$
$$\text{where} \quad \theta(t-\tau) = \theta(t) + f_0[(t-\tau) - t]$$

The clock phase error attributable to the oscillator on board a GPS satellite corresponds to the term $f_0 b_s(t)$ .

Replacing the above equations into the carrier beat phase measurement general expression stated in (3.3-6), the following equation is achieved

$$\text{(3.3-11)} \quad \phi_b(t) = \overbrace{\theta(t) + f_0 b_r(t)}^{\phi_{lo}(t)} - \overbrace{[\theta(t) + f_0 b_s(t-\tau) - f_0 \tau]}^{\phi_s(t-\tau)}$$
$$\phi_b(t) = f_0 \tau + f_0[b_r(t) - b_s(t-\tau)]$$

The oscillator frequency can also be defined in terms of its wavelength $\lambda$ as $f_0 = c/\lambda$, where the term $c$ corresponds to the speed of light in vacuum.

As it was commented in the case of pseudo-range measurements, the transit time term $f_0\tau$ consists of two components. The main one corresponds to the time it took the signal to travel from satellite to receiver describing a straight-line path (that is, covering the real geometric range between the satellite's location at transmission time and the receiver's position at reception time). The second component accounts for the lag in signal path caused by atmosphere effects; these generate refractions and dispersions that change the velocity (speed and direction) at which GPS signals travel. Those phenomena are modelled as *time delays, phase delays* or as an increase in the covered distance and considered in the observation equations as several *phase correction terms* grouped on the factor $\phi_{atm}$. The signal transit time component is therefore expressed as

$$f_0\tau = \frac{f_0}{c} Range(t, t-\tau) + \phi_{atm}(t) \qquad (3.3\text{-}12)$$

Where *Range(t,t-τ)* corresponds to the geometric distance between the receiver position at time $t$ and the satellite location at $t$-$\tau$. The term $\phi_{atm}$ can be broken down into components for the different parts of the atmospheric delay, through the ionosphere and troposphere.

Combining the equation (3.3-12) and the model (3.3-11), the ***observation equation for an individual carrier-phase measurement*** is derived as

$$\phi_b(t) = \frac{f_0}{c} Range(t, t-\tau) + f_0[b_r(t) - b_s(t-\tau)] + \phi_{atm}(t) \quad \text{in cycles} \qquad (3.3\text{-}13)$$

$$\Phi_b(t) = Range(t, t-\tau) + c[b_r(t) - b_s(t-\tau)] + \lambda\phi_{atm}(t) \quad \text{in metric units} \qquad (3.3\text{-}14)$$

where $\lambda$ is the wavelength of the respective carrier ($\lambda = c/f_0$).

**Measured carrier-phases**

The measured carrier-phases obtained within the GPS receiver slightly differ from the above posed observation model (3.3-13) or (3.3-14) in several aspects.

*First of all*, random noise generated within the GPS receiver processes might affect the measurements. Additionally, multipath signals reaching the receiver's antennas might also cause interferences. As in the case of pseudo-range measurements, a term is added to take account of these errors $\phi_{noise}$.

*Secondly*, the real derived phase measurement is the *integrated carrier beat phase* that depends not only on the fractional part of the measured carrier phase, but also on the integral part coming from the counter registering the number of elapsed cycles since lock-on. That is, all the whole missing satellite-to-user cycles (or wavelengths) since lock on need to be considered on the observation equation. This quantity is unique for a particular satellite-receiver pair and remains constant as long as the receiver keeps on tracking and counting the elapsed cycles from the time the satellite signal was first acquired. The parameter *N* will be added to consider this effect.

*Thirdly*, tracking the correct number of full cycles on which satellite-to-user distance is changing is very critical. This magnitude will be miscalculated if a cycle is missed or an extra cycle is added when, for example, the receiver fails to track the signal from a satellite at any time. In this situation, the integer ambiguity term *N* might not remain fixed between these observation epochs. In GPS terminology, this phenomenon is referred to as "***cycle slip***", which is like missing the centimetre or metre marks while you are concentrating on reading the millimetre ticks. Cycle slips can cause large errors, most GPS systems are thus able to detect and repair them.

*Finally*, as in the case of pseudo-range measurements, atmosphere effects will be modelled separately into ionosphere and troposphere terms. Ionosphere is a dispersive medium, that is, the carrier and its modulating signal (i.e. the code and navigation

message) propagate at different speeds through this atmosphere layer. In fact, the code phase is delayed (i.e. is measured larger than it is in reality) and the carrier phase is advanced *by the same amount* (i.e. is measured shorter). Therefore, in the case of carrier measurements, the ionosphere term on the observation equation has negative sign. Troposphere effects on carrier phases are analogous to the case of code measurements.

On the final measurement model, cycle slips will not be considered because they are usually detected previously in independent processes. Hence, dropping references to the measurement epoch, the ***mathematical model for the measured carrier phase*** is

$$\text{(3.3-15)}\quad \phi = \frac{f_0}{c} Range + f_0\left(b_r - b_s\right) + \phi_{atm} + \phi_{noise} + N \qquad \text{in cycles}$$

$$\text{(3.3-16)}\quad \Phi = Range + c\left(b_r - b_s\right) + \Phi_{atm} + \Phi_{noise} + \lambda N \qquad \text{in metres}$$

Considering ionosphere and troposphere effect separately

$$\textbf{(3.3-17)}\quad \Phi = Range + c\left(b_r - b_s\right) - I + T + \Phi_{noise} + \lambda N$$

This mathematical development has been obtained from references [3.1] [3.2] and [3.5]. As it was mentioned before, constant running oscillator frequency is assumed in these studies, that implies equal phases in satellite oscillator and receiver oscillator at the time of arrival. If differences in the initial phases of the receiver and satellite clocks are taken into consideration, a new term must be added on the equations above.

The atmosphere and noise terms depend on the receiver, satellites layout and epoch (day or night). However, these effects vary slowly between consecutive observation epochs. Thus, the change with time in observed carrier phases is equal to the change in satellite-to-user geometric range, receiver and satellite clock errors, atmosphere effects and measurement noise and signal multipath. The change in carrier phase measurement over a time interval is referred to as integrated Doppler or *delta pseudo-range*.

In the following section, an example of the carrier-phase measurements used in these studies is shown. Figure 27 shows carrier-phase measurements obtained from the studies previously introduced in Figure 23. Observations have been collected on July 19 2007 during 4 hours (9:00 – 13:00) by the same permanent GPS station located on *E.T.S.I of Topography, Geodesy and Cartography* in *Polytechnic University* of Madrid.

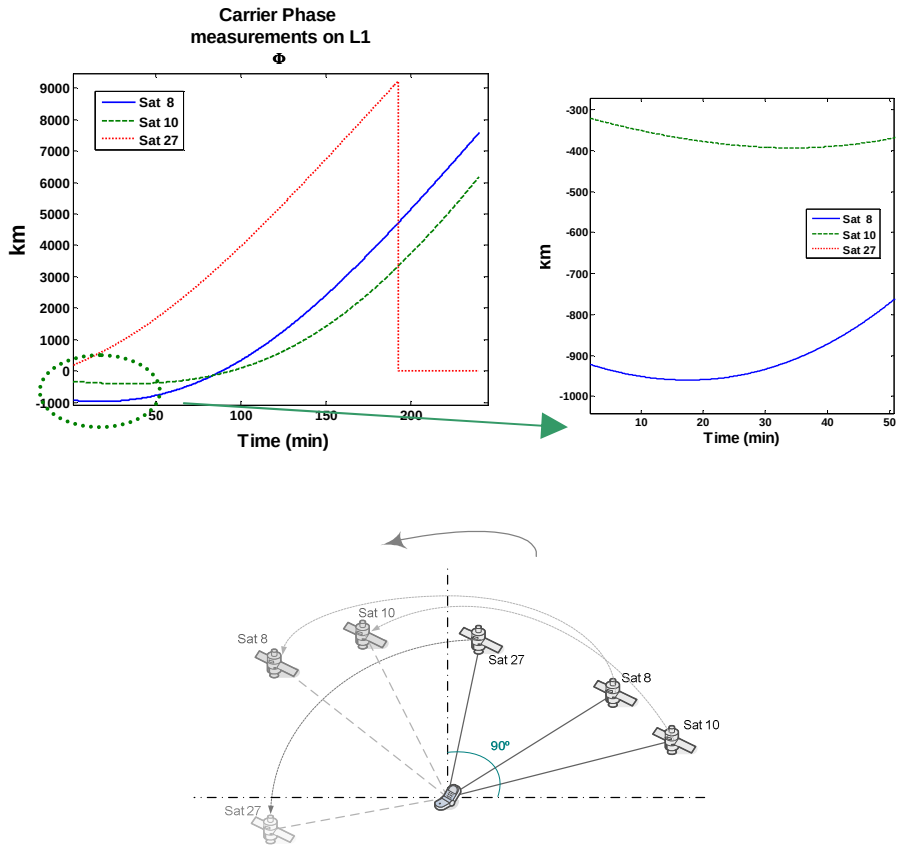


Figure 27 **Example of carrier-phase measurements taken by a stationary receiver** that observed three satellites during a time period of 4 hours on July 19, 2007 from 9:00 to 13:00. Unlike code pseudo-ranges, carrier phases are not affected by receiver clock readjustments discontinuities.

It is worth highlighting that unlike code-based measurements carrier-phases are not affected by receiver clock readjustments (i.e. the discontinuities affecting pseudo-ranges in Figure 23). Anyway, large ambiguities are corrupting these carrier measurements (almost the whole satellite-to-user distances ≈ 21000 km). In the next section, it will be shown that the change over time in carrier phases reflects the trace of satellite-to-user ranges in a more reliable way than the change over time in pseudo-ranges. The negative sign of some carrier-phases is due to the fact that these are measured regarding to the

local oscillator located at receiver site, that is, the received carrier-phase can be "advanced" or "delayed" with respect to the phase of the reference oscillator.

### 3.3.3 Carrier-phase time variations: Delta pseudo-ranges

The carrier-phase observation model (3.3-17) appears similar to the one of the pseudo-range measurements based on code tracking (3.2-8). Both the code and carrier phase measurements are corrupted by the same error sources (measurement noise, atmosphere effects, clock errors), but there is an important difference. Code tracking provides essentially unambiguous pseudo-ranges (though coarse). The carrier phase measurements are however extremely precise, but encumbered with integer ambiguities (as shown previously in Figure 27).

One way to get at least a partial benefit of the precise carrier phases, without being degraded by the integer ambiguities, is via *delta pseudo-ranges* obtained from the change in the carrier phase measurement over a time interval. These delta pseudo-ranges are derived by differencing carrier-phase measurements between consecutive epochs (i.e. computing time differences). In that way, if the carrier is tracked continuously between epochs, the integer ambiguity term is cancelled.

Delta pseudo-ranges between time instants $t_{k-1}$ and $t_k$ can be defined as the following time differences

$$\Delta\phi_{k-1,k} = \phi(t_k) - \phi(t_{k-1}) \approx \frac{Range_k - Range_{k-1}}{\lambda} + \tilde{\phi}_{noise} \quad \text{in cycles} \tag{3.3-18}$$

$$\Delta\Phi_{k-1,k} = \Phi(t_k) - \Phi(t_{k-1}) \approx Range_k - Range_{k-1} + \tilde{\Phi}_{noise} \quad \text{in metric units} \tag{3.3-19}$$

The error in the above measurement type is related to the rates of change in the offsets of the satellite and receiver clocks, and the rates of change in the atmosphere effects.

Furthermore, the millimetre-level resolution on carrier-phases implies a lower measurement noise, in comparison with achievable metre-level pseudo-ranges resolution.

An experimental example derived while performing these studies is shown in this section. The data analysis was carried out considering an ensemble of observations taken by the previously quoted stationary GPS station. The observation interval on which measurements were collected was shorter (9:00– 10:00) in order to speed up the period of computation and reading from RINEX files. Measurements were taken from one monitored satellite that stayed in view during the whole observation interval. This satellite set and, therefore, the respective pseudo-ranges increased. Code and carrier observables (i.e. pseudoranges and carrier-phases) are shown in the following figure.

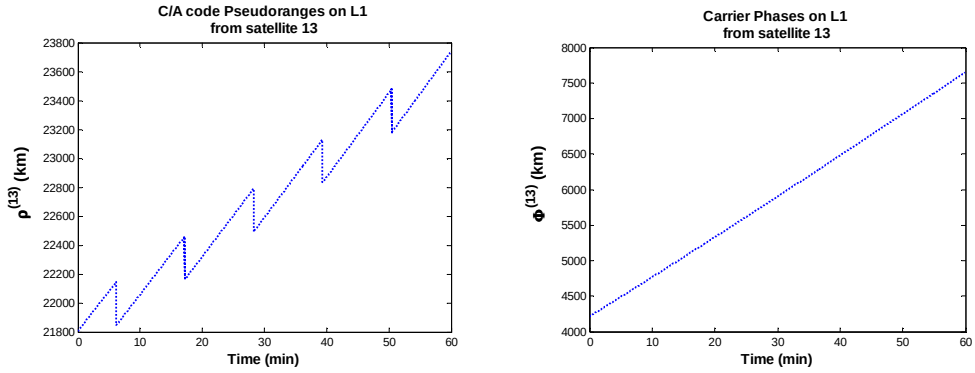


Figure 28 **Example of code and carrier measurements from a descending satellite**, collected during one hour of observations (9:00– 10:00 on July 19 2007)

The time variations of the above illustrated measurements were evaluated by computing differences between epochs of observations. The resultant inherent measurement noise is considerable lower on carrier-based time differences (see the following Figure 29). Specifically, code-based time differences, denoted by $\Delta\rho$, are affected not only by higher noise levels but also by clock readjustments. Nevertheless, time differences derived from carrier-phases (i.e. delta pseudo-ranges, denoted by $\Delta\Phi$) describe a finer trace of the time variations in pseudo-ranges since they are not affected by clock readjustments and, furthermore, they exhibit lower levels of measurement noise.

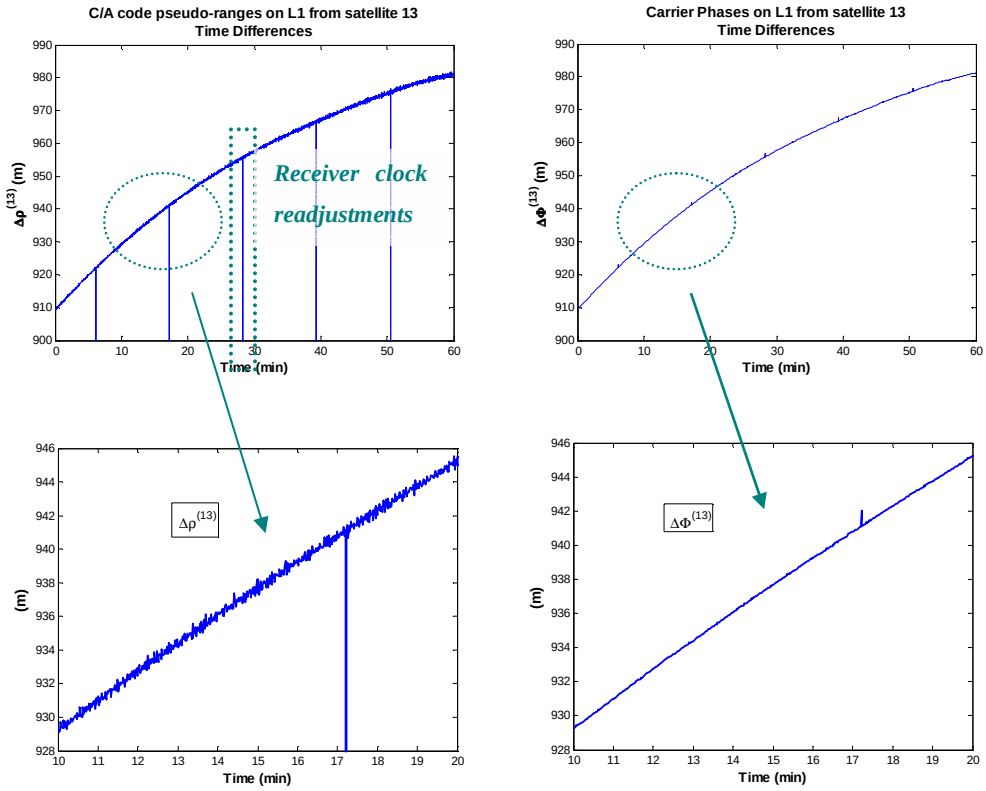


Figure 29 **Comparison between code pseudo-ranges (ρ) and carrier-phases (Φ) in terms of changes over time**, differences between adjacent time-instants have been computed as $\Delta\rho = \rho(t_{k+1}) - \rho(t_k)$ and $\Delta\Phi = \Phi(t_{k+1}) - \Phi(t_k)$.

On these studies, the files that contained the processed GPS data also included a rough approximation of where the stationary GPS station that gathers the measurements is located. This position was used to show more realistic outcomes. In that way, traces to theoretical ranges were roughly assessed with the aid of the satellites positions derived from the broadcast navigation parameters. In the following figures, the resultant theoretical ranges, referred to as *R*, are compared with the measured pseudo-ranges and carrier phases as well as their time differences (denoted by ρ, Φ, Δρ and ΔΦ, respectively). It can be observed how code-based measurements are much noisier than carrier-based ones.

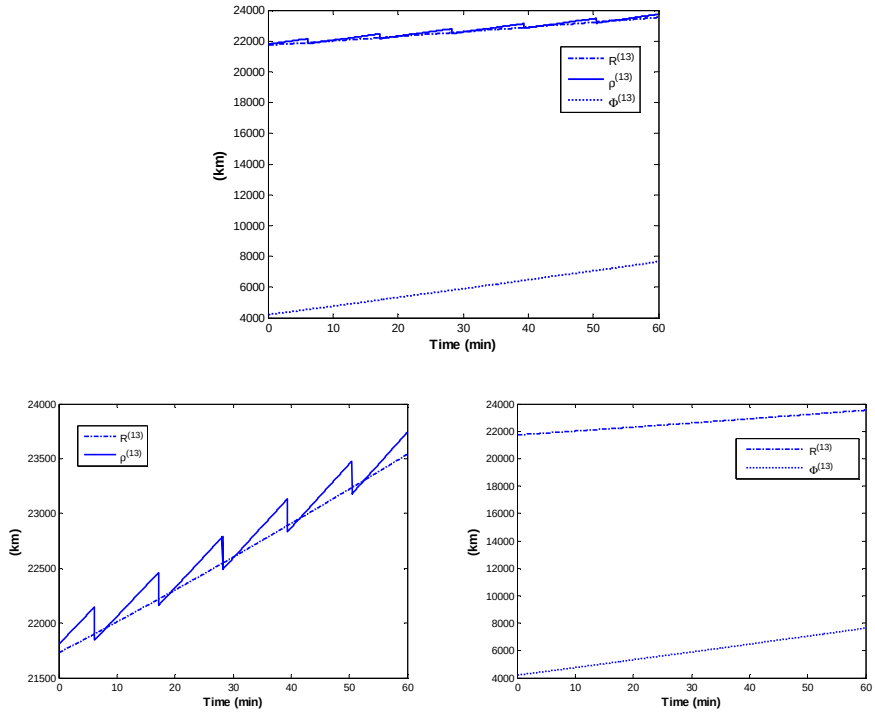


Figure 30 **Example of the theoretical ranges to satellites (R)** compared with measured pseudo-ranges (ρ) and carrier-phase measurements (Φ).

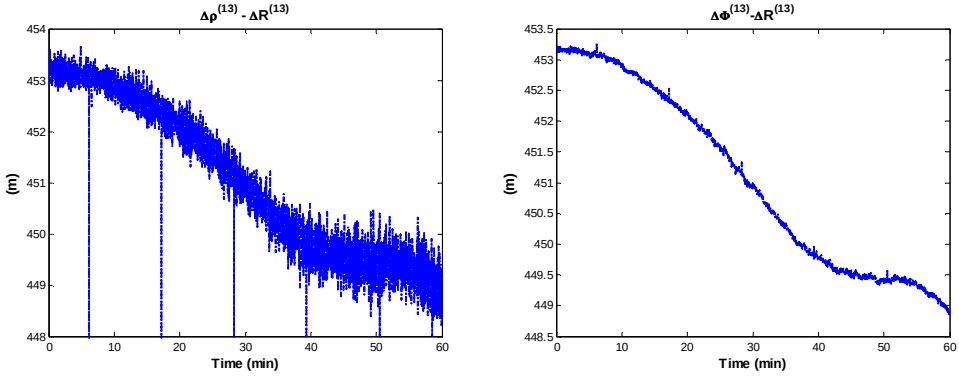


Figure 31 **Example of the time variations in the theoretical ranges to satellites (ΔR)** compared with the ones of measured pseudo-ranges (Δρ) and carrier-phase measurements (ΔΦ).

Differenced measurements like *delta pseudo-ranges* $\Delta\Phi$ are usually processed on GPS equipments, these approaches are applied in order to handle some of the effects caused by errors degrading the derived GPS measurements (such as clock deviations from general GPS time frame or cycle ambiguities). For example, as it was mentioned before, the observation dependent ambiguity in carrier-phase measurements is assumed to remain constant for an extended period of uninterrupted tracking. The effect of this error can thus be eliminated by differencing between consecutive epochs (as shown in figures above), avoiding then the cycle ambiguity estimation. Nevertheless, cycle ambiguities can also be explicitly estimated to apply the proper corrections on GPS carrier measurements, in that way, measurement differentiation will not be necessary. These "non-differenced schemes" imply time penalties and algorithms complexities that might not be interesting in terms of conventional real-time GPS positioning.

The effect of computing differences on GPS measurements will be explained in more detail in chapter 4.

## 3.4 GPS Observation Model Errors

Errors degrading code and carrier-based measurements are often categorized as ***noise*** or ***bias*** according to their rate of change over time.

*Noise* generally refers to quickly varying phenomena that average out to zero over a 'short' time interval, where short is defined in relation to the tracking loops within receiver equipments. A *bias* tends to persist over a period of time. Measurement biases in GPS are referred to as those influences on the observations that cause the measured satellite-to-user distance (or "range") to be different from the true distance by a *systematic amount*[18].

For example, the errors associated with the satellites and receiver clocks are regular enough to be characterized as bias terms. Propagation errors can be highly variable depending upon the user location, satellite elevation angle, and state of the medium. However, if the GPS receiver remains fixed or moves slowly, these effects change slowly and might also be thought as biases, except for atmosphere scintillations. Hence, bias is considered as a time correlated effect (low frequency component) and noise as a time uncorrelated effect (high frequency component).

It is worth pointing out that the dominant biases in GPS are those due to the receiver equipment and satellite clocks deviations regarding to general GPS time scale (GPST). Furthermore, both affect the respective measurements by the same amount.

In this section, the most important sources of errors affecting GPS measurement are mentioned describing the principal characteristics and effects on positioning accuracy.

[18] *Systematic errors* are biases in measurements which lead to measured values being "systematically" too high or too low.

### 3.4.1 Satellite Errors

Satellite errors are caused by errors in the satellite position and clock parameters as specified in the 50-bits/s navigation message broadcast by each satellite. These inaccuracies are common on both code- and carrier-based measurements. In fact, the most important one is that due to the purposeful *"dithering"*[19] of the satellite clock frequency under the policy of *Selective Availability (SA)*[20] . Such scheme introduces deviations in the timing marks on the broadcast signals which can be taken out only by authorized users. The size of this error can apparently be raised or lowered by the U.S. Government. According to reference [3.6], this error remains stable at about 80 ns rms (root-mean-square), or 24 m rms. President George Bush recently accepted the recommendation of the DoD to end procurement of GPS satellites that have the capability to intentionally degrade the accuracy of civil signals by means of SA (October 2007). This policy, thus, will no longer be present in GPS III satellites.

Prediction of the satellite ephemeris is processed on the basis of orbits fitted to the tracking data obtained over several preceding days. The net effect of the error caused by these parameters on a pseudo-range measurement can easily be considered to be the projection of the satellite position error vector on the satellite-to-user line of sight. According to reference [3.6], experimental results have shown this error to be as large as 10 m. Schemes to reduce the ephemeris errors are focused on improvements in satellite tracking and prediction algorithms.

[19] *Dithering* consists of the addition of noise into the satellite clock used to derive broadcast GPS signals in order to degrade position accuracy for civil users.

[20] *Selective Availability (SA)* is a policy adopted by the DoD of USA to introduce some intentional clock noise into the GPS satellite signals thereby degrading their accuracy for civilian users.

### 3.4.2 Signal Propagation Errors: Ionosphere and troposphere

As mentioned before, all but the final 5% of the signal travel can be regarded as in a vacuum or free space, through which the radio waves broadcast by GPS satellites propagate at a constant speed (c ≈ 299792458 m/s). In fact, the propagation medium changes the velocity of signals (speed and direction) causing uncertainties in the measurements of satellite-to-user distances. These effects have a variation dependent upon the state of the medium.

Close to the surface of the earth, at a height of about 1000 km, the signals enter an atmosphere of charged particles, called the ionosphere**.** *In the case of GPS signals, the ionosphere acts as a refractive and dispersive medium.* As a result, the carrier and its modulating signal (i.e. the code and navigation message) propagate at different speeds through this atmosphere layer. In fact, the code phase is delayed (i.e. *group delay*) while the carrier phase is advanced (i.e. *phase advance*) by the same amount. This implies that code measurements are measured longer and carrier-based observables are measured shorter than they are in reality.

The physical characteristics of the ionosphere depend upon the solar activity; hence they change widely between day and night, even from day to day. Additionally, phase delays vary as the physical path of the crossing signal changes due to satellite motion and dynamics of the atmosphere itself. In fact, the zenith path delay can vary from about 1 m at night to 5-15 m in the mid-afternoon (according to reference [3.6]). The delay can be larger at low elevation angles, because signal traverses a larger ionosphere path.

Dual frequency (L1-L2) GPS receivers can estimate ionosphere group delays and phase advances. Receivers limited to L1-only measurements have recourse to an ionosphere model whose parameters are broadcast by the satellites. According to reference [3.6], this model reduces the errors due to uncompensated ionosphere delays by about 50% on average. In reference [3.6], it is mentioned that, at mid-latitudes, the remaining error can be up to 10 m during the day.

After crossing the ionosphere, at a height of about 40 km, the signals encounter a layer composed of dry gases and water vapour. This electrically neutral gaseous atmosphere is called the *troposphere* and acts as a refractive medium in terms of GPS radio waves. Hence, the propagation velocity is once again modified.

Unlike the ionosphere, the troposphere is "nondispersive" for the GPS frequencies, therefore the path delay is the same for both code and carrier measurements at L1 and L2 frequencies. This effect depends on the refractive index of the air mass along the path of the signal. As mentioned in reference [3.2], this error is about 2.5 m in the zenith direction and 10-15 m for satellites at low elevation angles. Troposphere delay cannot be estimated directly from the GPS measurements and the receiver has to apply mathematical models with accuracies decreasing at low elevation angles.

### 3.4.3 Receiver Measurement Errors and Multipath

Measurement errors due to receiver noise depend on signal strength characterized as carrier-to-noise spectral density ratio. According to reference [3.2], this error is below 1 m rms for code measurements, and about 2 mm for carrier phase measurements.

GPS broadcast signals can be reflected from structures in the vicinity of the receiver's antenna, or from the ground. Hence, receiver gathers not only the line-of-sight signal but also one or more of its reflections. This interference phenomenon is named as *multipath* and depends upon the environment, antenna placement, and antenna design. As mentioned in [3.2], multipath errors can be reduced in previous signal processing steps; in fact, receiver manufacturers have developed and implemented proprietary techniques. Typical *multipath* error in pseudo-range measurements can range from 1 m in a benign environment to more than 5 m in highly reflective environments. The corresponding errors in the carrier measurements are typically two orders of magnitude smaller.

*Satellites layout in the sky* affects measurements qualities. For example, both atmosphere and multipath errors are magnified when satellites are at low elevation angles. As a result, observables from high satellites are more reliable than low ones. Figure 32 illustrates an example of this fact. Graphics show the time change in pseudo-range measurements gathered from two observed satellites. Data was gathered in the afternoon July 19, 2007 at a rate of 1 Hz during the 18:00-18:06 time period. Both satellites were visible the whole observation interval. One of them was placed low in the sky with elevation angles ranging from 70 to 80 degrees; in contrast, the other satellite was monitored at lower elevation angles that do not exceeded 20 degrees. It can be observed how "time differenced" pseudo-ranges from the satellite placed at lower elevation angles are affected by higher noise levels.

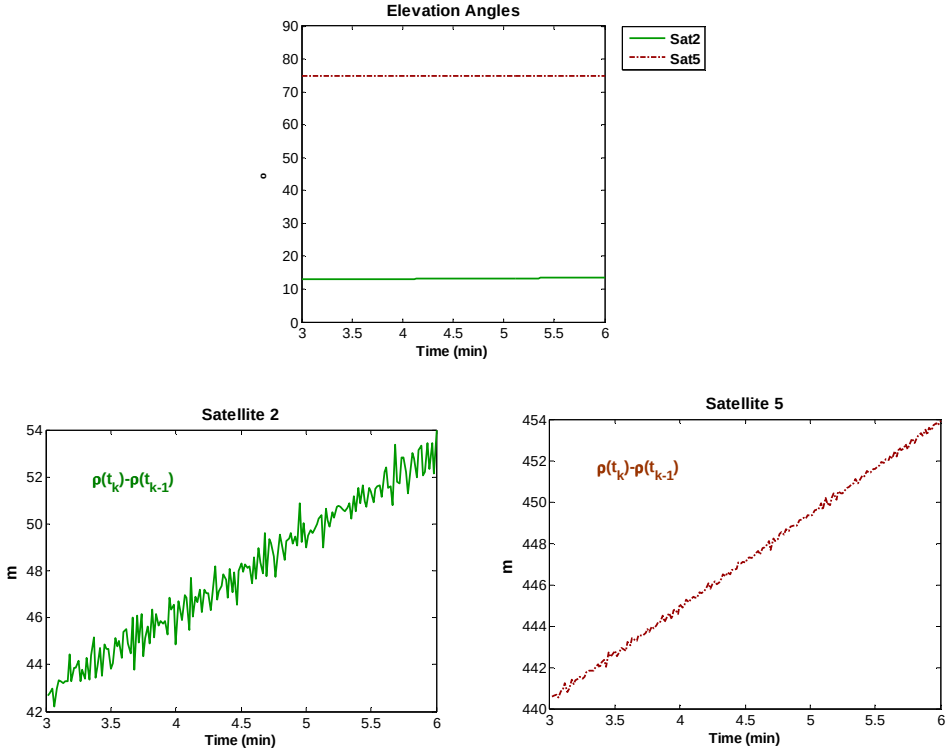


Figure 32 **Example of GPS measurements taken from high and low satellites.** The satellites were observed on July 19, 2007 during 6 minutes (18:00-18:06). Satellite 2 was located at low elevation angles that do not exceeded 20 degrees; in contrast, satellite 5 was placed at higher positions in the sky with elevation angles ranging from 70 to 80 degrees. Between-epoch differences computed on measured pseudo-ranges (i.e. changes with time) are shown in the graphics above, it is noticed that measurements from satellite 2 are affected by higher noise levels.

If measurements from low satellites can be excluded as a precaution, the impact of these errors on the position estimates could be reduced. However, this is not always practical because the GPS receiver may not have the luxury to drop measurements. According to reference [3.6], elevation cut-off of 5º-7.5º appears to offer a good trade-off between the loss of measurements and potential for large errors. The studies performed on this work were all based on measurements taken from satellites with elevation angles beyond 10º (see Figure 32).

# Chapter 4

# Combining GPS Measurements

*"Two types of measurements can be obtained from the GPS Navstar Satellites (…). Code tracking measurements are normally referred to as pseudorange measurements (…). The relative phase between the received, reconstructed carrier phase and the receiver clock phase at a particular epoch may be measured. This is like a very fine and precise measurement of pseudorange but with all the most significant (whole cycles) missing (…) more economical processing of the measurements can be obtained via a simple combination procedure prior to their inclusion in the position solution equations (…)"*

Ron Hatch – 'The Synergism of GPS Code and Carrier Measurements', 1982

The information redundancy provided by the diverse types of GPS measurements, such as pseudo-ranges and carrier phases, offers an exceptional opportunity to improve accuracy of position estimates. Conventional GPS equipments use C/A code pseudo-ranges to compute the navigation solution (i.e. position, velocity and time). These code measurements are affected by errors due to satellite and receiver clocks, ephemeris parameters and atmosphere effects just like the measured carrier phases. However, the error due to multipath and receiver noise in the carrier observables, at centimetre level, is about one-hundredth of that in the pseudo-ranges. But there is an important drawback: ambiguities affecting carrier measurements involve extra complications while computing the navigation solution.

These studies were aimed at examining the benefits of combining the above noisy and unambiguous code measurements with the precise but ambiguous carrier phases for absolute positioning in a single-frequency receiver. In this chapter, different approaches that allow the integration of these measurements in order to achieve better position accuracies are developed theoretically. The resultant test results are shown in chapter 5.

## 4.1 Carrier smoothing code pseudo-ranges (CSC algorithms)

Firsts attempts to combine GPS code and carrier measurements were posed at the beginning of the nineteen eighties with the name of *carrier-aided smoothing code (CSC) algorithms*.

The term "*smoothing*" implies the suppression or, at least, reduction of high frequency noise components inherent in signals that contain certain desired information. In GPS terminology, the information about satellite-to-user distances embedded in the noisy pseudo-ranges is essential to allocate the receiver equipment; therefore, efforts to reduce pseudo-range noise levels, that make difficult the identification of this range information, are the main goal in the design of CSC algorithms (see Figure 33). In that way, the preciser or finer carrier-phases are used to filter or "smooth" out the noise on code pseudo-ranges.

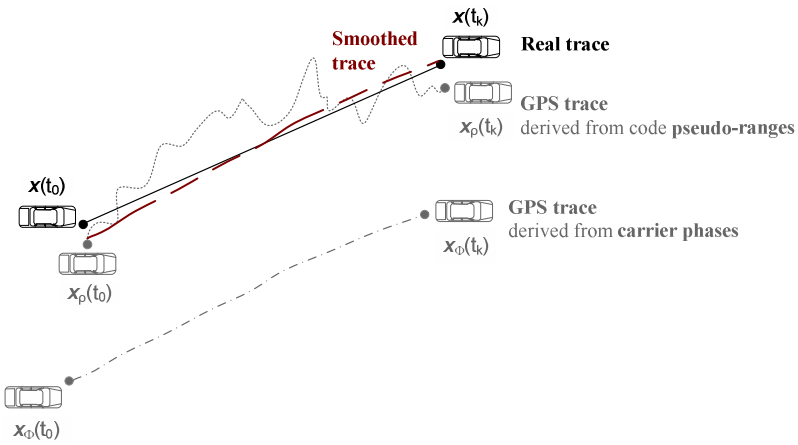


Figure 33 **Illustrative example of smoothing in GPS positioning**. Positions derived from pseudo-ranges are "noisier" than the ones obtained from carrier-phases. However, carrier-based outcomes contain an inherent ambiguity that must be solved to yield absolute positioning (the sketch does not fit the reality). If both sources of information are combined, a "cleaner" or "smoothed" trace of positions can be obtained.

Basically, a phase smoothing filter might start with raw pseudo-range measurements to establish an absolute position. Progressively, higher weights will be placed on the derived carrier phase information and less on the raw pseudo-range based data to

provide a smoothed pseudo-range output. Such a technique was firstly described in a paper by Ronald R. Hatch, entitled "*The synergism of GPS code and carrier measurements*" [4.1].

### 4.1.1 Evolution of CSC Algorithms

In 1982, Ron Hatch posed one of the first proposals to perform carrier-smoothing-code pseudo-ranges algorithms [4.1]. In fact, some of these techniques were later named as *Hatch filters*.

As P. Cheng mentioned in [4.10], Hatch himself posed improvements four years later (1986) that applied epoch-dependent smoothing weight factors [4.2].

Variants of Hatch's algorithms were developed by Lachapelle in 1986 [4.6] on which the smoothing weight factors were reduced by a constant from epoch to epoch. Similar proposals were also released by Meyerhoff and Evans in 1986 [4.7].

During the next decade, innovative designs were analyzed by Hofmann-Wellenhof (1997) [4.3], [4.4]. In fact, an implicit smoothing scheme of code pseudo-ranges with carrier observations was used in a DGPS differential correction model by Jin (1996) [4.5].

### 4.1.2 CSC Domains: range and position.

Two domains of carrier phase smoothing schemes have been analyzed since the first Hatch's investigations were performed in 1982. These are referred to as *range* and *position domain algorithms*.

*Range domain (RD)* algorithms place the combination of code and carrier measurements before the computation of the navigation solution, that is, pseudo-ranges are *directly*

*filtered* with the aid of carrier-phases in order to smooth out inherent noise affecting the code-based measurements; a 'smoothed pseudo-range profile' is then output and processed subsequently in order to estimate the receiver's position. *Position domain (PD) CSC* algorithms are, however, performed within the process that estimates the receiver's position; in that way, both pseudo-ranges and carrier-phases are processed while computing the navigation solution. The following figure shows these two CSC domain variants. In both approaches, carrier-phases are previously differenced in time in order to process the resultant differenced measurements (denoted by $\Delta\Phi$).

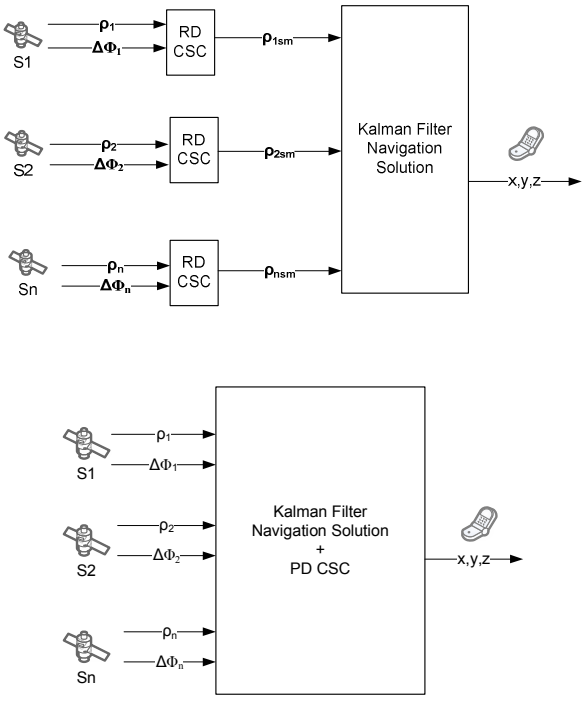


Figure 34 **Domains to perform carrier-phases smoothing code pseudo-ranges:** Range (RD) and Position (PD) domains.

Smoothing schemes posed by Ronald R. Hatch are good examples of range domain CSC algorithms. They involve the use of a group of parallel filters (one for each visible satellite – see Figure 34) in order to smooth out the noise on code pseudo-ranges with the aid of 'time-differenced' carrier-phases. Compared with other types of precise

differential positioning[21], these procedures do not require the specification of a dynamic model; furthermore, corrections from a second reference GPS station are not necessary. Using this type of filters within a single-frequency receiver, the noise affecting pseudo-range measurements is considerably reduced; test results shown this fact and will be commented in section 5.2.2 (in fact, the noise is reduced more than 1 metre in some experiments).

Ideally, it would appear to make sense to apply as much carrier-smoothing as possible in order to eliminate the inherent noise. Unfortunately, some references such as [3.3][3.6][3.8][3.9] mention that enlarged smoothing intervals can have negative effects on the GPS receiver performance, because of the cumulative effect of ionosphere delay – this fact was verified in the performed experiments and will be explained in 4.2.1. To achieve a more effective and efficient use of Hatch's algorithms, the rate of ionosphere delay and noise characteristics should be known. However, since these effects are usually unknown to a single-frequency user, the above quoted references pose the use of a conservative constant carrier smoothing time (the cost of considering this option is a efficiency reduction in the smoothing approach).

After the introduction of Ron Hatch algorithms, several position-domain (PD) schemes were also posed. According to H.K. Lee and C. Rizos [4.8], the most representative examples are referred to as the complementary filter designed by Hwang and Brown [4.11] and the phase-connected filter posed by Bisnath and Langley in [4.12]. These algorithms exhibit less sensitivity to changes in the visible satellite constellation in comparison to the above RD schemes. Otherwise RD filtering is, in general, more susceptible to information losses than PD filtering if signal lock of a channel is lost, even for short periods of time.

The present study was focused on implementations of both RD and PD schemes. Specifically, the Hatch filter algorithm has been implemented as an example of RD CSC schemes. This algorithm is theoretically introduced in the next section and test

[21] *Precise Differential Positioning* - Precise measurement of the relative positions of two receivers tracking the same GPS signals.

results are shown in chapter 5. In the case of PD CSC schemes, a modified position/velocity Kalman filter has been implemented. This approach was posed by Thomas Ford in the article [4.14].

In the following sections, the theory that allows computing these RD and PD CSC schemes is developed. Test results are shown next in chapter 5.

## 4.2 Range Domain CSC

In this section, the mathematical background of a conventional method used to combine single-frequency GPS code pseudo-ranges and carrier-phases will be introduced.

So far, carrier-phase measurements have been represented in both cycles and metric units. When combining code and carrier measurements it is more convenient to represent carrier phases in units of length, like the code pseudo-ranges. Therefore, considering the measurement models previously stated in equations (3.3-17) and (3.2-8), and individual carrier-phase and pseudo-range measurement taken from a certain satellite *j* will be defined as

$$\begin{aligned}\Phi^{(j)}(t_k) &= \lambda\phi^{(j)}(t_k) \\ &= Range^{(j)}(t_k) + c\left[b_r(t_k) - b_s{}^{(j)}(t_k)\right] - I^{(j)}(t_k) + T^{(j)}(t_k) + \Phi^{(j)}_{noise}(t_k) + \lambda N^{(j)}(t_k)\end{aligned} \tag{4.2-1}$$

$$\rho^{(j)}(t_k) = Range^{(j)}(t_k) + c\left[b_r(t_k) - b_s{}^{(j)}(t_k)\right] + I^{(j)}(t_k) + T^{(j)}(t_k) + \rho^{(j)}_{noise}(t_k) \tag{4.2-2}$$

where $\phi(t_k)$ corresponds to the measured carrier phase (in cycles) at any observation epoch $t_k$ and $\rho(t_k)$ is the code pseudo-range measurement obtained at the same observation epoch. The above carrier phase measurement is mapped into units of length just by multiplying by the respective wavelength λ.

Considering that both code- and carrier-based measurements are gathered from the same satellite, references to satellites will be dropped in order to simplify the following mathematical expressions. Subscripts will be used to denote the epoch at which measurements were taken. Consequently, the above mathematical models (4.2-1) and (4.2-2) will be stated as

$$\Phi_k = Range_k + c\left(b_{r_k} - b_{s_k}\right) - I_k + T_k + \Phi_{noise\,k} + \lambda N_k \quad (4.2\text{-}3)$$

$$\rho_k = Range_k + c\left(b_{r_k} - b_{s_k}\right) + I_k + T_k + \rho_{noise\,k} \quad (4.2\text{-}4)$$

It is worth highlighting that broadcast satellite signals contain a group of navigation parameters that are used to estimate satellite clock deviations $b_s$ in a really accurate way. In fact, these corrections are considered while processing the GPS measurements to obtain the navigation solution and the residual error can be considered negligible compared to other errors affecting outcomes. Therefore, the effect of satellite clock offset $b_s$ will be disregarded in the following mathematical development.

$$\Phi_k = Range_k + c.b_{r_k} - I_k + T_k + \Phi_{noise\,k} + \lambda N_k \quad (4.2\text{-}5)$$

$$\rho_k = Range_k + c.b_{r_k} + I_k + T_k + \rho_{noise\,k} \quad (4.2\text{-}6)$$

The above measurements appear to be similar; both are corrupted by the same error sources such as the common receiver clock error $b_r$, atmosphere effects ($I$, $T$) and multipath and measurement noise ($\Phi_{noise}$, $\rho_{noise}$). Nevertheless, there is an inherent ambiguity term $N$ embedded in the carrier-phases and ionosphere effects affect code- and carrier-based measurements in an opposite way. As mentioned before, the carrier frequency is advanced while it goes through the ionosphere and the lower frequency code sequences are, in contrast, delayed. These effects are considered as a delay or enlargement in the derived code pseudo-ranges ($+I$) and as an advance or shortening ($-I$) in the case of carrier-phases.

Let's study more deeply the effects of all these error sources affecting code pseudo-ranges and carrier-phases in order to find a convenient way to combinate both GPS measurements. Both observables contain the information of interest, denoted by $Range_k + c.br_k$ and referred to as the "*error-free pseudo-range*". In fact, the term $Range_k$ corresponds to the satellite-to-user distance required to estimate the receiver's position in terms of trilateration methods (see chapter 2, section 2.2).

**Multipath and measurement noise ($\Phi_{noise}$, $\rho_{noise}$)**

Inherent multipath and measurement noise affecting pseudo-ranges and carrier-phases largely depend upon the precision of processes within both the code tracking loop and the carrier tracking loop (see chapter 3, section 3.1). These effects are denoted by $\Phi_{noise}$ and $\rho_{noise}$ in eq. (4.2-5) and (4.2-6).

According to Robert G. Brown and Patrick Y. C. Hwang [4.9], the accuracy of the code tracking measurement processes (that derive the pseudo-ranges) is considered to be about 1 meter under nominal signal reception strengths. In the same way, though multipath effects depend upon the environment, antenna placement, and antenna design, reference [3.2] states that the errors caused by this interference phenomena can range, in the case of code pseudo-ranges, from 1 m in a benign environment to more than 5 m in highly reflective environments. The noise term on pseudo-ranges can be considered to be about several metres.

Nevertheless, multipath and measurement noise effects adopt lower values in the case of carrier-based measurements. As stated in by Hwang and Brown in [4.9], the noise generated by the tracking processes deriving carrier-phase measurements may adopt values lower than 1 percent of the wavelength, in the case of stationary receivers (most navigation-type receivers may generate stronger noise levels in the case of high dynamics environments - as high as 2 percent). Considering that L1 carrier wavelength is about 19 cm, measurement noise affecting carrier-phases can be therefore considered

negligible compared to the one affecting code pseudo-ranges. Additionaly, multipath errors in carrier-based measurements are typically two orders of magnitude smaller than the ones affecting code pseudo-ranges.

Consequently, code measurements can be considered as *unambiguous* measurements of *error-free pseudo-ranges*, albeit noisy. In contrast, carrier-phases provide a finer and almost noiseless profile of pseudo-ranges with inherent ambiguities affecting them, denoted by $\lambda N_k$ in eq. (4.2-5) and (4.2-6) (compare Figure 23 and Figure 27 shown in chapter 3, code pseudo-ranges are not ambiguous and carrier-phases contain an important ambiguity, i.e. they are not absolute measurements of satellite-to-user distances). The measurement noise affecting carrier-phases can be considered negligible compared to the one affecting pseudo-ranges.

In the following figure, a conceptual view of these two GPS measurements is illustrated. The higher code measurement noise and the ambiguity of the carrier phases are shown.

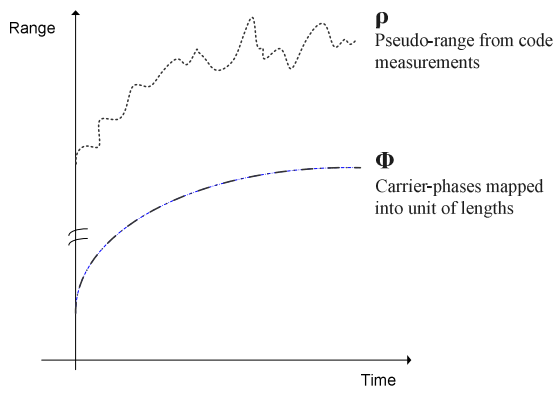


Figure 35 **Conceptual view of code pseudo-ranges and carrier-phase measurements.** Pseudo-ranges ρ are noisy while carrier-phases Φ are precise but ambiguous.

**Carrier-phases ambiguity**

In eq. (4.2-5) and (4.2-6), the unknown number of whole cycles $N_k$ affecting carrier-phases can be considered to remain fixed if continuous carrier tracking is assured. The effect of this ambiguity term on carrier-phases will be then suppressed if the change in

carrier measurements between two consecutive measurement epochs is evaluated. This variation between epoch $t_{k-1}$ and epoch $t_k$ can be defined by means of the time differenced measurements as

$$\Delta\Phi_k = \Phi(t_k) - \Phi(t_{k-1}) = \Delta Range_k + c.\Delta b_{r_k} - \Delta I_k + \Delta T_k + \Delta\Phi_{noise_k} \quad (4.2\text{-}7)$$

As mentioned before, the satellite clock error term $b_s$ was not considered in the equation above since the satellite clock is previously synchronized by considering the clock model broadcast on the navigation message. Additionaly, the carrier-phase measurement noise is considered to be negligible.

The term $\Delta Range_k + c.\Delta br_k$ in the equation above is the change in the "*error-free pseudo-range*" between the two measurement epochs. Similarly $\Delta I$ and $\Delta T$ are the corresponding changes in ionosphere and troposphere delays. Several methods have been stated in order to combine the GPS code- and carrier-based measurements defined by the above equations (4.2-6) and (4.2-7) in order to take advantage of the low-noise on carrier-phases, and the unambiguous nature of code pseudo-ranges (see [4.1], [4.3], [4.13]). In terms of the rates of change in atmosphere effects, an appealing alternative is posed by P. Misra and P. Enge in [4.13], in this scheme both ionosphere and troposphere effects are assumed to change slowly. Therefore, variations in ionosphere and troposphere effects are disregarded in the above quoted measurement models since these quantities usually would be small if the measurement epochs are close (about 1 or 5 seconds in between). Under the above circumstances, the change in carrier-phases might be thought as a precise and unambiguous profile of the change in the "*error-free pseudo-range*", that is,

$$\Delta\Phi_k = \Phi(t_k) - \Phi(t_{k-1}) = \Delta Range_k + c.\Delta br_k \quad (4.2\text{-}8)$$

Consequently, the above mentioned carrier-based time differences, denoted by $\Delta\Phi_k$, are considered as an accurate estimate of pseudo-ranges and thus exploited to smooth out the inherent noise on the measured code pseudo-ranges, denoted by $\rho_k$ and defined in the eq. (4.2-6). As a result, a smoothed or finer pseudo-range profile is derived. This is the basic concept of *carrier-smoothing-code (CSC)* approaches carried out in the range domain. An illustrative example of this procedure is shown in the following figure.

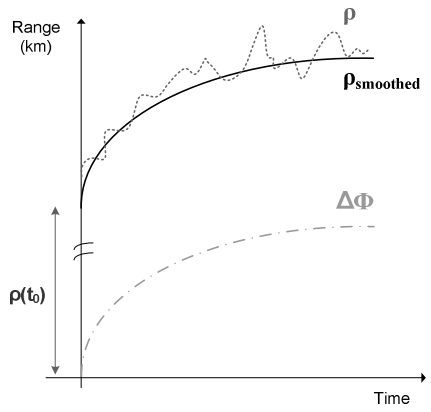


Figure 36 **Range Domain Carrier Smoothing Code pseudo-ranges (CSC).** If a fine estimate of pseudo-range at initial epoch $\rho(t_0)$ can be approximated, a smoothed pseudo-range trace would be yielded with the aid of the change in carrier-phases Φ, denoted by Δ Φ.

*If a fine estimate of pseudo-range at the initial epoch could be approximated* (denoted by $\rho(t_0)$ in the above Figure 36)*, it is possible to yield a smoothed pseudo-range profile using the differences over time on carrier-phases (i.e. a good reference of the change in the "error-free pseudo-range") to update the measured code pseudo-ranges.*

Actually, an estimate of pseudo-range at initial epoch could be derived from any epoch $t_k$ as

$$\hat{\rho}(t_0)_k = \rho(t_k) - [\Phi(t_k) - \Phi(t_0)] \qquad (4.2\text{-}9)$$

where $\rho(t_k)$ is the pseudo-range measured at that k-th epoch and $\Phi(t_k) - \Phi(t_0)$ corresponds to the carrier-phase difference between the current epoch $t_k$ and the initial epoch $t_0$, respectively.

A more precise estimate would be obtained if a simple average over *n* epochs is processed

$$\bar{\rho}(t_0) = \frac{1}{n}\sum_k \hat{\rho}(t_0)_k \qquad (4.2\text{-}10)$$

Once the proper estimate of pseudo-range at initial epoch has been obtained, a "*smoothed pseudo-range profile*" can be reconstructed as

$$\rho_{sm}(t_k) = \bar{\rho}(t_0) + [\Phi(t_k) - \Phi(t_0)] \qquad (4.2\text{-}11)$$

This is the basic mathematical procedure of a conventional range domain CSC algorithm. According to [4.13], CSC schemes are nowadays included in GPS receivers and offer a modest improvement in terms of positioning accuracy. However, the storage of all the pseudo-ranges taken on previous epochs from each of the observed satellites is required in order to compute the average stated in (4.2-10). Additionaly, a group of *n-1* additions need to be processed in each epoch for each of the satellites. This is not therefore an efficient computational technique in terms of real-time applications. In these studies, a more efficient performance of the previously exposed CSC algorithm has been considered and implemented. This idea was posed by P. Misra and P. Enge as well as B. Hoffman-Wellenhof in references [4.13] and [4.3], respectively. It consists of a *recursive filter* that only needs the smoothed pseudo-ranges from the previous time step and the current measurements (both pseudo-ranges and time-differenced carrier-phases) in order to compute the estimate of the current smoothed pseudo-ranges. In contrast to the above mentioned batch smoothing technique, no history of measurements and/or smoothed pseudo-ranges is required. This recursive algorithm is defined as

$$\begin{aligned} &\rho_{sm}(t_k) = \frac{1}{M_k}\rho(t_k) + \frac{M_k - 1}{M_k}[\rho_{sm}(t_{k-1}) + (\Phi(t_k) - \Phi(t_{k-1}))] \\ &\rho_{sm}(t_0) = \rho(t_0) \end{aligned} \qquad (4.2\text{-}12)$$

The filtering scheme (4.2-12) embodies two inputs and one output. The inputs are the measured pseudo-ranges ρ and the measured carrier-phases Φ, taken from the respective observed satellite. Additionally, the resultant smoothed pseudo-ranges $\rho_{sm}$ corresponds to the filter's output. Therefore, at each measurement epoch $t_k$, the smoothed pseudo-ranges $\rho_{sm}(t_k)$ are estimated as a linear combination of the pseudo-ranges measured at the same epoch $\rho(t_k)$, the smoothed pseudo-ranges obtained at the previous epoch $\rho_{sm}(t_{k-1})$ and the carrier-phases differenced between current and previous epochs $\Phi(t_k)- \Phi(t_{k-1})$. Hence two multiplications and two additions are required to be computed on each measurement epoch for each observed satellite, this conveys an important reduction in terms of computational requirements. Furthermore, it is only required the storage of the smoothed pseudo-ranges obtained on the previous measurement epoch instead of the whole set of measurements since the initial epoch. In some literature, this algorithm is usually referred to as the ***Hatch filter***.

It is worth highlighting that the above exposed RD CSC approach adopts a more conservative solution by considering the raw pseudo-ranges at the initial epoch $\rho(t_0)$ as the initial estimate of the smoothed pseudo-ranges $\rho_{sm}(t_0)$. Anyway, ionosphere and troposphere corrections are applied on this measurement on previous steps and, therefore, this initial estimate of smoothed pseudo-range can be considered as a convenient approximation.

In eq. (4.2-12), the weight factors affecting code pseudo-ranges and the smoothed pseudo-ranges (updated by the carrier-phases) are *time dependent.* In fact, an increase of the term $M_k$ is carried out from epoch to epoch. At the first epoch, $M_k$ is set to 1 in order to lay the full weight on the measured pseudo-range. For consecutive epochs, $M_k$ is increased in order to emphasize the influence of the carrier-phases on previous smoothed pseudo-ranges. In that way, as mentioned before, this recursive scheme uses the noisy but unambiguous measured pseudo-ranges in order to set an "absolute" estimation of the initial smoothed pseudo-ranges and, from epoch to epoch, lays more reliability on the estimated smoothed pseudo-ranges from previous epoch (augmented by the carrier-phases differenced between epochs).

B. Hoffman-Wellenhof, H. Collins and J. Lichtenegger posed in [4.3] a reduction of the weight factor *1/M*$_k$ by 0.01 from epoch to epoch with a data sampling rate of 1 Hz. After 100 seconds, only the smoothed value of the previous epoch (augmented by the carrier phase difference) is taken into account. In the experiments developed on these studies, $M_k$ is considered as the number of epochs on which smoothing is continuously applied, i.e. the number of consecutive pseudo-ranges taken from a certain satellite that is consecutively processed in the Hatch filter. Therefore, the weight factors $\frac{1}{M_k}$ and $\frac{M_k - 1}{M_k}$ change in an exponentially way, as shown in the following figure.

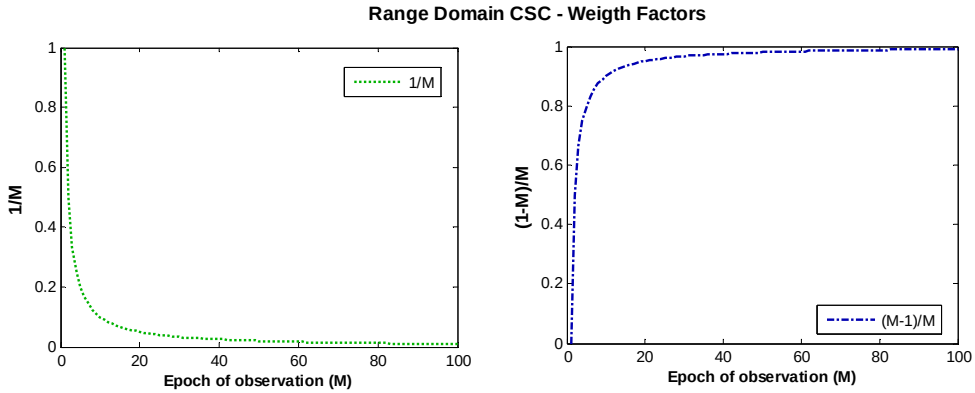


Figure 37 **Range Domain CSC schemes –** Hatch filter's weight factors.

The recursive CSC scheme stated in equation (4.2-12) is supposed to improve over time, that is, the higher the maximum of consecutive smoothing epochs, i.e $M_k$, the stronger carrier measurements information is emphasized and more efficient filtering would be achieved. In that way, more pseudo-range noise would be filtered out. However, in the next sections it will be shown that cumulative effects caused by atmosphere changes limit this efficiency. It is worth hightlighting that the Hatch filter approach defined in eq. (4.2-12) is independently carried out for the measurement set taken from each of the observed satellites. Therefore, the resultant smoothing algorithm consists of a bank of parallel filters, each one defined by the equation (4.2-12). The following figure illustrates this procedure.

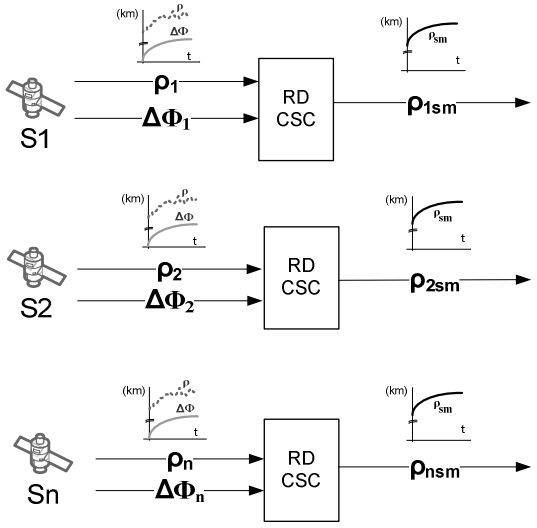


Figure 38 **Bank of parallel Hatch filters to perform a range domain CSC approach**. Time differenced carrier-phases are denoted by ΔΦ.

In the following section, experimental outcomes will be shown in order to observe smoothing effects on the measured pseudo-ranges and the positioning outcomes while applying the bank of parallel Hatch filters.

Measurements were collected on July 19 2007 during 5 minutes (13:00 - 13:05). The GPS receiver consists of a stationary station located at the *E.T.S.I. Topography, Geodesy and Cartography* in Madrid (Spain) as part of a GNSS stations ensemble belonging to *Universidad Politécnica de Madrid.* Observations were taken at a rate of 1 Hz and stored in files under the *Receiver Independent Exchange Format* (RINEX) Version 2.10. These RINEX files are available as a free download on the website http://gps.topografia.upm.es/.

Since the processed pseudo-ranges were not affected by high levels of measurement noise (maybe because of the antenna's location or the receiver's equipment features), a normally distributed gaussian random noise with a standard deviation of 2 meters has been added on pseudo-ranges in order to facilitate the analysis. This idea was

considered following the guidelines of reference [3.6] where real experimental results of receiver and multipath noise show variations around 2.5 metres.

First of all, the code- and carrier-based observables (i.e. measured pseudo-ranges and carrier-phases) taken from a certain satellite were compared. Additionaly, their changes over time were evaluated by computing differences between epochs, the resultant differenced measurements are denoted by $\Delta\Phi_k = \Phi_k - \Phi_{k-1}$ and $\Delta\rho_k = \rho_k - \rho_{k-1}$ and referred to as "*delta measurements*". Why were these time differenced measurements evaluated? Considering the above mathematical background, the "*between epochs*" code- and carrier-based measurements are stated as

$$\Delta\Phi_k = \Phi_k - \Phi_{k-1} = \Delta Range_k + c.\Delta b_{r_k} - \Delta I_k + \Delta T_k + \Delta\Phi_{noise_k} \quad (4.2\text{-}13)$$

$$\Delta\rho_k = \rho_k - \rho_{k-1} = \Delta Range_k + c.\Delta b_{r_k} + \Delta I_k + \Delta T_k + \Delta\rho_{noise\,k} \quad (4.2\text{-}14)$$

Considering that the elapsed time between epochs is 1 second (i.e. sampling rate of 1 Hz), the change in the atmosphere effects can be assumed to be negligible. Furthermore, it was previously mentioned that the noise term affecting carrier-phases is insignificant with respect to the one affecting code pseudo-ranges. Therefore, the difference between code and carrier delta measurements can be considered as the inherent noise affecting pseudo-ranges (that is reduced when applying the Hatch filter smoothing scheme stated in eq. (4.2-12)).

$$\Delta\rho_k - \Delta\Phi_k = \Delta\rho_{noise\,k} - \Delta\Phi_{noise\,k} \approx \Delta\rho_{noise\,k} \quad (4.2\text{-}15)$$

The difference between code and carrier delta measurements stated in the above eq. (4.2-5) was evaluated and the results are shown in the following figure. The resultant sequence seems to be essentially time uncorrelated and is considerably reduced when applying the Hatch filter smoothing scheme. Mean and standard deviation values were computed on the first and the last 120 samples. On the first two minutes of measurements, the mean error slightly enhanced (from 3.59 cm to 2.03 cm) and the standard deviation, however, decreased from metre level to centimetre level (from

almost 3 metres to 1.5 decimetres approximately). On the last two minutes of observations statistical results verify the improvement over time when smoothing is applied on the measured pseudo-ranges since the noise reduction is even stronger (mean and standard deviation reach the millimetre-level).

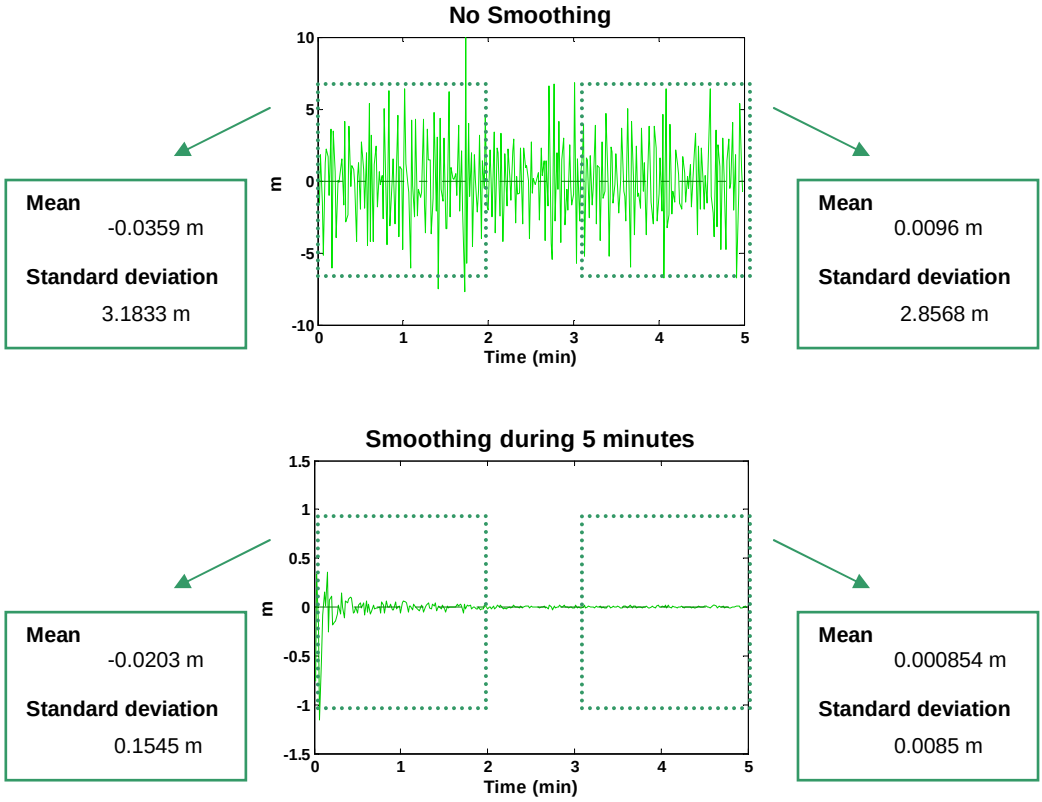


Figure 39 **Example of smoothing - comparison between time variations in pseudo-ranges and carrier-phases.** The error in pseudo-range time variations is shown with respect to carrier phases (i.e. $\Delta\Phi_k - \Delta\rho_k$ and $\Delta\Phi_k - \Delta\rho sm_k$). Data were taken on July 19, 2007 during 5 minutes. The error is computed as $\Delta\Phi_k - \Delta\rho sm_k = (\Phi_k - \Phi_{k-1}) - (\rho sm_k - \rho sm_{k-1})$.

Secondly, the experimental results were also evaluated in terms of the receiver's positioning. In that way, a posision error profile was computed as the distance between and the position estimates and an approximation of receiver's location (available among RINEX data). This error in position was calculated as

$$e_u = \left\| u_{ap} - u_{es} \right\| = \sqrt{\left(x_{ap} - x_{est}\right)^2 + \left(y_{ap} - y_{est}\right)^2 + \left(z_{ap} - z_{est}\right)^2} \quad (4.2\text{-}16)$$

where $u_{ap} = \left(x_{ap}, y_{ap}, z_{ap}\right)$ is the RINEX location and $u_{es} = \left(x_{es}, y_{es}, z_{es}\right)$ corresponds to the estimate. The resultant error is shown in the following figure. Fluctuations on the position error were drastically reduced when smoothing was applied on pseudo-ranges. In the first minute, the mean error decreased by almost one metre (from 2.634 to 1.978 metres) while the standard deviation was reduced by half a metre (from 1.518 to 1.090 m). In contrast, during the last minute of observations, although the standard deviation decreased from decimetre-level to centimetre level, the mean error increased a few decimetres. This effect will be explained in the next section.

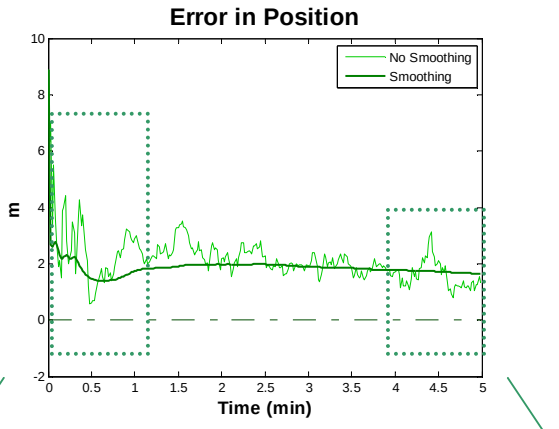


| | No smoothing | Smoothing |
|---|---|---|
| **Mean** | 2.634 m | 1.978 m |
| **Standard Deviation** | 1.518 m | 1.090 m |

| | No smoothing | Smoothing |
|---|---|---|
| **Mean** | 1.581 m | 1.721 m |
| **Standard Deviation** | 0.489 m | 0.044 m |

Figure 40 **RD CSC schemes - example of error in position estimation.** Effects of applying Hatch filter CSC schemes on measured pseudo-ranges.

### 4.2.1 RD code-carrier divergence

When deriving the smoothing scheme defined in eq. (4.2-12) any change in the ionosphere delay between consecutive measurement epochs was disregarded. It is relevant to consider that such a change would generally be insignificant over a few seconds. However, as time goes by, this variation accumulates and might become significant over a large number of epochs, i.e. a large *M* factor.

In the above Figure 40, the mean error in position estimation slightly increases in the last minute of observations (from 1.581 m to 1.721 m), this deviation might be caused by the double effect derived from the ionosphere effect since this goes in one direction for the carrier-phases and in the opposite direction for the code pseudo-ranges - see eq. (4.2-5), (4.2-6) and (4.2-12). Therefore, as a result of the combination of code- and carrier-based measurement in the Hatch filter of eq. (4.2-12), a price is paid for large smoothing intervals in the form of positioning deviations due to changes in atmosphere effects. In some literature this effect is referred to as *code-carrier divergence*.

If it were possible to estimate the rate of ionosphere delay, more effective and efficient use of the Hatch filtering schemes would be achieved. However, this effect is usually unknown to a single-frequency receiver and, therefore, a *conservative constant carrier-smoothing time* is typically applied, i.e. a fixed maximum weight factor $M_k$ is determined in the equation (4.2-12). When this specified maximum is achieved, the factor $M_k$ is set to its initial value and the smoothing process is restarted.

The following figure shows an illustrative example of the code-carrier divergence effects on position estimates. These experimental results were obtained by processing the same data used to achieve the test results shown in the previous section (Figure 39 and Figure 40). Observations were taken during 5 minutes at midday July 19, 2007. Different maximum for the smoothing interval (i.e. maximum factor $M_k$) were applied: 10 seconds, 50 seconds, 100 seconds and the whole observation time, that lasts 5 minutes. Induced biases due to code-carrier divergence can be slightly appreciated

during the last minute. The mean of the position error is highlighted as the filter length (i.e. maximum factor $M_k$) becomes larger. Nevertheless, fluctuations decrease with higher filter lengths, that is, standard deviations of the error in position estimates decrease as smoothing interval is enlarged. If the atmosphere (specifically the ionosphere) had been more active, the divergence would have become manifest for a shorter filter length.

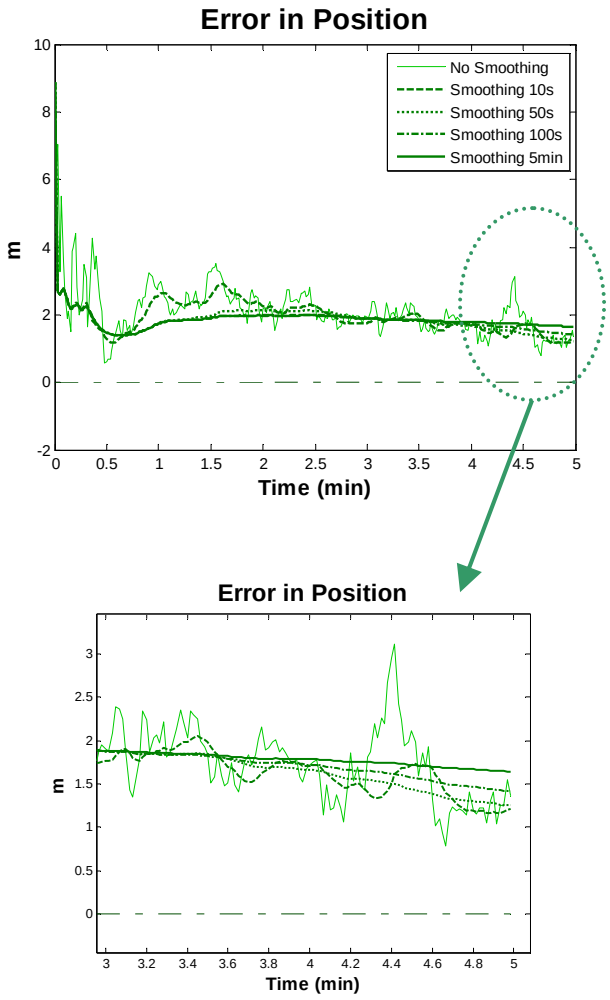


| 13:03-13:05 | No Smoothing | Smoothing 10s | Smoothing 50s | Smoothing 100s | Smoothing 5min |
|---|---|---|---|---|---|
| **Mean** | 1,739 | 1,631 | 1,626 | 1,694 | 1,779 |
| **Standard Deviation** | 0,424 | 0,240 | 0,203 | 0,139 | 0.070 |

Figure 41 **Effects of code-carrier divergence on position estimates** applying different filter lengths – error in estimation of position.

### 4.2.2 Cycle slip drawbacks

It is worth pointing out that, in the case of cycle slips (see page 61), Hatch filter algorithms defined in eq. (4.2-12) would fail. A simple check of the carrier-phase difference between two consecutive epochs and the Doppler shift multiplied by the elapsed time may detect data irregularities such as cycle slips.

In this work, not all the available RINEX data contained Doppler measurements. Consequently, other methods were taken into consideration to detect these irregularities in the processed carrier-phases. In that way, the change in pseudo-ranges was evaluated when no Doppler measurement was available in observation data. In case of a cycle slip in the carrier-phases, an extremely high 'jump' or discontinuity was detected on the mapped delta phases when they were compared with the measured pseudo-ranges.

Therefore, the algorithms implemented in these studies reset the Hatch filter's weight factor $M_k$ of eq. (4.2-12) to its initial value, that is $M_k = 1$, when a cycle slip is detected. This process fully eliminates the influence of the erroneous carrier-phase data.

## 4.3 Position Domain CSC

In conventional GPS receivers, techniques for obtaining the receiver's location are derived generally from the measured code pseudo-ranges. Since these code observables are corrupted by noise and other error sources, filtering and smoothing methods are required to achieve convenient position estimates. In general, the parameters of interest in GPS (usually receiver's position), or the dominant system errors (for example, clock errors), or both, are time-varying. In addition, the time variation is more or less predictable. Fur such situations, the data processing techniques that are the most efficient and optimal, and therefore the most appropriate, are those based on the principles of Least Squares prediction, filtering and smoothing, specifically a recursive algorithm called the *Kalman filter*. Such a filter provides optimum estimates of user position (even velocity and local time) based on noise statistics and current GPS measurements.

As well as changes in satellite-to-user distances, information about variations in the position of the GPS receiver can also be extracted from carrier measurements when they are differenced over time. In the last two decades, several lines of investigation have posed modified Kalman schemes that also incorporate carrier-phase measurements to compute the navigation solution (see references [4.9], [4.11], [4.14]). According to these works, some techniques for integrating pseudo-ranges and carrier-phases as observables in a Kalman filter have been studied. The idea is to treat a carrier-based measurement as a position difference observable between previous and current time epochs, hence current as well as previous position information needs to be included among filter's states. As a result, a position difference can be derived, that is directly observable by the phase difference measured between the previous and current time epochs.

In this section, a general view of the conventional Kalman filter used in GPS receivers to compute the navigation solution is exposed. Then, methods that integrate carrier-phases together with pseudo-ranges are posed by determining modifications in the

conventional Kalman configuration. Additionally, the formulation of the “observation equations” is also described, as well as the modifications made on the “measurement models” to incorporate the new carrier-based observables.

### 4.3.1 Position determination using Kalman filters

The central problem for the GPS receiver is the precise *estimation* of position, velocity, and time based on noisy observations taken from the gathered satellite signals. This is, in fact, an ideal setting for Kalman filter schemes.

This filtering scheme was firstly introduced in 1960 on a paper written by R. E. Kalman [4.17]. He described a recursive solution of the discrete-data linear filtering problem. The idea revolved around the estimation of a random process with prior knowledge of its dynamics and the statistical nature of inherent errors. Additionally, external observations were also considered to reach finer estimates.

Advances in digital computer technology made it possible to consider implementing this recursive solution in a number of real-time applications, such as GPS.

The design of Kalman filters requires knowledge in the *dynamic behaviour* of the random process to be estimated, that is, the GPS receiver motion described at least by its position. Furthermore, a linear relationship between the “state” of the process (i.e. position and maybe velocity, acceleration, jerk and local time) and the gathered measurements need to be established so that the behaviour of the process can be thought as “observable”.

In the following sections, these aspects are theoretically defined by means of mathematical models. Subsequently, position determination regarding to these models is described by means of the conventional Kalman algorithm and the equations of the GPS positioning Kalman filter are introduced.

**Dynamics of the observed random process: The GPS receiver**

In terms of GPS, the random process to be estimated is the receiver platform motion. The dynamic behaviour of this process can be derived by a Taylor series expansion about the true position of the receiver. Let $\bar{u}$ represent the receiver (or *user*) location; then at time *t*, shortly after time $t_0$, the receiver will be at

$$\bar{u}(t) = \bar{u}(t_0) + \left.\frac{d\bar{u}(t)}{dt}\right|_{t=t_0} (t-t_0) + \frac{1}{2!}\left.\frac{d\bar{u}^2(t)}{dt^2}\right|_{t=t_0} (t-t_0)^2 + \frac{1}{3!}\left.\frac{d\bar{u}^3(t)}{dt^3}\right|_{t=t_0} (t-t_0)^3 \ldots \quad (4.3\text{-}1)$$

where the term $\left.\frac{d\bar{u}(t)}{dt}\right|_{t=t_0}$ corresponds to *velocity*, $\frac{1}{2!}\left.\frac{d\bar{u}^2(t)}{dt^2}\right|_{t=t_0}$ defines the system's *acceleration* and $\frac{1}{3!}\left.\frac{d\bar{u}^3(t)}{dt^3}\right|_{t=t_0}$ is the *jerk*. The terms following the third derivative are usually considered negligible.

It is worth highlighting that the determination of non-negligible terms depends on the system being modelled. In the case of most GPS users, position and velocity change relatively slowly over the time period of observations, hence the estimates are reasonably close. The same may not be true for acceleration or jerk in some cases such as aircrafts or racing cars. Following the guidelines stated in reference [4.9], an assumption is often considered in terms of a constant velocity receiver's movement; acceleration and jerk are therefore supposed to be negligible. The resultant model derived from the one defined in equation (4.3-1) describes a rectilinear motion

$$\bar{u}(t) = \bar{u}(t_0) + \left.\frac{d\bar{u}(t)}{dt}\right|_{t=t_0} (t-t_0) \quad (4.3\text{-}2)$$

Considering that GPS positioning usually consist of a three dimensional process, at least, three equations analogous to (4.3-2) need to be solved for the three unknown coordinates of receiver's position $\bar{u}(t) = \lfloor u_x(t), u_y(t), u_z(t) \rfloor$, that is

$$
\begin{aligned}
u_x(t) &= u_x(t_0) + \left.\frac{du_x(t)}{dt}\right|_{t=t_0} (t - t_0) \\
u_y(t) &= u_y(t_0) + \left.\frac{du_y(t)}{dt}\right|_{t=t_0} (t - t_0) \\
u_z(t) &= u_z(t_0) + \left.\frac{du_z(t)}{dt}\right|_{t=t_0} (t - t_0)
\end{aligned}
\qquad \text{(4.3-3)}
$$

Furthermore, if velocity coordinates $\frac{d\bar{u}(t)}{dt} = \left[\frac{du_x(t)}{dt}, \frac{du_y(t)}{dt}, \frac{du_z(t)}{dt}\right]$ need to be also estimated, a total of six differential equations need to be solved. Considering the above mentioned constant velocity model, the ensemble of differential equations that determine the GPS receiver's movement will be

$$
\begin{aligned}
u_x(t) &= u_x(t_0) + \left.\frac{du_x(t)}{dt}\right|_{t=t_0} (t - t_0) \qquad \frac{du_x(t)}{dt} = \left.\frac{du_x(t)}{dt}\right|_{t=t_0} \\
u_y(t) &= u_y(t_0) + \left.\frac{du_y(t)}{dt}\right|_{t=t_0} (t - t_0) \qquad \frac{du_y(t)}{dt} = \left.\frac{du_y(t)}{dt}\right|_{t=t_0} \\
u_z(t) &= u_z(t_0) + \left.\frac{du_z(t)}{dt}\right|_{t=t_0} (t - t_0) \qquad \frac{du_z(t)}{dt} = \left.\frac{du_z(t)}{dt}\right|_{t=t_0}
\end{aligned}
\qquad \text{(4.3-4)}
$$

In order to develop the formulation of a Kalman filter, *state space models*[22] are considered since they are better suited for computer simulation in the case of n-th order input-output differential equations.

In that way, a system's ***state-vector*** $\bar{x}(t) \in V_n$ will determine the *process status* at any time, that is, the unknown navigation solution. For a stand-alone GPS model, this array usually consists of three position states and two clock states in its most basic form.

[22] The *state space model* represents a physical system as n first order coupled differential equations.

According to reference [4.9], this 5-state model is ideal for a stationary receiver (i.e. constant position). Anyway, overlooking possible enhancements in this model an 8-state model has been considered in these studies by integrating three velocity states. Therefore, the GPS model of receiver's motion will be defined by *six system states*: three coordinates of position $\bar{u} = (u_x, u_y, u_z)$ and three coordinates of velocity $\bar{v} = (v_x, v_y, v_z)$ considering a 3-D reference frame[23]. Additionally, receiver clock offset and receiver clock drift are also considered as system states. It is worth highlighting that both clock offset and drift are determined in units of lengths (i.e. multiplied by the speed of light in vacuum *c*). In the following studies, clock states will be omitted focusing in the position and velocity state-models.

The ***continuous state model*** of a random process is reasonably general in form. All that is required is that the process under consideration be related to *white noise* via a linear differential equation as

$$\dot{\bar{x}}(t) = F\bar{x}(t) + G\bar{n}(t) \qquad (4.3\text{-}5)$$

where $\bar{x}(t) \in V_n$ is the vector of process states that embodies position and velocity coordinates and its derivative is denoted by a dot $\dot{\bar{x}}(t) \in V_n$. Perturbations affecting the ideal "noise-free" behaviour $\dot{\bar{x}}(t) = F\bar{x}(t)$ are considered in the vector $\bar{n}(t) \in V_n$ and referred to as *process noise*. It is worth highlighting that Kalman filters are formulated assuming that the process noise is time-uncorrelated with a gaussian probability density distribution. Therefore, $\bar{n}(t)$ is assumed to be an array of *white-noise driving functions*. The white noise component $\bar{n}(t) \in V_n$ can be considered "coloured" by defining a linear relationship $G \in M_{nxn}$ that relates it with the process model. According to [4.9], an appropriate stochastic model for the GPS receiver motion defined in (4.3-2) might be an *integrated random walk model* as shown in the following Figure 42.

[23] The reference frame considered for the computation will be the earth-centered, earth-fixed (ECEF) frame.

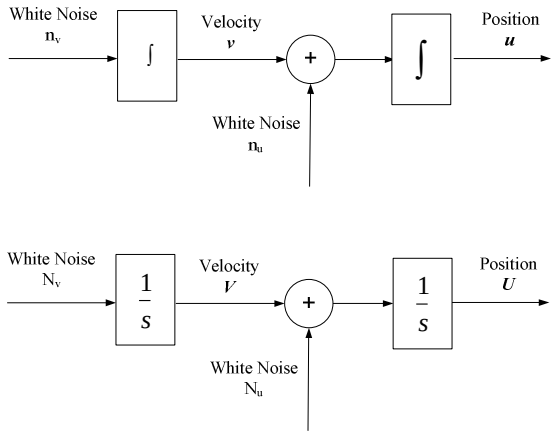


Figure 42 **Diagram of the integrated random walk model for position and velocity states –** time and Laplace domains**.**

For example, if the system is considered to be defined by a 6-state position-velocity model $\bar{x}(t)=\left[u_x(t),u_y(t),u_z(t),v_x(t),v_y(t),v_z(t)\right]$, the ensemble of differential equations related to the above integrated random walk motion is given by

$$\dot{\bar{x}}(t)=\frac{d\bar{x}(t)}{dt}=F\bar{x}(t)+G\bar{n}(t)\begin{cases}\dot{u}_x(t)=v_x(t)+n_{u_x}(t)\\ \dot{u}_y(t)=v_y(t)+n_{u_y}(t)\\ \dot{u}_z(t)=v_z(t)+n_{u_z}(t)\\ \dot{v}_x(t)=n_{v_x}(t)\\ \dot{v}_y(t)=n_{v_x}(t)\\ \dot{v}_z(t)=n_{v_x}(t)\end{cases} \tag{4.3-6}$$

where $F=\begin{bmatrix}0&0&0&1&0&0\\0&0&0&0&1&0\\0&0&0&0&0&1\\0&0&0&0&0&0\\0&0&0&0&0&0\\0&0&0&0&0&0\end{bmatrix}$ $G=\begin{bmatrix}1&0&0&0&0&0\\0&1&0&0&0&0\\0&0&1&0&0&0\\0&0&0&1&0&0\\0&0&0&0&1&0\\0&0&0&0&0&1\end{bmatrix}=I_6$ and $\bar{n}(t)=\begin{bmatrix}n_{u_x}(t)\\n_{u_y}(t)\\n_{u_z}(t)\\n_{v_z}(t)\\n_{v_z}(t)\\n_{v_z}(t)\end{bmatrix}$

In GPS positioning, measurement constraint allows observations of receiver's motion only at certain points in time. Therefore, the process model defined in (4.3-6) must be specified in the discrete-time domain. Considering samples of this process at times $t_0$, $t_{1,}$... $t_{k;}$ the solution of (4.3-6) at time $t_{k+1}$ may be written as

$$\text{(4.3-7)} \qquad \bar{x}(t_k) = A(t_{k-1}, t_k)\bar{x}(t_{k-1}) + \int_{t_{k-1}}^{t_k} A(t_k, \tau)G(\tau)\bar{n}(\tau)d\tau$$

The discretization of the physical problem exposed in (4.3-6) is given by

$$\text{(4.3-8)} \qquad \bar{x}_k = A_k \bar{x}_{k-1} + \bar{w}_k \qquad \textbf{\textit{discrete-time state model}}$$

$\bar{x}_k = \bar{x}(t_k) \in V_n$ and $\bar{x}_{k-1} = \bar{x}(t_{k-1}) \in V_n$ are the process state-vectors at time $t_k$ and $t_{k-1}$, respectively. The vector $\bar{w}_k = \bar{n}(t_k) \in V_n$ corresponds to the noise affecting process states. According to reference [4.15], the sequences $\bar{w}_k$ are also white noise with known covariance structures given by

$$\text{(4.3-9)} \qquad E\left[\bar{w}_k \bar{w}_i^T\right] = \begin{cases} Q_k, & i = k \\ 0, & i \neq k \end{cases}$$

Additionally, $A_k \in M_{n\times n}$ relates the state-vectors $\bar{x}_{k-1}$ and $\bar{x}_k$ in the absence of noise. This matrix corresponds to the solution of the ***deterministic portion*** in the system (4.3-6) and is called the *state transition matrix* for the time-step from $t_{k-1}$ to $t_k$. Since $F$ matrix has constant coefficients, $A_k$ can be written by analyzing the Taylor Series of the exponential function as

$$\text{(4.3-10)} \quad A(t_{k-1}, t_k) = A_k = e^{Ft} = \sum_{k=0}^{\infty} \frac{(Ft)^k}{k!} = I + Ft + \frac{F^2}{2!}t^2 + \frac{F^3}{3!}t^3 + \ldots$$

Considering that the terms $F^2$, $F^3$, … cancel the state transition matrix is defined by the mathematical expression stated above

$$(4.3\text{-}11)\quad A_k = e^{F(t_k - t_{k-1})} = I + F(t_k - t_{k-1}) = I + F\Delta t \qquad A_k = \begin{bmatrix} 1 & 0 & 0 & \Delta t & 0 & 0 \\ 0 & 1 & 0 & 0 & \Delta t & 0 \\ 0 & 0 & 1 & 0 & 0 & \Delta t \\ 0 & 0 & 0 & 1 & 0 & 0 \\ 0 & 0 & 0 & 0 & 1 & 0 \\ 0 & 0 & 0 & 0 & 0 & 1 \end{bmatrix}$$

Where $\Delta t$ is the elapsed time between epochs of observation $t_{k-1}$ and $t_k$.

Evaluation of the ***stochastic portion*** of (4.3-6) is made by deriving the covariance matrix $Q_k$ associated with the process noise $\overline{w}_k$ - this matrix was previously defined in (4.3-9). This procedure may not be obvious; following the guidelines specified in [4.9], *process noise covariance matrix* can be obtained by

$$(4.3\text{-}12)\quad \begin{aligned} Q_k &= E\left[\overline{w}_k \overline{w}_k^T\right] = E\left\{\left[\int_{t_{k-1}}^{t_k} A(t_k,\xi)G(\xi)\overline{n}(\xi)d\xi\right]\left[\int_{t_{k-1}}^{t_k} A(t_k,\eta)G(\eta)\overline{n}(\eta)d\eta\right]^T\right\} \\ &= \int_{t_{k-1}}^{t_k}\int_{t_{k-1}}^{t_k} A(t_k,\xi)G(\xi)E\left[\overline{n}(\xi)\overline{n}^T(\eta)\right]A^T(t_k,\eta)G^T(\eta)d\xi d\eta \\ &= \int_{t_{k-1}}^{t_k}\int_{t_{k-1}}^{t_k} A(t_k,\xi)E\left[\overline{n}(\xi)\overline{n}^T(\eta)\right]A^T(t_k,\eta)d\xi d\eta \end{aligned}$$

The mathematical expectation $E\left[\overline{n}(\xi)\overline{n}^T(\eta)\right]$ is known as the *spectral density matrix for the process noise*. In fact, due to the fact that the process noise is assumed to be white, $E\left[\overline{n}(\xi)\overline{n}^T(\eta)\right]$ is defined as a matrix of Dirac delta functions known from the continuous model. Assuming independence of velocity in terms of position errors the spectral density matrix is given by

$$(4.3\text{-}13)\quad E\left[\overline{n}\overline{n}^T\right] = \begin{bmatrix} q_u & 0 & 0 & 0 & 0 & 0 \\ 0 & q_u & 0 & 0 & 0 & 0 \\ 0 & 0 & q_u & 0 & 0 & 0 \\ 0 & 0 & 0 & q_v & 0 & 0 \\ 0 & 0 & 0 & 0 & q_v & 0 \\ 0 & 0 & 0 & 0 & 0 & q_v \end{bmatrix}$$

The terms $q_u$ and $q_v$ in the matrix (4.3-13) correspond to the common spectral densities of process noise $\overline{w}_k = \overline{n}(t_k) \in V_n$ for all the position and velocity elements, respectively (see the *integrated random walk model* specified in Figure 42). In general, spectral amplitudes associated with process noise are not known. In these studies, $q_u$ and $q_v$ were chosen heuristically following guidelines specified in [4.14]. In fact, experiments were developed with GPS data collected by stationary receivers, these parameters were therefore specified at extremely low values around 0.000033.

Then the process noise covariance matrix, is derived from equation (4.3-12) and is zero except for the following elements

$$Q_k = E\left[\overline{w}_k \overline{w}_k^T\right] = \int_{t_{k-1}}^{t_k} A(t_k, \eta) E\left[\overline{n}\overline{n}^T\right] A^T(t_k, \eta) d\eta \tag{4.3-14}$$

$$Q_k = E\left[\overline{w}\overline{w}^T\right] = \begin{bmatrix} \left(q_u \Delta t + q_v \frac{\Delta t^3}{3}\right) I_3 & \left(q_v \frac{\Delta t^2}{2}\right) I_3 \\ \left(q_v \frac{\Delta t^2}{2}\right) I_3 & (q_v \Delta t) I_3 \end{bmatrix}$$

$I_3$ is the identity matrix of size 3.

In conclusion, the GPS receiver motion is defined by a discrete-time state space model given by

$$\overline{x}_k = A_k \overline{x}_{k-1} + \overline{w}_k \tag{4.3-15}$$

$$A_k = \begin{bmatrix} 1 & 0 & 0 & \Delta t & 0 & 0 \\ 0 & 1 & 0 & 0 & \Delta t & 0 \\ 0 & 0 & 1 & 0 & 0 & \Delta t \\ 0 & 0 & 0 & 1 & 0 & 0 \\ 0 & 0 & 0 & 0 & 1 & 0 \\ 0 & 0 & 0 & 0 & 0 & 1 \end{bmatrix} \qquad Q_k = E\left[\overline{w}\overline{w}^T\right] = \begin{bmatrix} \left(q_u \Delta t + q_v \frac{\Delta t^3}{3}\right) I_3 & \left(q_v \frac{\Delta t^2}{2}\right) I_3 \\ \left(q_v \frac{\Delta t^2}{2}\right) I_3 & (q_v \Delta t) I_3 \end{bmatrix}$$

Where the *state-vector* $\bar{x}_k \in V_n$ embodies, in this case, position and velocity coordinates and the *process error* $\bar{w}_k \in V_n$ consists of white noise sequences affecting each of the system's states. Spectral amplitudes of these noise sequences are defined by $q_u$ , $q_v$ and *process noise covariance matrix* corresponds to $Q_k \in M_{n\times n}$ . Additionally, the *state-transition matrix* $A_k \in M_{n\times n}$ relates state-vectors of consecutive measurement epochs in the absence of noise; being $\Delta t$ the elapsed time between the considered epochs.

For example, let's consider a 6-state state vector that embodies position and velocity coordinates $\bar{x} = (u_x, u_y, u_z, v_x, v_y, v_z)^T$ . If the sampling rate is 1 Hz, that is, the estimation of the process states will be computed at each second of observations. In any step from epoch $t_{k-1}$ to epoch $t_k$ on which the elapsed time is a second, the receiver motion will be defined by the following discrete-time state space model

$$\bar{x}_k = A_k \bar{x}_{k-1} + \bar{w}_k \qquad A_k = \begin{bmatrix} 1 & 0 & 0 & 1 & 0 & 0 \\ 0 & 1 & 0 & 0 & 1 & 0 \\ 0 & 0 & 1 & 0 & 0 & 1 \\ 0 & 0 & 0 & 1 & 0 & 0 \\ 0 & 0 & 0 & 0 & 1 & 0 \\ 0 & 0 & 0 & 0 & 0 & 1 \end{bmatrix}$$

$$Q_k = E\left[\bar{w}\bar{w}^T\right] = \begin{bmatrix} q_u + \frac{q_v}{3} & 0 & 0 & \frac{q_v}{2} & 0 & 0 \\ 0 & q_u + \frac{q_v}{3} & 0 & 0 & \frac{q_v}{2} & 0 \\ 0 & 0 & q_u + \frac{q_v}{3} & 0 & 0 & \frac{q_v}{2} \\ \frac{q_v}{2} & 0 & 0 & q_v & 0 & 0 \\ 0 & \frac{q_v}{2} & 0 & 0 & q_v & 0 \\ 0 & 0 & \frac{q_v}{2} & 0 & 0 & q_v \end{bmatrix}$$

**GPS measurements and receiver's motion mathematical relations**

GPS code pseudo-ranges can be considered as rough measurements of satellite-to-user distances (or *ranges*). In fact, a mathematical relationship between the receiver's coordinates $\bar{u} = (u_x, u_y, u_z)$ and an individual pseudo-range ρ taken from a certain *j*-satellite at any epoch of observations can be defined as

$$\rho^{(j)} = \sqrt{\left(s_x^{(j)} - u_x\right)^2 + \left(s_y^{(j)} - u_y\right)^2 + \left(s_z^{(j)} - u_z\right)^2} + c.b_r - c.b_s^{(j)} \quad (4.3\text{-}16)$$

Where $s^{(j)}=(s_x^{(j)},s_y^{(j)},s_z^{(j)})$ corresponds to this *j*-satellite three dimensional coordinates. It is noticed that the real geometric distance between satellite and user is given by

$$\Psi^{(j)} = \sqrt{\left(s_x^{(j)} - u_x\right)^2 + \left(s_y^{(j)} - u_y\right)^2 + \left(s_z^{(j)} - u_z\right)^2} \quad (4.3\text{-}17)$$

This is the *basic range equation*, in which the geometric range (Ψ) is a function of the satellite and receiver coordinates, that are the parameters of interest (see Figure below). For simplicity, references to the time epoch have not been considered in the equations above.

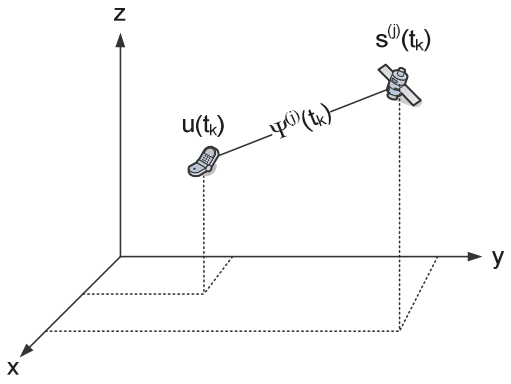


Figure 43 **Geometric range between a GPS satellite and the receiver.** The receiver coordinates are parameterised as Cartesian coordinate components in the same reference system as the satellite coordinates.

In the case of GPS, the coordinates of the satellites are assumed to be known. In fact, these positions are typically evaluated from the broadcast parameters within the navigation message (see section 2.3.3).

In the equation (4.3-16), the receiver clock error $c.b_r$ and satellite clock error $c.b_s$ are generally considered to be "nuisance" parameters as they do not appear explicitly in the basic range equation (4.3-17). However, it is required to include these parameters in the GPS model equations in order to account for the measurement biases present in the data being processed.

As well as satellite coordinates, satellite clock errors are assumed to be known $c.b_s$ because they are generally evaluated with the aid of the broadcast navigation parameters. In contrast, the receiver clock error needs to be solved to achieve an absolute estimation of receiver's position. As mentioned before, conventional GPS Kalman filters consider this parameter as an unknown parameter together with receiver's position coordinates. Anyway, it will be mentioned in subsequent sections how the effect of these clock biases can be suppressed by forming measurement differences in order to construct observables that are, to a large extent, free of biases.

Moreover, atmosphere effects are not considered because ionosphere and troposphere corrections are generally applied on measured pseudo-ranges. In fact, the algorithms performed in these studies apply these corrections just before pseudo-ranges are processed in the Kalman filter.

As well as in the case of receiver's dynamics, a *discrete-time measurement model* that relates process states $\bar{x} = \left(u_x, u_y, u_z, c.b_r\right)$[24] with pseudo-range observables can also be specified from the mathematical relation posed in (4.3-16). However, in the case of Kalman algorithms, linear relationships are required and that is not the case. In order to obtain a linear system that mathematicaly relates process states (i.e. *position*) with

[24] Conventional Kalman filter models include clock error as a system state in order to solve for it if there are enough satellites

measurements (i.e *pseudo-ranges*), the geometric relationship (4.3-16) is "linearized" about an approximate receiver's position.

For any given function $\rho = h(x)$, a certain value *h(x)* can be approximated if it is near a known point. The most basic requisite is that, where $h_{\tilde{x}}(x)$ is the linearization of *h(x)* at the known point $x = \tilde{x}$, $h_{\tilde{x}}(\tilde{x}) = h(\tilde{x})$. The general form of the linearized *h(x)* is the equation of a line given by $h_{\tilde{x}}(x) = K + Z(x - H)$ where *(K,H)* is a known point and *Z* is the line's slope. Hence, using the point *(x,h(x))*, $h_{\tilde{x}}(x)$ becomes $h_{\tilde{x}}(x) = x + M(x - h(x))$. Because continuous functions are locally linear, the best slope to substitute in would be the slope of the line tangent to *h(x)* at $x = \tilde{x}$. Therefore, the equation for the linearization of the function $\rho = h(x)$ at $x = \tilde{x}$ would be

(4.3-18) $\quad h_{\tilde{x}}(x) \approx h(\tilde{x}) + h'(\tilde{x})(x - \tilde{x})$ where $h_{\tilde{x}}(\tilde{x}) \approx h(\tilde{x})$

Where $h(\tilde{x})$ is *h(x)* at $\tilde{x}$ and $h'(\tilde{x})$ is the derivative of *h(x)* evaluated in $\tilde{x}$, that is, the slope of *h(x)* at $\tilde{x}$. Therefore, the linearization of a function corresponds to the first order term of its Taylor expansion around the point of interest.

In the linearization of the geometric relationship (4.3-16) an approximation of receiver's states is chosen such that the error in this approximation regarding to the real receiver's location is small compared with the pseudo-range measurements. Therefore, $\tilde{x} \in V_n$ is an "a priori" estimation of the process state-vector based on all that the receiver knows about the process prior to the current epoch. Additionally, the term $h(\tilde{x}) = \tilde{\rho} \in V_m$ corresponds to a vector of "*anticipated*" pseudo-ranges derived from this a priori state-vector and $h_{\tilde{x}}(x) = \rho \in V_m$ embodies the current pseudo-range measurements. Finally, the term $h'(\tilde{x}) \in M_{m \times n}$ is a matrix obtained by simply evaluating the partial derivatives of (4.3-16) about the considered approximate state-vector $\tilde{x}$.

As a result, a new linear system of equations is obtained that relates the *state-vector errors* $(x - \tilde{x})$ to pseudo-ranges $\rho$. For example, if the state-vector embodies position

coordinates and receiver clock offset as $x=(u_x,u_y,u_z,c.b_r)$ and the approximate state-vector is defined by $\tilde{x}=\left(\tilde{u}_x,\tilde{u}_y,\tilde{u}_z,c.\tilde{b}_r\right)$, the resultant system of equations related to a certain satellite $j$ would be

$$\rho^{(j)} \approx \tilde{\rho}^{(j)} + \left[\frac{\delta\rho^{(j)}}{\delta u_x} \quad \frac{\delta\rho^{(j)}}{\delta u_y} \quad \frac{\delta\rho^{(j)}}{\delta u_z} \quad \frac{\delta\rho^{(j)}}{\delta c.b_r}\right](x-\tilde{x}) \tag{4.3-19}$$

The partial derivatives are defined as

$$\begin{aligned}
&\frac{\delta\rho^{(j)}}{\delta u_x} = \frac{-(s_x^{(j)}-\tilde{u}_x)}{\tilde{\Psi}^{(j)}} \\
&\frac{\delta\rho^{(j)}}{\delta u_y} = \frac{-(s_y^{(j)}-\tilde{u}_y)}{\tilde{\Psi}^{(j)}} \\
&\frac{\delta\rho^{(j)}}{\delta u_z} = \frac{-(s_z^{(j)}-\tilde{u}_z)}{\tilde{\Psi}^{(j)}} \\
&\frac{\delta\rho^{(j)}}{\delta c.b_r} = 1
\end{aligned} \tag{4.3-20}$$

In fact, $\tilde{\Psi}^{(j)}=\sqrt{\left(s_x^{(j)}-\tilde{u}_x\right)^2+\left(s_y^{(j)}-\tilde{u}_y\right)^2+\left(s_z^{(j)}-\tilde{u}_z\right)^2}$ is the geometric distance (or *range*) between $j$-satellite position $s^{(j)}=(s_x^{(j)},s_y^{(j)},s_z^{(j)})$ and the anticipated user position $\tilde{u}=\left(\tilde{u}_x,\tilde{u}_y,\tilde{u}_z\right)$. Actually, more than one satellite is observed in each of the measurement epochs. Therefore, the linear relationship between receiver's position and each of the obtained pseudo-ranges becomes

$$\begin{bmatrix}\rho^{(1)}\\ \rho^{(2)}\\ \dots\\ \rho^{(m)}\end{bmatrix} = \begin{bmatrix}\tilde{\rho}^{(1)}\\ \tilde{\rho}^{(2)}\\ \dots\\ \tilde{\rho}^{(m)}\end{bmatrix}_{x=x^-} + \underbrace{\begin{bmatrix}\frac{\delta\rho^{(1)}}{\delta u_x} & \frac{\delta\rho^{(1)}}{\delta u_y} & \frac{\delta\rho^{(1)}}{\delta u_z} & 1\\ \frac{\delta\rho^{(2)}}{\delta u_x} & \frac{\delta\rho^{(2)}}{\delta u_y} & \frac{\delta\rho^{(2)}}{\delta u_z} & 1\\ \dots & \dots & \dots & 1\\ \frac{\delta\rho^{(4)}}{\delta u_x} & \frac{\delta\rho^{(4)}}{\delta u_y} & \frac{\delta\rho^{(4)}}{\delta u_z} & 1\end{bmatrix}}_{H}(x-\tilde{x}) \tag{4.3-21}$$

The matrix $H$ in equation (4.3-21) is called the ***measurement matrix*** and describes the ideal, i.e. noiseless, connection between measurements and process states.

State-space models are also considered to specify the above measurement model in terms of Kalman algorithms. Therefore, the corresponding discrete-time measurement model to (4.3-21) will be

(4.3-22) $$z_k \approx \tilde{z}_k + H_k\left(x_k - \tilde{x}_k\right) + V v_k$$

Where $x_k \in V_n$ and $z_k \in V_m$ are the actual state and measurement vectors; $\tilde{x}_k \in V_n$ and $\tilde{z}_k \in V_m$ are the "anticipated" or approximates for state and measurement vectors. As well as the process noise $w_k \in V_n$ in (4.3-15), the random variable $v_k \in V_m$ represents the measurement noise that is considered as a white process than can be "coloured" by defining the linear mathematical relation $V \in M_{m\times m}$ . The measurement matrix $H_k \in M_{m\times n}$ embodies the partial derivatives of (4.3-16) with respect to the state-vector *x* and the matrix $V$ would contain the partial derivatives of (4.3-16) with respect to the measurement noise *v*.

As mentioned before, both process and measurement noises are assumed to be white and to have known covariance structures. Furthermore, they are uncorrelated to each other, that is, the cross-correlation between them is zero. Hence, the covariance matrices are given by

(4.3-23) $$E\left[w_k w_i^T\right] = \begin{cases} Q_k, & i = k \\ 0, & i \neq k \end{cases} \qquad E\left[v_k v_i^T\right] = \begin{cases} R_k, & i = k \\ 0, & i \neq k \end{cases} \qquad E\left[w_k v_i^T\right] = 0 \qquad \forall k, i$$

It is worth highlighting that the covariance matrix *R* is typically defined based on the particular design of the receiver device and the system (e.g. the signal bandwidth or the received signal power). In these studies, following the guidelines stated in reference [4.9], the errors affecting measurements taken from different satellites are assumed to be uncorrelated, that is, the matrix *R* is defined as diagonal. The variance of the error in pseudo-range measurements $v_k$ is determined by taking into consideration a broadcast parameter within the navigation message. This parameter is referred to as *User-Range-*

*Accuracy (URA)* and corresponds to the contribution to the range-measurement error from an individual error source (apparent clock and ephemeris prediction accuracies). When the variance of the receiver measurement noise is somehow known, it is also considered on the covariance matrix *R*.

For example, let's consider the GPS data processed in previously mentioned experiments. As it was said, this data was collected on July 19 2007 at a rate of 1 Hz. The receiver was a stationary station located at the *E.T.S.I. Topography, Geodesy and Cartography* in Madrid (Spain). For example, in the first minute of observations (i.e. after 60 samples) a total of 8 GPS satellites were visible in the sky. Anyway, it will be considered only 5 of them to simplify the mathematical expressions – as shown in the following figure.

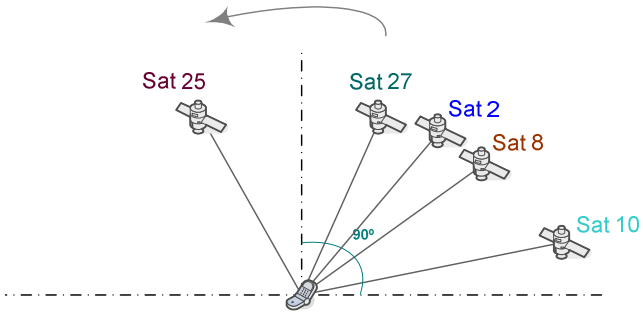


Figure 44 **Example of satellites visibility** - July 19, 2007 - 9:00 am

In the 60th epoch of observations, the considered approximate state-vector is denoted as $\tilde{x}_{60} = \left(\tilde{u}_{x_{60}}, \tilde{u}_{y_{60}}, \tilde{u}_{z_{60}}, c.\tilde{b}_{r_{60}}\right)$. In this example, it is only considered the three position coordinates $(u_x,u_y,u_z)$ together with receiver clock offset $c.b_r$.

Additionally, satellite positions and clock corrections are computed at each epoch of observations and are denoted by

$$s_{60}^{(j)} = \begin{bmatrix} s_{x60}^{(10)} & s_{y60}^{(10)} & s_{z60}^{(10)} \\ s_{x60}^{(8)} & s_{y60}^{(8)} & s_{z60}^{(8)} \\ s_{x60}^{(2)} & s_{y60}^{(2)} & s_{z60}^{(2)} \\ s_{x60}^{(27)} & s_{y60}^{(27)} & s_{z60}^{(27)} \\ s_{x60}^{(25)} & s_{y60}^{(25)} & s_{z60}^{(25)} \end{bmatrix} \qquad c.b_{s60}^{(j)} = \begin{bmatrix} c.b_{s60}^{(10)} \\ c.b_{s60}^{(8)} \\ c.b_{s60}^{(2)} \\ c.b_{s60}^{(27)} \\ c.b_{s60}^{(25)} \end{bmatrix}$$

The discrete-time measurement model for this time step will be determined as

$$z_{60} \approx \tilde{z}_{60} + H_6\left(x_{60} - \tilde{x}_{60}\right) + Vv_{60}$$

The actual *state vector* in the previous equation is considered as

$$x_{60} = \begin{bmatrix} u_{x60} & u_{y60} & u_{z60} & c.b_{r60} \end{bmatrix}^T \in V_4$$

and the *measurement vector* $z_{60}$ embodies the code pseudo-ranges obtained in the current epoch.

$$z_{60} = \begin{bmatrix} \rho_{60}^{(10)} & \rho_{60}^{(8)} & \rho_{60}^{(2)} & \rho_{60}^{(27)} & \rho_{60}^{(25)} \end{bmatrix}^T \in V_5$$

Moreover, the computed satellite positions and clock corrections are processed to obtain the *approximate or anticipated measurement vector* as

$$\tilde{z}_{60} \approx \begin{bmatrix} \tilde{\Psi}_{60}^{(10)} + c.\tilde{b}_{r60} - c.b_{s60}^{(10)} \\ \tilde{\Psi}_{60}^{(8)} + c.\tilde{b}_{r60} - c.b_{s60}^{(8)} \\ \tilde{\Psi}_{60}^{(2)} + c.\tilde{b}_{r60} - c.b_{s60}^{(2)} \\ \tilde{\Psi}_{60}^{(27)} + c.\tilde{b}_{r60} - c.b_{s60}^{(27)} \\ \tilde{\Psi}_{60}^{(25)} + c.\tilde{b}_{r60} - c.b_{s60}^{(25)} \end{bmatrix}$$

Where, in the case of each satellite, the *anticipated geometrical range* is computed by

$$\tilde{\Psi}_{60}^{(j)} = \sqrt{\left(s_{x60}^{(j)} - \tilde{u}_{x60}\right)^2 + \left(s_{y60}^{(j)} - \tilde{u}_{y60}\right)^2 + \left(s_{z60}^{(j)} - \tilde{u}_{z60}\right)^2}$$

It is worth highlighting that other biases affecting pseudo-range measurements need to be taken into consideration while computing the approximate measurement vector $\tilde{z}_{60}$, if they are known in advance or can be predicted during the data processing. In these studies, atmosphere corrections are applied on the measured pseudo-ranges in previous steps so these biases do not need to be considered.

Finally, the measurement matrix is obtained with the aid of the computed satellite positions and the approximate state-vector

$$H_{60} = \begin{bmatrix} \frac{-(s_{x60}^{(10)} - \tilde{u}_{x60})}{\tilde{\Psi}_{60}^{(10)}} & \frac{-(s_{y60}^{(10)} - \tilde{u}_{y60})}{\tilde{\Psi}_{60}^{(10)}} & \frac{-(s_{z60}^{(10)} - \tilde{u}_{z60})}{\tilde{\Psi}_{60}^{(10)}} & 1 \\ \cdots & \cdots & \cdots & 1 \\ \cdots & \cdots & \cdots & 1 \\ \cdots & \cdots & \cdots & 1 \\ \frac{-(s_{x60}^{(25)} - \tilde{u}_{x60})}{\tilde{\Psi}_{60}^{(25)}} & \frac{-(s_{y60}^{(25)} - \tilde{u}_{y60})}{\tilde{\Psi}_{60}^{(25)}} & \frac{-(s_{z60}^{(25)} - \tilde{u}_{z60})}{\tilde{\Psi}_{60}^{(25)}} & 1 \end{bmatrix} \in M_{5x4}$$

The covariance matrix of error affecting pseudo-ranges was determined by considering as independent sources of error: the clock deviations, errors in the ephemeris parameters, and the receiver measurement noise. The variance of the measurement noise was considered in the range of a few meters following guidelines stated in reference [4.9]. For example, experimental outcomes have shown that, when a gaussian white noise component was added on pseudo-ranges with a standard deviation of 2 metres, a measurement error variance of $3^2\ \mathrm{m}^2$ provides good approximations in test results.

$$R_{60} = \begin{bmatrix} \sigma_{60}^{(10)} & 0 & 0 & 0 & 0 \\ 0 & \sigma_{60}^{(8)} & 0 & 0 & 0 \\ 0 & 0 & \sigma_{60}^{(2)} & 0 & 0 \\ 0 & 0 & 0 & \sigma_{60}^{(27)} & 0 \\ 0 & 0 & 0 & 0 & \sigma_{60}^{(25)} \end{bmatrix} \quad \text{where} \quad \sigma_{60}^{(j)} = \underbrace{3 \times URA_{60}^{(j)}}_{\substack{clock \\ ephemeris}} + \underbrace{}_{\substack{estimation \\ data}} 3^2$$

**Kalman filter equations**

Once, both GPS process and measurement models are specified. The Kalman filter equations can be introduced. As mentioned before, the Kalman filter is a recursive estimator; this means that only the estimated process-states from the previous time step and the current measurements are needed to compute the estimate for the current states. As well as the Hatch filter, no history of observations and/or estimates is required. Generally, Kalman filters are purely defined in the time domain.

The state of the observed process is represented in the form of two variables denoted by $\hat{x}_k$ and $P_k$. The estimate of the state at time k is stored in $\hat{x}_k$. In addition, $P_k$ corresponds to the *error covariance matrix*, a measure of the estimated accuracy of the state estimate. Therefore, the smaller $P_k$ elements are, the more accurate the state estimates are. The notation $\hat{x}_k$ represents the estimate of $x_k$ at time $t_k$ given observations up to, and including the initial epoch of time $t_0$.

Basically, a Kalman filter estimates the state of an observed process (i.e. the GPS receiver motion) by using a form of *feedback control*: the algorithm uses the state estimate from the previous epoch to "*predict*" an estimate of the state at the current epoch, provided a dynamic model of the states. Then, it obtains feedback in the form of external noisy measurements taken at the current epoch. In that way, measurement information at the current epoch is used to "*correct*", refine or filter the prediction in order to achieve a new more accurate state estimate for the current epoch, provided some functional relationship exists between the state and the measurements. Therefore, the equations for the Kalman filter are processed in two different phases: the "*prediction*" or *time update* and the "*correction*" or *measurement update.* The time update is responsible for "projecting forward" (propagating or predicting) in time the state $\hat{x}_k$ and error covariance $P_k$ estimates to reflect the effects of dynamics over time. The measurement update is responsible for the "prediction refinement" with the aid of information provided by external observations or measurements.

Furthermore, measurement update utilizes a weighting function, called the *Kalman gain,* which is optimized to produce a minimum error variance. For this reason, the Kalman filter is called an optimal filter. Moreover, this filter is structured to produce an *unbiased estimate,* in terms of linear system models.

***Time update – Propagation or Prediction step***

In the Kalman time update, an initial estimate of the process state and error covariance is "predicted" based on all that the receiver knows about the process prior to the actual epoch. These prior, or *a priori,* estimates will be denoted in the following mathematical expressions as $\hat{x}_k^-$ and $P_k^-$ where the "hat" denotes estimate and the minus superscript identifies estimates prior to assimilating measurements at current epoch. In that way, both state and covariance are "*propagated*" from the previous epoch to the current one according to the dynamic model (4.3-15). The error in these "*a priori"* estimates is defined as $e_k^- = x_k - \hat{x}_k^-$ and assumed to have zero mean. The predicted error covariance matrix is defined as $P_k^- = E\left\{e_k^- e_k^{-T}\right\}$.

Under these circumstances, the ***Kalman time update step*** is determined by the following matrix equations

(4.3-24) $\hat{x}_k^- = A\hat{x}_{k-1}$ A priori estimation of state

(4.3-25) $P_k^- = AP_{k-1}A^T + Q_k$ A priori estimation of error covariance matrix

***Measurement update***

After the time update, *ephemeris data*[25] gathered from satellite signals is extracted from navigation messages to allocate satellites within their orbits. Using the time updated receiver position contained in the "a priori" state estimate $\hat{x}_k^-$ , an "anticipated" pseudo-range measurement is then derived for each of the allocated satellites taking into consideration the basic range equation stated in (4.3-16). Differences between measured and anticipated pseudo-ranges are evaluated in order to minimize the estimation error. These differences are called *residuals* or *innovation* and reflect the discrepancy between the current measurements and the anticipated ones. According to [4.9], a linear blending of the noisy measurements and the anticipated ones is applied in accordance with

$$\hat{x}_k = \hat{x}_k^- + K_k\left(z_k - H_k\hat{x}_k^-\right) \qquad (4.3\text{-}26)$$

The vector $\hat{x}_k$ is called the *updated estimate* and the difference $\left(z_k - H_k\hat{x}_k^-\right)$ embodies the above mentioned *residuals*, where $z_k$ are the measured pseudo-ranges and $H_k\hat{x}_k^-$ corresponds to the anticipated ones.

The Kalman filter thus adjusts the estimation of system's states $\hat{x}_k$ to minimize the residuals by means of the weighting function $K_k \in M_{n\times m}$. This matrix is called the *Kalman gain* and it is normally obtained by means of *minimum mean squared error criteria*[26]. According to reference [4.15], the minimization can be accomplished by first substituting (4.3-26) in the definition of the *measurement update error* $e_k = x_k - \hat{x}_k$. Then, the resultant expression is substituted into the covariance matrix expression $P_k = E\left[e_k e_k^{\,T}\right]$ and the mathematical expectation is performed. The Kalman gain $K$ matrix is finally obtained by taking the derivative of the resultant trace with respect to

[25] GPS satellites include ephemeris data in the broadcast signals, this set of parameters can be used to accurately calculate the location of a GPS satellite at a particular point in time. They describe the path that the satellite is following as it orbits Earth.

[26] A *minimum mean square error (MMSE)* approach minimizes the mean square error, that is, the amount by which an estimate differs from the true value of the quantity being estimated.

*K*, setting the result equal to zero, and then solving for K (i.e. looking for the minimum mean square error $P_k = E\left[e_k e_k^{\,T}\right]$). For more details, see reference [4.9]. One form of the resultant matrix[27] is given by

$$K = P_k^- H_k^{\,T}\left(H_k P_k^- H_k^{\,T} + R_k\right)^{-1} \tag{4.3-27}$$

Therefore, according to equation (4.3-26), when the measurement error covariance *R* approaches zero, the actual measurement $z_k$ is "trusted" more and more, while the predicted measurement $H_k \hat{x}_k^-$ is trusted less and less. On the other hand, as the *a priori* estimate error covariance $P_k^-$ approaches zero, the actual measurement is trusted less and less, while the predicted measurement is trusted more and more.

Under these circumstances, the ***Kalman measurement update step*** is finally defined by the following matrix equations

$$K = P_k^- H_k^{\,T}\left(H_k P_k^- H_k^{\,T} + R_k\right)^{-1} \tag{4.3-28}$$ Kalman Gain

$$\hat{x}_k = \hat{x}_k^- + K\left(z_k - H_k \hat{x}_k^-\right) \tag{4.3-29}$$ State measurement update

$$P_k = \left(I - KH_k\right)P_k^- \tag{4.3-30}$$ Error Covariance measurement update

The resultant adjusted estimates $\hat{x}_k$ and $P_k$ are the navigation solution output to the user, they are also fed back to the dynamical model to repeat then this recursive estimation process.

[27] Kalman filter equations can be algebraically manipulated into several forms. Equation (4.3-27) represents the Kalman gain in one popular form.

In conclusion, the specification of seven basic elements defines the Kalman filter to the extent that it can be implemented as

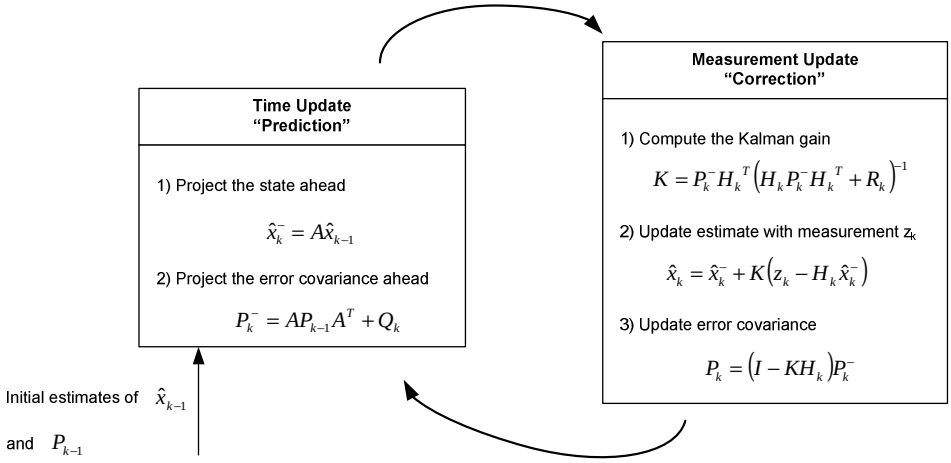


Figure 45 **Kalman filter recursive algorithm – matrix equations defining this filtering scheme.**

*x* and *P* are the state vector and state covariance matrix. The s*tate transition matrix A* and the *covariance matrix of system's error Q* are determined in terms of the modelled system dynamics. The vector *z* contains the measurements used while computing navigation solution. Additionally, measurements perturbations are characterized by means of their respective covariance matrix *R*, and mathematical relationships between states and measurements are specified in the *measurement matrix H*.

The recursive Kalman algorithm is first initialized with rough approximations of the system's states. In most cases, the initialization data had been stored in receiver non-volatile memory when the equipment was last turned off. On these studies, a rough 3-D trilateration method (Bancroft algorithm) has been used to determine a rough position and time estimates on the first epoch of observations, initialization notwithstanding.

It is worth mentioning that the *initial uncertainty*, specified in the covariance matrix *P* that is associated with the errors in the state-estimation, is initialized as a diagonal matrix with large diagonal elements. Values have been considered according to the guidelines of reference [4.14], as the seed position for the system is provided by a Bancroft algorithm, position error states were assumed to have initial variance of (100

m)$^2$ and the velocity error states were considered to have an initial variance of 2x(100 m/s)$^2$ .

For example, let's consider the process-state position/velocity model $x = (u_x\ u_y\ u_z\ v_x\ v_y\ v_z)^T$. The initial position and velocity are assumed to be not known perfectly; therefore, the covariance matrix should be initialized with a suitably large number. Following the guidelines stated in reference [4.14], the initial covariance matrix $P$ could be

$$P_0 = \begin{bmatrix} 100^2 & 0 & 0 & 0 & 0 & 0 \\ 0 & 100 & 0 & 0 & 0 & 0 \\ 0 & 0 & 100^2 & 0 & 0 & 0 \\ 0 & 0 & 0 & 2(100)^2 & 0 & 0 \\ 0 & 0 & 0 & 0 & 2(100)^2 & 0 \\ 0 & 0 & 0 & 0 & 0 & 2(100)^2 \end{bmatrix}$$

Hence, in this initial time step, the Kalman filter will then prefer the information from the first measurements over the information already provided by the model since the variances embodied in the covariance matrix P are extremely high – as mentioned before, this matrix represents a measure of the estimated *accuracy* of the state estimate, it its elements are high quantities, the estimated accuracy will not be quite good. In the experiments performed with the GPS data obtained on July 19, 2007 the P matrix obtained after the first state estimation was

$$P_1 = \begin{bmatrix} 1.935 & 0.070 & 1.998 & 0 & 0 & 0 \\ 0.070 & 0.465 & 0.062 & 0 & 0 & 0 \\ 1.998 & 0.062 & 3.700 & 0 & 0 & 0 \\ 0 & 0 & 0 & 20000 & 0 & 0 \\ 0 & 0 & 0 & 0 & 20000 & 0 \\ 0 & 0 & 0 & 0 & 0 & 20000 \end{bmatrix}$$

After five minutes of observations the covariance matrix obtained after the 300$^{th}$ state estimation was

$$P_{300} = \begin{bmatrix} 0.152 & 0.011 & 0.122 & 0.007 & 0 & 0.004 \\ 0.011 & 0.057 & 0.003 & 0 & 0.004 & 0 \\ 0.122 & 0.003 & 0.260 & 0.004 & 0 & 0.010 \\ 0.007 & 0 & 0.004 & 0.001 & 0 & 0 \\ 0 & 0.004 & 0 & 0 & 0.001 & 0 \\ 0.004 & 0 & 0.010 & 0 & 0 & 0.001 \end{bmatrix}$$

Therefore, as the variances of the error in the state estimation decreased (i.e. P matrix elements decreased), the Kalman filter trusted less and less the measurements, while the filter relied on the state estimations more and more. Furthermore, the initial P "diagonality" is lost, that is, the initial assumption of uncorrelated state-estimate errors is not trusted by the Kalman filter and some correlation appear among errors in the different state-estimates.

According to Figure 45 the covariance matrix estimate $P_k$ depends on the measurement noise affecting pseudo-ranges (R matrix) and the process noise affecting receiver's movement (Q matrix) together with the current set of measurements and satellites layout in the sky, as determined by the $H_k$ matrix.

According to [2.1], the two key benefits of applying Kalman filtering schemes are the possibility of operating even when only a partial set of measurements is available and the adjustment of state estimation in order to weight the effects of measurement noise. This type of filter provides a navigation solution even in the case of low visibility environments. Furthermore, as the measurement noise increases, the filter decreases the weights of the measurement information while relying more on the user state estimates. When the noise variance decreases, the filter utilizes the measurement information more and relies on the estimates less. This is, in fact, a smoothing filtering algorithm.

A flowchart showing the main steps on the Kalman recursive algorithm used in GPS positioning is shown in the following figure.

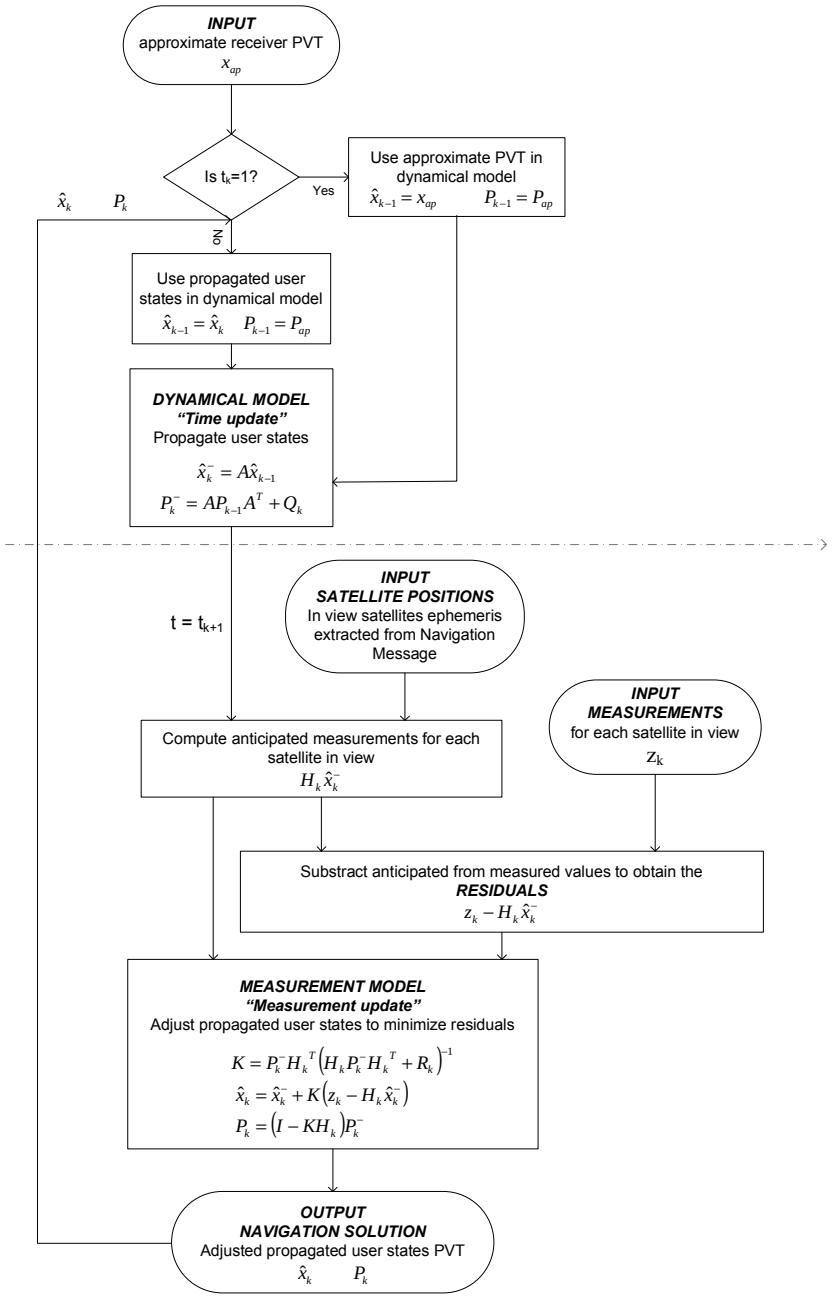


Figure 46 **User Position-Velocity-Time (PVT) determination with Kalman filtering**

### 4.3.2 Modifications to incorporate carrier-phase measurements

As mentioned before, the change in carrier phases over time can provide a fine trace of "noise-free" pseudo-range variations. Previously, some linear equations relating pseudo-ranges and positions were posed; in this section it will be shown that estimates about GPS receiver location can also be obtained from carrier-based measurements.

Let's start by assuming an individual carrier-phase measurement taken from a satellite, say $j$, at a certain time step $t_k$. As stated before in equation (3.3-17), the mathematical model related with this measurement is defined by

$$\Phi^{(j)}(t_k) = \Psi^{(j)}(t_k) + c.b_r(t_k) - c.b_s^{(j)}(t_k) + \Phi_{atm}^{(j)}(t_k) + N^{(j)} \quad (4.3\text{-}31)$$

Only the geometric range $\Psi^{(j)} = \sqrt{\left(s_x^{(j)} - u_x\right)^2 + \left(s_y^{(j)} - u_y\right)^2 + \left(s_z^{(j)} - u_z\right)^2}$ contains the coordinate parameters of interest in GPS positioning. The unknown receiver position is $u = (u_x, u_y, u_z)$ and the location of satellite $j$ is identified by $s^{(j)} = (s_x^{(j)}, s_y^{(j)}, s_z^{(j)})$ that is derived from navigation parameters broadcast on GPS signals.

The above non-linear mathematical relationship (4.3-31) links receiver position at any epoch with carrier-phases $\Phi^{(j)}(t_k)$, derived at the same epoch. As mentioned in chapter 3, all biases (atmosphere effects $\Phi_{atm}^{(j)}$, ephemeris and satellite clock deviations $c.b_s^{(j)}$, etc.) basically influence both the pseudo-range and carrier-phase observations by the same amount (despite some frequency-dependent effects in terms of ionosphere). However, only the carrier-phases contain the ambiguity bias $N^{(j)}$, which is a constant for a satellite-receiver pair as long as the instrument remains locked onto the satellite.

Depending upon the level of accuracy sought, the various GPS biases and errors may be considered significant or not, and different options are used in accounting for these effects. According to reference [3.5], the standard approach to GPS phase data processing is to construct new observables by differencing carrier-phase measurements

in such a way that some (or all) the clock biases are eliminated, and the impact of several other measurement biases is significantly reduced. Several differencing schemes have been considered by researchers, the figure below shows and illustration of them.

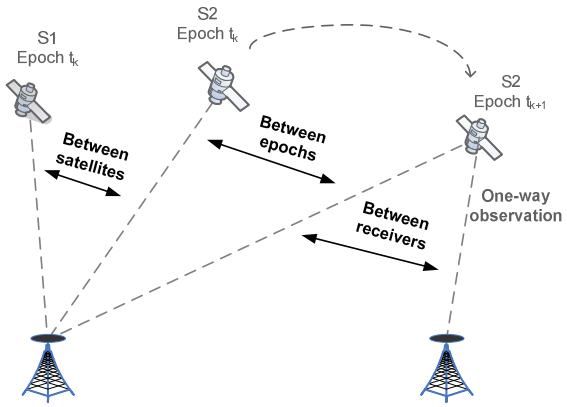


Figure 47 **GPS measurement differencing schemes**

*Differences between-receivers* may (almost) suppress the effects of satellite clock errors. The differences are formed between observations taken by two GPS receivers to one satellite, at the same epoch (see Figure 47 above). Nevertheless, the transit time of the satellite signals are not equal because of the different satellite-to-user distances (according to [3.5] this difference may be up to 1 millisecond for a distance of 300 km between receivers) and satellite clock errors cannot, therefore, completely cancel because they may refer to different transmission times. However, as the satellites use stable atomic oscillators, it is usual to assume that the satellite clock errors are identical and thus cancel when the between-station difference is formed. As a result, remaining clock bias terms are the “between-receivers” clock errors and the “between-receivers” cycle ambiguity. Influences of the orbit error terms have approximately equal magnitude and will therefore cancel in between-receiver differencing (according to [3.5], this assumption becomes wrong with increasing receiver separation). However, in this differenced approach, ambiguity estimates are still required to be solved.

These studies have been performed with measurement taken from an individual GPS station. Therefore, it was not possible to compute between-receivers differences and other differencing schemes needed to be considered. For example, bias parameters which remain constant with time may be eliminated by forming the *between-epoch difference* (the well-known *time-difference* or *delta-measurement*). Moreover, the common receiver clock bias can be eliminated by differencing simultaneous measurements taken from different satellites. In that way, a ***double-difference*** can be obtain by forming *between-epoch* and *between-satellites differences*.

**Double-differenced carrier-phases**

When the system do not have enough observations to generate an instantaneous position and clock estimate, position errors from a filter that includes clock states would be adversely affected. Since measurements from different satellites that have been taken simultaneously are affected by receiver clock error as the same way, *between-satellite differences* can be formed to eliminate this common clock offset. The considered observations are taken simultaneously by one GPS receiver to two satellites (see the previous Figure 47). Considering two simultaneous carrier-phase measurements taken by the same GPS receiver from two observed satellites, the difference between satellites can be written as

$$\nabla\Phi^{(lj)}(t_k) = \Phi^{(l)}(t_k) - \Phi^{(j)}(t_k) \tag{4.3-32}$$

where the operator $\nabla$ identifies a between-satellite difference and the superscript *jl* corresponds to the considered satellites (being $l \neq j$). Remaining clock bias terms are the "between-satellite" clock error and the "between-satellite" cycle ambiguity as shown in the following equation

$$\nabla\Phi^{(lj)}(t_k) = \Psi^{(l)}(t_k) - \Psi^{(j)}(t_k) - c\left[b_s^{(l)}(t_k) - b_s^{(j)}(t_k)\right] + N^{(l)} - N^{(j)} + \nabla\Phi_{atm}(t_k) \tag{4.3-33}$$

As a result, receiver clock error has been suppressed. However, ambiguity estimates are still required for each of the satellite measurements.

Now consider that both *l* and *j* satellites have been tracked continuously without no losses of lock between two consecutive epochs, say $t_{k-1}$ and $t_k$. Under these circumstances, ambiguities $N^{(l)}$ and $N^{(j)}$ embedded in carrier-phases remain constant. If a second difference measurement is formed between these epochs, integer ambiguities will thus be eliminated.

$$\begin{aligned}\Delta\nabla\Phi^{(lj)}(t_{k-1},t_k) &= \nabla\Phi^{(lj)}(t_k)-\nabla\Phi^{(lj)}(t_{k-1}) \\ &= \left[\Psi^{(l)}(t_k)-\Psi^{(j)}(t_k)\right]-\left[\Psi^{(l)}(t_{k-1})-\Psi^{(j)}(t_{k-1})\right] \\ &\quad -c\left[b_s^{(l)}(t_k)-b_s^{(j)}(t_k)\right]+c\left[b_s^{(l)}(t_{k-1})-b_s^{(j)}(t_{k-1})\right]+\Delta\nabla\Phi_{atm}(t_k)\end{aligned} \tag{4.3-34}$$

The operator $\Delta$ is used to represent differences computed between epochs of measurements (i.e. time-differences or delta measurements). Note that both common receiver clock bias and integer ambiguities have been suppressed from the double-differenced measurement model. If the assumption that integer ambiguities are constant is wrong, an extra term is required to account for any possible cycle slip. As mentioned in reference [3.5], not only have the above unknown biases been removed, but in addition, the effect of other biases arising from atmospheric effects and satellite ephemeris error, have been substantially reduced by the process of double-differencing.

The above posed double-differenced measurement based on carrier observations can be applied in the Kalman filter to obtain, as well as in the case of pseudo-ranges, information about receiver's location. But some aspects need to be considered while processing these double-differenced carrier-phases. According to [4.14], these measurements would be very reliable except that over time, changes in satellite allocation and in atmosphere delays all occur.

First of all, time differences computed on carrier-phases relate change in satellite-to-user distances to change in user location between consecutive epochs. These variations are in the direction of the satellite generating the broadcast carrier, i.e. the line-of-sight

path to the satellite. Therefore, *satellite motion must to be taken into consideration*. Receiver can guess, in a really accurate way, where the satellite is or has been placed by considering satellite orbit parameters broadcast as part of the navigation message. Thomas J. Ford and Jason Hamilton claim in [4.14] that the residual errors in satellite motion resulting from ephemeris shortcomings can be considered small in comparison with the atmospheric error changes.

Secondly, atmosphere also changes with time. Following the guidelines specified in [4.14], errors caused by atmosphere effects changes are accounted for in part in the error models associated with the measurements and in part by the process noise applied to the position in the Kalman time updates.

In addition, information about the current position as well as the previous one needs to be incorporated within the states of the Kalman filter.

**Kalman modifications to incorporate differenced measurements**

The measurements considered on this new Kalman filter will be the double-differenced carrier-phases introduced in (4.3-34) together with between-satellite differences computed on pseudo-ranges given by the following “error-free” equations

$$\Delta\nabla\Phi_k^{(lj)} = \left(\Psi_k^{(l)} - \Psi_k^{(j)}\right) - \left(\Psi_{k-1}^{(l)} - \Psi_{k-1}^{(j)}\right) \tag{4.3-35}$$

$$\nabla\rho_k^{(lj)} = \Psi_k^{(l)} - \Psi_k^{(j)} \tag{4.3-36}$$

Where $\Psi = \sqrt{(s_x - u_x)^2 + (s_y - u_y)^2 + (s_z - u_z)^2}$ is the geometric *range* between a satellite position $(s_x, s_y, s_z)$ and the receiver position $(u_x, u_y, u_z)$. Subscripts *k* and *k-1* are used to specify the epoch at which differenced measurements are computed and the superscript *lj* identify each of the monitored satellites.

The above measurement models (4.3-35) and (4.3-36) require the availability of both current and previous positions among system's states. Therefore, the state-vector considered in the Kalman filter is expanded in order to include the position at the last epoch.

$$x = \left(u_{x_k}, u_{y_k}, u_{z_k}, v_x, v_y, v_z, u_{x_{k-1}}, u_{y_{k-1}}, u_{z_{k-1}}\right) \tag{4.3-37}$$

The current and previous positions are $\left(u_{x_k}, u_{y_k}, u_{z_k}\right)$ and $\left(u_{x_{k-1}}, u_{y_{k-1}}, u_{z_{k-1}}\right)$, respectively. Consequently, the time update requires modification in order to support not only current position states but also previous ones. In this way, $\left(u_{x_k}, u_{y_k}, u_{z_k}\right)$ states will be transferred to $\left(u_{x_{k-1}}, u_{y_{k-1}}, u_{z_{k-1}}\right)$during the Kalman time update. That is, the current position after the previous update becomes the previous position after the propagation. Therefore, a modification in the conventional state transition matrix is performed as

$$A_{k,k+1} = \begin{bmatrix} 1 & 0 & 0 & \Delta t & 0 & 0 & 0 & 0 & 0 \\ 0 & 1 & 0 & 0 & \Delta t & 0 & 0 & 0 & 0 \\ 0 & 0 & 1 & 0 & 0 & \Delta t & 0 & 0 & 0 \\ 0 & 0 & 0 & 1 & 0 & 0 & 0 & 0 & 0 \\ 0 & 0 & 0 & 0 & 1 & 0 & 0 & 0 & 0 \\ 0 & 0 & 0 & 0 & 0 & 1 & 0 & 0 & 0 \\ 1 & 0 & 0 & 0 & 0 & 0 & 0 & 0 & 0 \\ 0 & 1 & 0 & 0 & 0 & 0 & 0 & 0 & 0 \\ 0 & 0 & 1 & 0 & 0 & 0 & 0 & 0 & 0 \end{bmatrix} \tag{4.3-38}$$

Additionally, new measurement matrices are also required, one for each of the above differenced measurement models stated in (4.3-35) and (4.3-36). By definition, the measurement matrix is obtained by computing the partial derivatives of the non-linear measurement equations (4.3-35) and (4.3-36) with respect to system states about a prior point, known in advance. These equations are linear combinations of the conventional pseudo-range measurement model described in (4.3-16).

Therefore, ruling out clock error states, the conventional measurement matrix at any k-th epoch can be stated as

(4.3-39)
$$H_k = \begin{bmatrix} -\frac{s_x^{(1)} - u_x^-}{\tilde{\Psi}^{(1)}} & -\frac{s_y^{(1)} - u_y^-}{\tilde{\Psi}^{(1)}} & -\frac{s_z^{(1)} - u_z^-}{\tilde{\Psi}^{(1)}} \\ -\frac{s_x^{(2)} - u_x^-}{\tilde{\Psi}^{(2)}} & -\frac{s_y^{(2)} - u_y^-}{\tilde{\Psi}^{(2)}} & -\frac{s_z^{(2)} - u_z^-}{\tilde{\Psi}^{(2)}} \\ \cdots & \cdots & \cdots \\ -\frac{s_x^{(m)} - u_x^-}{\tilde{\Psi}^{m}} & -\frac{s_y^{(m)} - u_y^-}{\tilde{\Psi}^{m}} & -\frac{s_z^{(m)} - u_z^-}{\tilde{\Psi}^{m}} \end{bmatrix}$$

where $\tilde{\Psi}^{(j)} = \sqrt{\left(s_x^{(j)} - u_x^-\right)^2 + \left(s_y^{(j)} - u_y^-\right)^2 + \left(s_z^{(j)} - u_z^-\right)^2}$ is the geometric *range* between an "*a priori*" receiver position estimate $u^-$ and the computed j-th satellite position $\left(s_x^{(j)}, s_y^{(j)}, s_z^{(j)}\right)$.

Considering the new position/velocity state-vector (4.3-37), the resultant differenced measurement matrices regarding to *double-differenced* carrier phases, stated in (4.3-35), and *single-differenced* pseudo-ranges, stated in (4.3-36), will be

(4.3-40)
$$\Delta\nabla H_k^{(lj)} = \left[H_k^{(l)} - H_k^{(j)} \quad 0 \quad 0 \quad 0 \quad -H_{k-1}^{(l)} + H_{k-1}^{(j)}\right]$$

(4.3-41)
$$\nabla H_k^{(lj)} = \left[H_k^{(l)} - H_k^{(j)} \quad 0 \quad 0 \quad 0 \quad 0 \quad 0 \quad 0\right]$$

Therefore, the resultant "noise-free" state-space measurement models for the modified Kalman filter are specified as

(4.3-42)
$$\Delta\nabla\Phi_k^{(lj)} \approx \Delta\nabla\tilde{\Phi}_k^{(lj)}\Big|_{x=x^-} + \Delta\nabla H_k^{(lj)}\left(x_k - x_k^-\right)$$

(4.3-43)
$$\nabla\rho_k^{(lj)} \approx \nabla\tilde{\rho}_k^{(lj)}\Big|_{x=x^-} + \nabla H_k^{(lj)}\left(x_k - x_k^-\right)$$

Modifications on the variance of the resultant differenced measurement errors were also considered. An example of the covariance matrix for four between-satellite differences generated by differencing the observations from a first satellite with the ones gathered from the rest of monitored satellites is shown below

(4.3-44)
$$\nabla R = \begin{bmatrix} \sigma_1^2 + \sigma_2^2 & \sigma_1^2 & \sigma_1^2 & \sigma_1^2 \\ \sigma_1^2 & \sigma_1^2 + \sigma_3^2 & \sigma_1^2 & \sigma_1^2 \\ \sigma_1^2 & \sigma_1^2 & \sigma_1^2 + \sigma_4^2 & \sigma_1^2 \\ \sigma_1^2 & \sigma_1^2 & \sigma_1^2 & \sigma_1^2 + \sigma_5^2 \end{bmatrix}$$

Therefore, the variance of the between-satellite differenced measurements is represented by a non-diagonal matrix when $\sigma_1^2$ is large compared with any $\sigma_i^2$ (for i≠1). Different satellite combinations have been considered while performing experiments on these studies, as a result, the effect of errors is reduced somewhat by choosing a high satellite as the reference in the formation of the between-satellite differences. As mentioned in chapter 3, a high satellite will have smaller noise, multipath, and atmosphere errors than a low satellite will. Therefore, a covariance with a high satellite as reference will be closer to a diagonal than the one with a low satellite as reference.

This approach was performed by following the guidelines specified in reference [4.14]. Test results are shown in chapter 5 based on the simulations developed on these studies. This scheme helps maintain position accuracy when the number of satellites in view drops below four. It also helps reduce the effect of pseudo-range errors when the observed satellites are four or more. In fact, clear improvements have been achieved in terms of the degrading effects caused by receiver clock readjustments in position estimates (see Figure 78 and Figure 79).

Furthermore, carrier-phases need only be available since the previous time epoch, rather than over the last 100 seconds or so. In range domain smoothing techniques the same satellites set must be continuously tracked for the position accuracy to be maintained and improved. This is in contrast to the position domain schemes, in which the same set of satellites need only be continuously observed since the previous time epoch. Therefore, provided that some selection of four satellites is available over every epoch, the position accuracy of the system can be maintained and improved (3 double-differenced carrier-phases and 3 single-differenced pseudo-ranges are available to compute position and velocity estimates).

In addition, the carrier-phase time differences are explicitly treated as a position difference observable, instead of other position/velocity schemes that use delta-phases as velocity estimates. Therefore, no assumptions are made about the dynamics of the vehicle and a position difference is directly observable by at least four differenced measurements.

## 4.4 Other CSC schemes

The carrier-smoothing-code filtering posed by Hatch in [4.1] and the PDP Kalman filter posed by Thomas Ford in [4.14] are good examples of algorithms that maximally utilizes the information redundancy provided by GPS to improve positioning accuracy. But these are not the unique options to combine GPS code and carrier measurements.

After the introduction of the Hatch filter in 1982, several smoothing filters have also been designed. Ron Hatch himself released improvements on these range domain schemes by using epoch-dependent smoothing weight factors. In 1986 Lachapelle [4.6] posed other methodology on which the smoothing weight factors were reduced by a constant from epoch to epoch and similar approaches were also designed by Meyerhoff and Evans in 1986 [4.7] and Hofmann-Wellenhof in 1997 [4.3]. In terms of position domain smoothing, in reference [4.12] Bisnatch and Langley described a filter called the *phase-connected filter*.

It is worth highlighting two smoothing approaches posed by P.Y.C. Hwang and R.G. Brown in references [4.11] and [4.9]. These schemes efficiently integrate GPS code and carrier measurements considering that complementary information is embedded on these observables. Both algorithms involve stochastic least-squares filter theory and are based on Kalman filters.

One of them based the estimation of the smoothed pseudo-ranges in a general linear operation processed on the two noisy GPS measurements – as illustrated in the following figure.

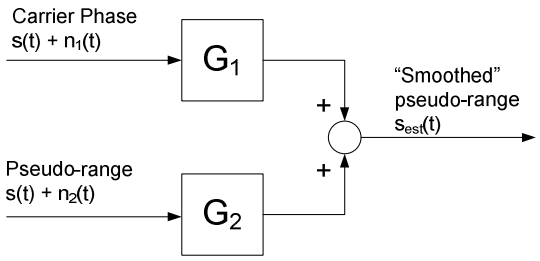


Figure 48 **Other CSC schemes - General linear measurement combination -** posed by P.Y.C. Hwang and R.G. Brown in [4.11]

The optimization problem of this general integrated filter is posed as follows: Given the mutual correlation structures of the signal and noises, what G1 and G2 will minimize the mean-square error? This is a standard Wiener or Kalman filter-type problem and the optimal model posed by Hwang and Brown is made up of 16 states that processes a pair of pseudo-range and carrier-phase measurements from each of the satellites in view. In this approach, the receiver motion is considered as being "noiselike" in character; this idea will not fit if, for example, the GPS receiver describes an intentional turn. Therefore, a second approach was posed by these researchers in order to avoid problems with deterministics inputs, this methodology is more conservative than the general linear combination. The following figure illustrates this idea.

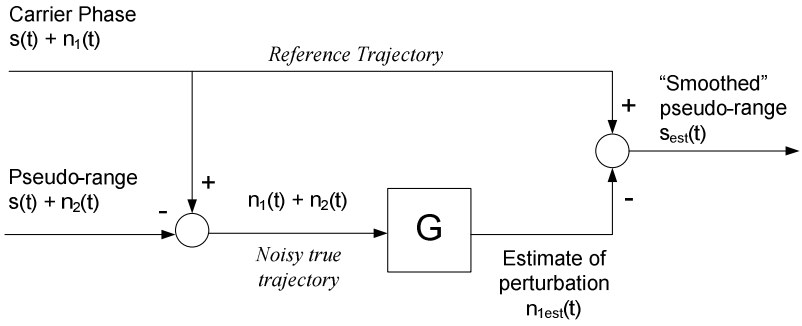


Figure 49 **Other CSC schemes - Complementary Kalman filter** combining continuous carrier-phase and pseudo-range data from GPS signal measurements - posed by P.Y.C. Hwang and R.G. Brown in [4.11] and [4.9] .

In the above illustrated complementary filter, the data provided by the carrier-phases is considered as a good reference trajectory, albeit a noisy one, and the other noisy measurement (i.e. the pseudo-ranges) is used to assist the first by providing corrections to the reference trajectory. The filter's job in this formulation is simply to estimate the perturbation affecting the reference trajectory derived from carrier-phases. Therefore, in optimizing the transfer function G it is not required assumptions about the stochastic character of the receiver's motion. According to Hwang and Brown in [4.9], an efficient way to implement this carrier-smoothing complementary filter is as a parallel bank of individual complementary filters as the one shown in Figure 49. Each filter is associated with a different observed satellite and all the filter outputs can be combined by a least-squares filter or a simple Kalman filter. According to Hwang and Brown, this method of complementary integration looks especially attractive as a mean of achieving good dynamical response while still retaining the benefits of filtering the pseudo-range data. An approach that achieves the same effect is mentioned by Thomas Ford in [4.14], in this process the previous position states from the Kalman state-vector are eliminated by reworking the gains, measurement covariance, and propagation equations to take advantage of the correlation between process noise and measurement noise that results when carrier-phase time difference is introduced as a position difference observation. The method in which the previous states are maintained was chosen while performing these studies because of its simplicity and intuitiveness.

In terms of range domain carrier-smoothing-code filters, the well-known Hatch filter was chosen to perform the experiments on this study. This algorithm is not the only one RD CSC scheme, in fact there are other approaches such as the stepwise-optimal RD filter posed by R. Rizos in the reference [4.20] and the Doppler-aided smoothing approach designed and described in [4.10] by P.Cheng in order to overcome problems due to cycle slips providing immunity to these phenomena. Additionally, motivated by the advantages of position-domain filtering compared to range-domain filtering, some references such as [4.8] posed Hatch filters that are performed in the position domain.

# Chapter 5

# Experimental Results

*"If you don't fail now and again,*
*it's a sign you're playing it safe."*

Woody Allen

The goal of this project is to study and implement different carrier-smoothing-code (CSC) schemes that blend together the “range information” contained in both code and carrier measurements in order to achieve better accuracies while computing the position of the GPS receiver.

Two different CSC approaches were considered in the performed studies. With respect to range domain (RD) smoothing algorithms, the Hatch filter stated in section 4.2 has been implemented since it has been the reference approach in these carrier-phase smoothing code pseudo-ranges techniques. In terms of position domain (PD) approaches, schemes based on Kalman filters have been considered. In that way, the modified Kalman filter expounded in section 4.3.2 has been implemented following the guidelines stated by Thomas J. Ford in references [4.14], [4.18] and [4.19]. This approach is generally called the *pseudo-range/delta-phase (PDP) Kalman filter*. Compared with other Kalman filter approaches posed by Patrick Y.C. Hwang and Robert G. Brown in references [4.11] and [4.9] , Ford’s algorithm was chosen because of its simplicity and intuitiveness.

These algorithms have been implemented with the aid of MATLAB R2006a. This computing language is extremely flexible with a wide variety of algorithm types. Furthermore, it facilitates programming environments dealing with matrix algebra.

The experiments carried out to test the positioning results were performed with real GPS data collected by a stationary receiver. The data was gathered by a GPS station located at the *E.T.S.I. Topography, Geodesy and Cartography* in Madrid (Spain) as part of a GNSS stations ensemble belonging to *Universidad Politécnica de Madrid.* Observations were taken at a rate of 1 Hz and stored in files under the *Receiver Independent Exchange Format* (RINEX) Version 2.10. These RINEX files are available as a free download on the website http://gps.topografia.upm.es/.

In this chapter, a brief description of the designed simulator is shown together with a set of test results. Position improvements are shown by means of both qualitative and quantitative experimental outcomes.

# 5.1 'Matlab GPS' Simulator

*Simulate, as defined by the* Concise Oxford Dictionary of Current English*, means to "imitate conditions of situation etc. with model, for convenience or training." Very often in the fields of science and engineering, we need to simulate a situation – just as the definition indicates – before it occurs to help us design or understand a system or its components. So it is with GPS*

Avram K. Tetewsky & Arnold Soltz – *GPS WORLD October 1998*

Because GPS simulation requires a broad spectrum of tools covering matrix algebra, digital signal processing, control theory, and navigation algorithms, a high-level programming language is desirable. MATLAB, from MathWorks, provides an easy-to-use matrix programming language that is both portable and third-party extendible. Although other simulation tools and matrix languages exist, industry and academia routinely use MATLAB for wide ranging analysis tasks in a variety of fields, including GPS.

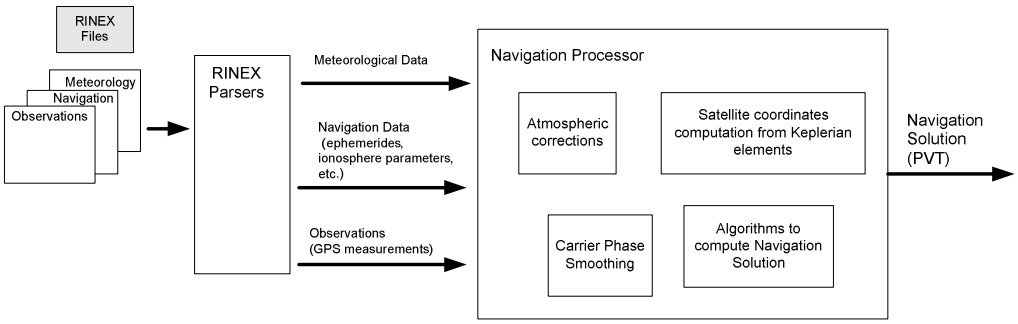


Figure 50 **Block diagram of the GPSMatlab Simulator**

In order to properly analyze the performance of the considered carrier smoothing algorithms, a set of MATLAB routines has been designed. This software allows the computation of satellites and receiver locations by processing GPS data stored under the *Receiver Independent Exchange Format* (RINEX) Version 2.10. This source code has

been developed in the Navigation Department at *Fraunhofer IIS* (Nuremberg - Germany).

Some of the features included in this software are a set of parsers to extract the GPS data stored in RINEX 2.10 files, satellite coordinates computation from Keplerian elements (broadcast on the navigation message), ionosphere and troposphere corrections on measurements, positioning algorithms to compute the navigation solution (position, velocity and time) together with carrier smoothing code pseudo-ranges (CSC) schemes. In the above Figure 50 the main components of this simulator are shown in a block diagram.

## 5.2 RD CSC experimental outcomes

As mentioned before, the range domain CSC algorithm specified in equation (4.2-12), referred to as Hatch's filter, was performed by programming a group of MATLAB simulation packages. In fact, this approach constitutes a group of parallel low pass filters (one for each satellite in view) that tries to smooth out the noise on the pseudo-ranges gathered from each of the observed satellites. The resultant "smoothed" pseudo-ranges are then the input to the navigation processor that computes position estimates by means of a conventional position/velocity Kalman filter. The following figure illustrates a conceptual view of this procedure.

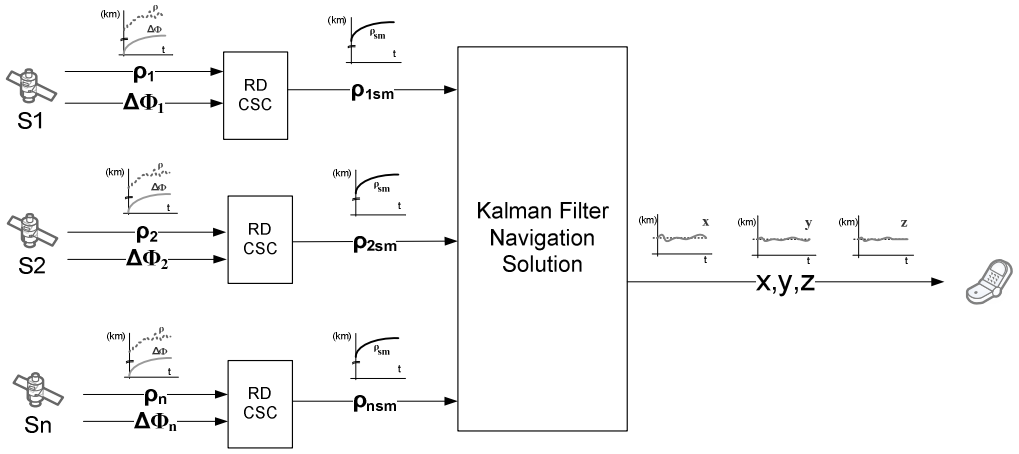


Figure 51 **Block diagram of the implemented RD CSC filtering scheme –** each RD CSC block corresponds to an individual Hatch filter.

Several experiments were carried out in order to analyze whether position accuracy is enhanced when performances are adjusted by the implemented CSC approach shown in Figure 51. Experimental outcomes were obtained by using real GPS data collected in the morning July 19, 2007 that can be downloaded freely in RINEX 2.10 files from the website http://gps.topografia.upm.es/.

The data was gathered by a stationary GPS station located at the *E.T.S.I. Topography, Geodesy and Cartography* in Madrid (Spain). Observations were taken during 6 minutes (9:00 – 9:06) at a rate of 1 Hz. A total of 8 satellites were visible in the sky during the whole observation time. In the following figure, the satellite visibility and the antenna's elevation angles are shown together with an illustrative example of the satellites layout in the sky.

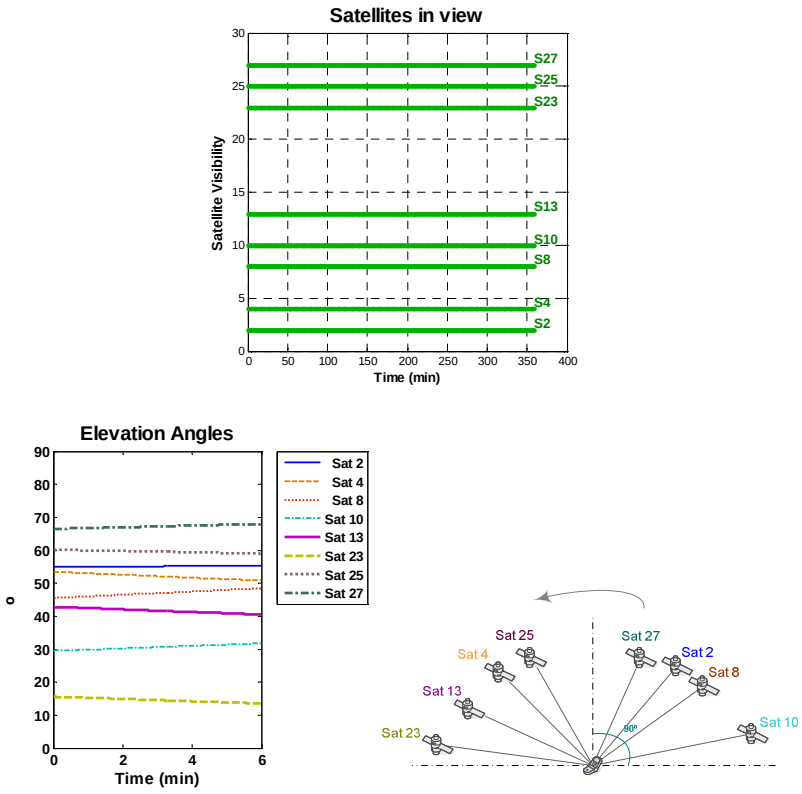


Figure 52 **July 19, 2007 Experiment - Satellites visibility and antenna's elevation angles.** Data were collected on July 19, 2007 from 9:01 to 9:06.

Since the available pseudo-range measurements are not severely affected by noise (maybe because of antenna's location or other characteristics in terms of receiver's feasibility), random noise was added on them. This random component is normally distributed with a standard deviation of 2 meters.

The navigation solution is performed by a conventional 8-state position/velocity Kalman filter that processes either unsmoothed or smoothed pseudo-ranges (atmospheric corrections are previously applied on them). The 3-D reference frame

considered for the position computation will be a Cartesian frame referred to as ECEF (Earth-Centred, Earth-Fixed) system, that is earth-centred and the earth itself remain static.

First of all, the effects on positioning when performances are adjusted by the implemented RD CSC approach are analyzed (see step 1 in Figure 53). Subsequently, this smoothing scheme will be more deeply examined by directly evaluating the effects on the filtered pseudo-range measurements (see step 2 in Figure 53). Finally, test results are summarized in order to assess if better positioning outcomes could be obtained when performances are adjusted by the implemented CSC approach.

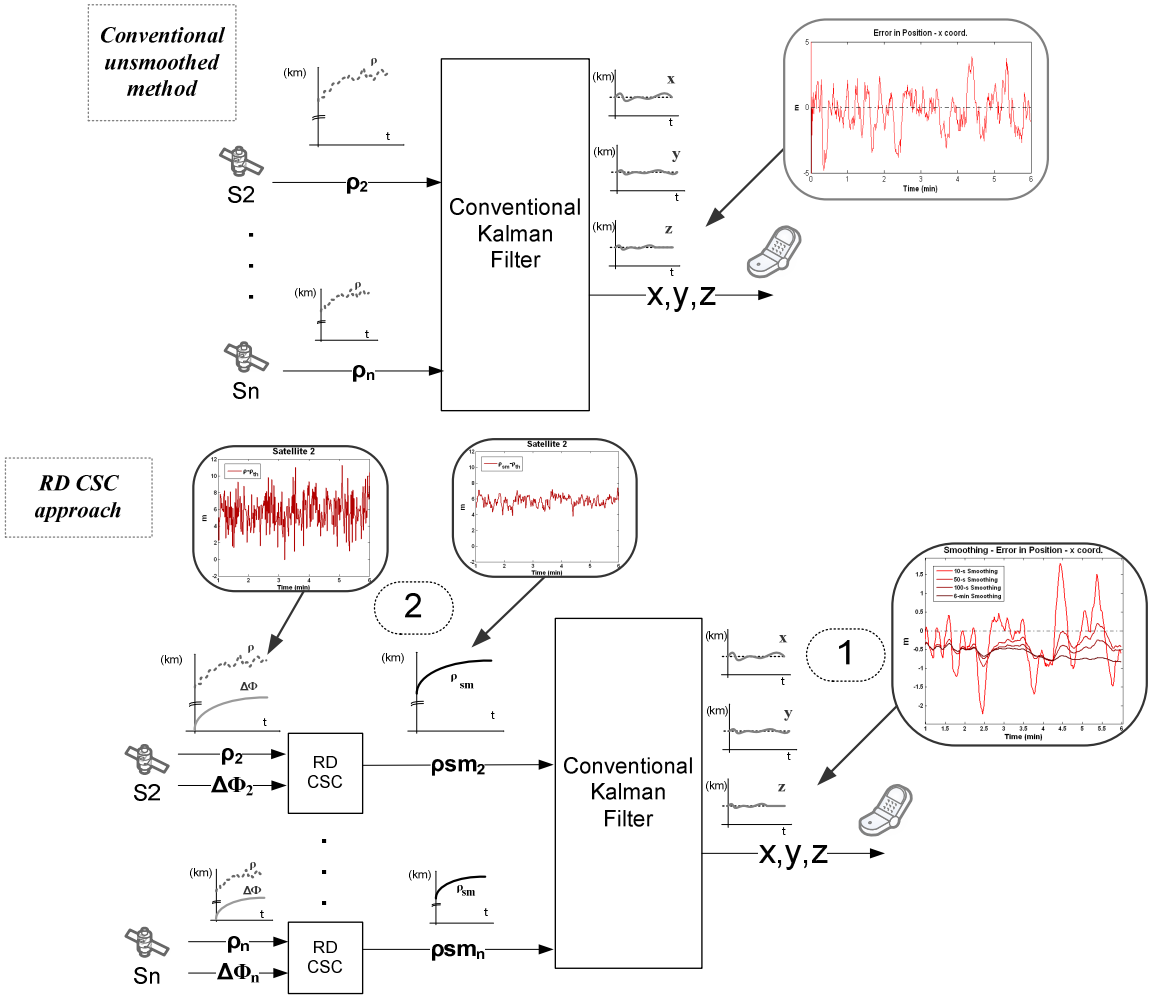


Figure 53 **Analysis performed on the implemented RD CSC scheme –** block diagrams of the conventional "unsmoothed" method (the first sketch) and the RD CSC method.

### 5.2.1 RD CSC effects on positioning

A position approximation for the GPS station that collects the measurements is available among the RINEX data. In order to properly analyze the effects of the implemented RD CSC schemes over position estimates, the resultant three-dimensional navigation solution was compared with this RINEX location to obtain a *positioning error profile* - as shown in the following figure.

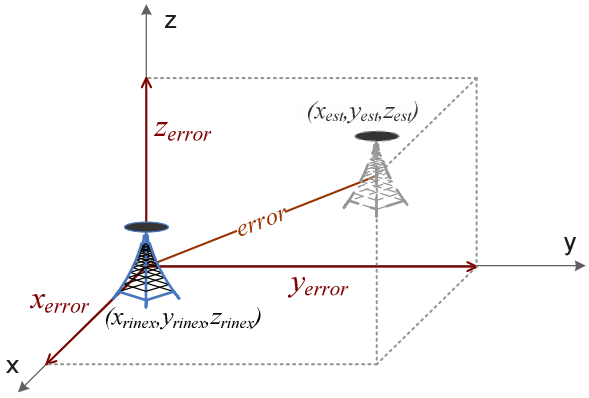


Figure 54 **Positioning error profile** considering the location approximation stored in RINEX files.

Test results performed by processing the GPS data collected in the morning July 19, 2007 are shown in Figure 55 and Figure 56. In fact, the errors in the estimation of each position coordinate ($x_{error}$, $y_{error}$ and $z_{error}$) are illustrated by means of graphics. Additionally, mean and standard deviations were also evaluated for the first and last sets of 120 samples. The first minute of observations was not considered in order to avoid possible system instabilities caused in the initialization. Considering that the measurements were taken at a rate of 1 Hz, the first and the last 120 samples correspond to the first and the last 2 minutes of observations (9:01-9:03 and 9:04-9:06). Numerical outcomes are also attached in the tables below the graphics.

First of all, the error in position estimates achieved when performances were adjusted by the *conventional "unsmoothed" method* is shown in Figure 55. The mean error in

positioning and its standard deviation were evaluated in terms of the outcomes derived from each position coordinate, as stated in the following mathematical expressions

(5.2-1) $$\mu_{error} = \sqrt{\mu_e(x)^2 + \mu_e(y)^2 + \mu_e(z)^2} \qquad \sigma_{error} = \sqrt{\sigma_e(x)^2 + \sigma_e(y)^2 + \sigma_e(z)^2}$$

being $\mu_e(x)$, $\mu_e(y)$, $\mu_e(z)$ the mean errors in position estimation for each Cartesian coordinate and $\sigma_e(x)$, $\sigma_e(y)$, $\sigma_e(z)$ the respective standard deviations. The mean error in position, denoted by $\mu_{error}$, is in the range of 1-2.2 metres and its standard deviation, denoted by $\sigma_{error}$, does not exceed 1.2 metres – see the following figure.

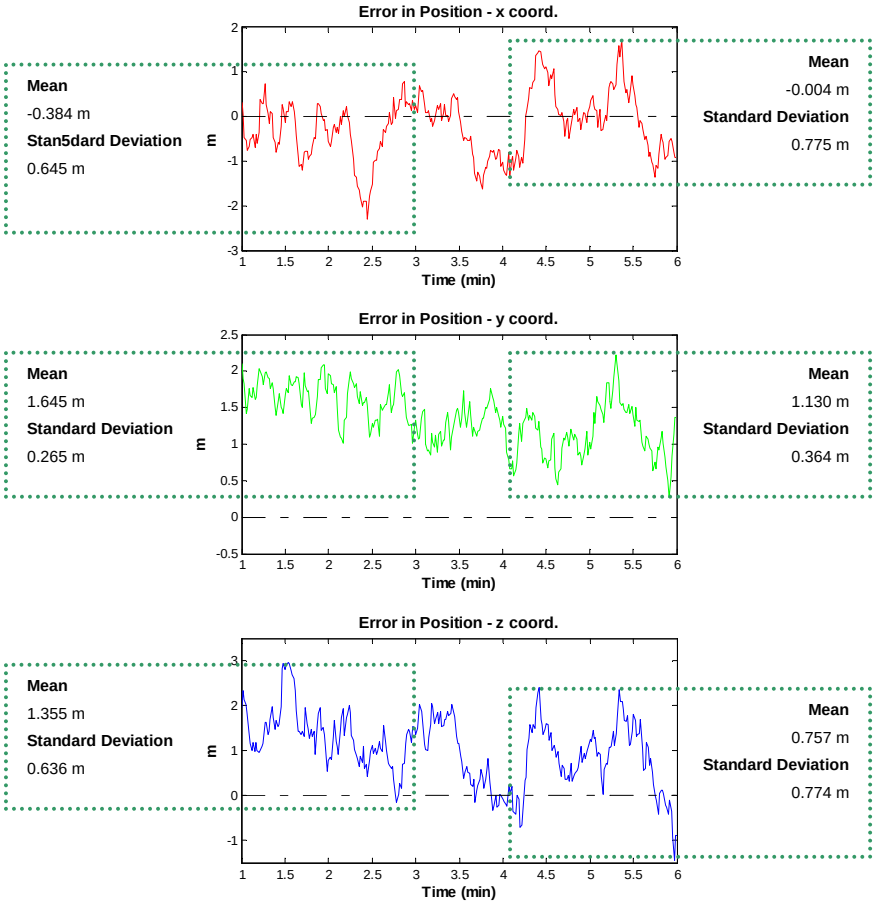


| July 19, 2007 9:00 – 9:06 | Error in position estimation | | | |
|---|---|---|---|---|
| | 9:01-9:03 | | 9:04-9:06 | |
| | $\mu_{error}$ | $\sigma_{error}$ | $\mu_{error}$ | $\sigma_{error}$ |
| **Unsmoothed** | 2.166 m | 0.944 m | 1.360 m | 1.154 m |

Figure 55 **July 19, 2007 Experiment - Error in the 3D stationary positioning solution derived from unsmoothed pseudo-ranges** taken on July 19, 2007 from 9:01 to 9:06.

In addition, Figure 56 embodies the error profiles obtained when performances were adjusted in order to smooth pseudo-range measurements by applying the implemented RD CSC approach illustrated in Figure 51. In fact, different maxima in the smoothing interval were considered in order to avoid the effects of code-carrier divergence, as mentioned in chapter 4. It is worth recalling that the concept of "maximum smoothing interval" refers to the period of time while pseudo-ranges, taken from a particular satellite, are smoothed in a continuous basis. This time interval is generally fixed in a maximum according to the time it takes the code-carrier divergence to become noticeable in terms of positioning (reference [3.1] mentioned a maximum in 100 seconds). When this maximum interval is achieved for a particular satellite, the smoothing process is reset, but only in the case of that satellite. As the implemented RD CSC filtering scheme (i.e. the Hatch filter) improves with time, the reset implies a loss of quality due to the return to the initial point of the smoothing process; this is in fact one of the drawbacks in this carrier-smoothing-code scheme.

The maximum smoothing intervals took 10 seconds, 50 seconds, 100 seconds and 6 minutes, that is, the whole observation time period (from 9:00 to 9:06). Mean and standard values of error in each position coordinate were likewise evaluated and the general positioning results derived from the mathematical expressions (5.2-1) are also shown in the table above the graphics.

The results of integrating carrier-phase measurements with code pseudo-ranges can be seen by comparing the plots shown in both figures (Figure 56 and Figure 55). Fluctuations in positioning error are reduced from almost one metre to a few centimetres when RD CSC schemes are applied on pseudo-ranges (see the evaluated standard deviations in tables above graphics). The mean error in positioning, however, slightly increases except in the case of smoothing intervals that last 50 seconds, 100 seconds, and 6 minutes (during the first 2-minutes interval). In these cases, the mean error is reduced below 2 metres.

In addition, in the last minutes of observations, it can be observed the effect of code-carrier divergence over the estimation of position since de error profile for the first and

second Cartesian coordinates (i.e. *x* and *y* graphics) slightly deviates from the "zero error".

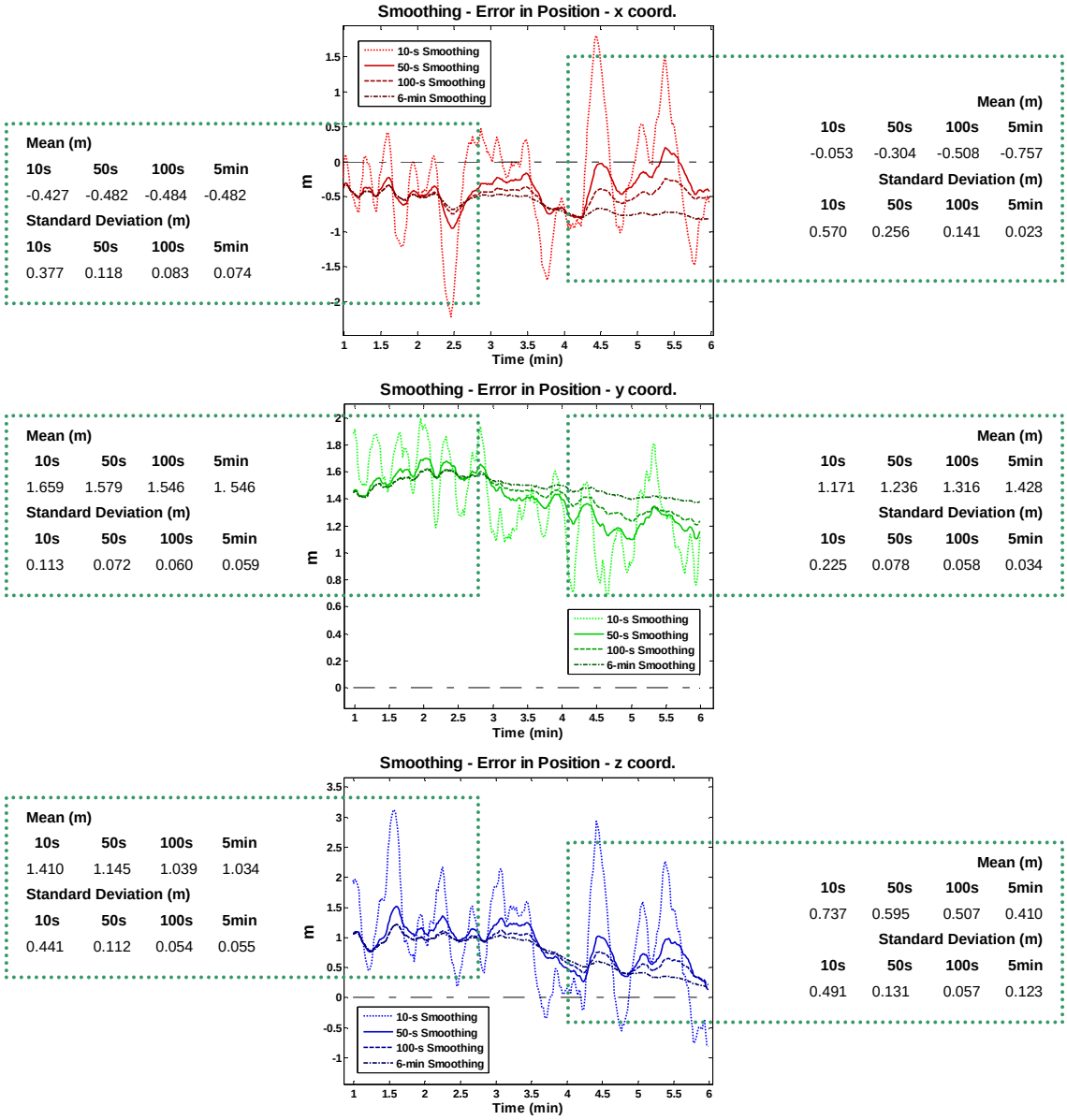


| July 19, 2007 9:00 – 9:06 | Error in position estimation | | | |
|---|---|---|---|---|
| | 9:01-9:03 | | 9:04-9:06 | |
| | $\mu_{error}$ | $\sigma_{error}$ | $\mu_{error}$ | $\sigma_{error}$ |
| **Unsmoothed** | 2.166 m | 0.944 m | 1.360 m | 1.154 m |
| **10 s RD CSC** | 2,219 m | 0.591 m | 1.385 m | 0.785 m |
| **50 s RD CSC** | 2.009 m | 0.179 m | 1.405 m | 0.298 m |
| **100 s RD CSC** | 1.925 m | 0.116 m | 1.499 m | 0.162 m |
| **6 min RD CSC** | 1.921 m | 0.110 m | 1.667 m | 0.130 m |

Figure 56 **July 19, 2007 Experiment - Error in the 3D stationary positioning solution derived from smoothed pseudo-range measurements** (from 9:01 to 9:06) – Different maximums for the smoothing interval were considered: 10 seconds, 50 seconds, 100 seconds and 6 minutes.

Now compare the statistical values derived from the positioning outcomes shown in Figure 56 and Figure 55. The following tables show the improvements achieved with respect to the outcomes derived from the conventional "unsmoothed" method - illustrated in Figure 55. Even when just the maximum smoothing interval lasts 10 seconds, the standard deviation of error in position, denoted by $\sigma_{error}$, decreases 30 percent approximately compared with the one obtained in the conventional "unsmoothed" method. In fact, these reductions reach values up to 88 percent when applying the largest feasible smoothing interval (in the case of these studies, this period corresponds to 6 minutes, that is, the whole observation interval). Hence, the original position error fluctuations, that reach almost one metre, are "smoothed" till they reach a few centimetres – see $\sigma_{error}$ values.

| **July 19, 2007 9:01-9:03 (120 samples)** | **Error in position estimation** | | | |
|---|---|---|---|---|
| | **$\mu_{error}$ (m)** | | **$\sigma_{error}$ (m)** | |
| **Unsmoothed** | 2,166 | **Improvement regarding unsmoothed** | 0,944 | **Improvement regarding unsmoothed** |
| **10 s RD CSC** | 2,219 | ↑ -2,45 % ☹ | 0,591 | ↓ 37,39 % ☺ |
| **50 s RD CSC** | 2,009 | ↓ 7,25 % ☺ | 0,179 | ↓ 81,04 % ☺ |
| **100 s RD CSC** | 1,925 | ↓ 11,13 % ☺ | 0,116 | ↓ 87,71 % ☺ |
| **5 min RD CSC** | 1,921 | ↓ 11,31 % ☺ | 0,110 | ↓ 88,35 % ☺ |

Table 5.1 **Mean values of error in the 3D smoothed stationary positioning solution computed on July 19, 2007 from 9:01 to 9:03 – 120 samples.**

| **July 19, 2007 9:04-9:06 (120 samples)** | **Error in position estimation** | | | |
|---|---|---|---|---|
| | **$\mu_{error}$ (m)** | | **$\sigma_{error}$ (m)** | |
| **Unsmoothed** | 1,360 | **Improvement regarding unsmoothed** | 1,154 | **Improvement regarding unsmoothed** |
| **10 s RD CSC** | 1,385 | ↑ -1,84 % ☹ | 0,785 | ↓ 31,98 % ☺ |
| **50 s RD CSC** | 1,405 | ↑ -3,31 % ☹ | 0,298 | ↓ 74,18 % ☺ |
| **100 s RD CSC** | 1,499 | ↑ -10,22 % ☹ | 0,162 | ↓ 85,96 % ☺ |
| **5 min RD CSC** | 1,667 | ↑ -22,57 % ☹ | 0,130 | ↓ 88,73 % ☺ |

Table 5.2 **Mean values of error in the 3D smoothed stationary positioning solution computed on July 19, 2007 from 9:04 to 9:06 – 120 samples.**

As it was mentioned before, the larger the smoothing interval, the more efficient smoothing would be achieved, that is, more pseudo-range noise would be filtered out. The experimental outcomes shown in the above tables verify this statement, that is, standard deviations of error (i.e $\sigma_{error}$) decrease more and more when the maximum smoothing interval is enlarged.

In contrast, the mean error in positioning, denoted by $\mu_{error}$, do not generally improves with respect to one derived from the conventional "unsmoothed" method (see 0 and 0). Small improvements, around 11 percent, are achieved in the first set of 120 samples (i.e. the first minutes of observations from 9:01 to 9:03). In contrast, in the last 2-minutes time interval the mean error increases more and more as the filter's length is enlarged. This effect might be caused, as mentioned before, by the cumulative effect of code-carrier divergence on the smoothed pseudo-ranges.

## 5.2.2 RD CSC effects on pseudo-ranges

Let's analyze more deeply the RD CSC approach that was performed to achieve the test results shown in previous section 5.2.1.

(5.2-2)
$$\rho_{sm}(t_k) = \frac{1}{M}\rho(t_k) + \frac{M-1}{M}[\rho_{sm}(t_{k-1}) + (\Phi(t_k) - \Phi(t_{k-1}))]$$
$$\rho_{sm}(t_0) = \rho(t_0)$$

This filtering scheme corresponds to an *estimator*. In statistics, an estimator is a function of an "observable sample" that is used to predict the values of an "unknown parameter". In this case, the observable samples are the pseudo-ranges, denoted by ρ, and the carrier-phase, denoted by Φ. In addition, the unknown parameter to be estimated is the smoothed pseudo-range referred to as $\rho_{sm}$.

Ideally, the perfect estimator would have the true "ideal" pseudo-range as expected value, that is, the geometric range corrupted by receiver and satellite clock errors.

(5.2-3)
$$\rho^{(j)} = \sqrt{\left(s_x^{(j)} - u_x\right)^2 + \left(s_y^{(j)} - u_y\right)^2 + \left(s_z^{(j)} - u_z\right)^2} + c.b_r - c.b_s^{(j)}$$

where $(s_x^{(j)}, s_y^{(j)}, s_z^{(j)})$ is the satellite position for a certain *j* satellite, receiver's location corresponds to $(u_x, u_y, u_z)$ and satellite and receiver clock errors are denoted by $c.b_r$ and $c.b_s^{(j)}$. This ideal pseudo-range profile is not available on these studies. Anyway, let's analyze which are the GPS parameters that are available in these studies; maybe, it is possible to obtain a proper "theoretical" pseudo-range profile that approaches the ideal model defined in equation (5.2-3).

*Firstly*, as it was previously mentioned, a position approximation of the GPS station that collects the measurements is stored in the processed RINEX files. Therefore, this information can be used as receiver's location $(u_x, u_y, u_z)$ in equation (5.2-3). Furthermore, the computation of satellite positions and their clock errors is performed within the routines of the "*GPS Matlab Tool*" used in these studies – see Figure 50.

These parameters are necessary to estimate the receiver's location by means of Kalman filtering and are obtained by using the navigation data that satellites broadcast embedded on L1 and L2 frequencies. Hence, estimates of the terms $(s_x^{(j)},s_y^{(j)},s_z^{(j)})$ and $c.b_s^{(j)}$ of the model stated in equation (5.2-3) are also available. In addition, the receiver clock error estimated by the 8-state Kalman filter can also be considered as the term $c.b_r$. Therefore, a "theoretical" pseudo-range can be obtained by processing all these parameters according to equation (5.2-3).

In the following figures, an illustrative example brings face to face an ensemble of measured pseudo-ranges, the respective "theoretical" profile and the resultant "smoothed" pseudo-ranges obtained when the maximum Hatch filter smoothing interval was set to 100 seconds. These test results were obtained by considering the GPS data gathered from a satellite observed in the morning July 19, 2007 (satellite 2 - see satellite visibility in Figure 52). Measured $\rho$, smoothed $\rho_{sm}$ and theoretical $\rho_{th}$ pseudo-ranges are seemingly equivalent. To check this fact, the differences in between were also evaluated.

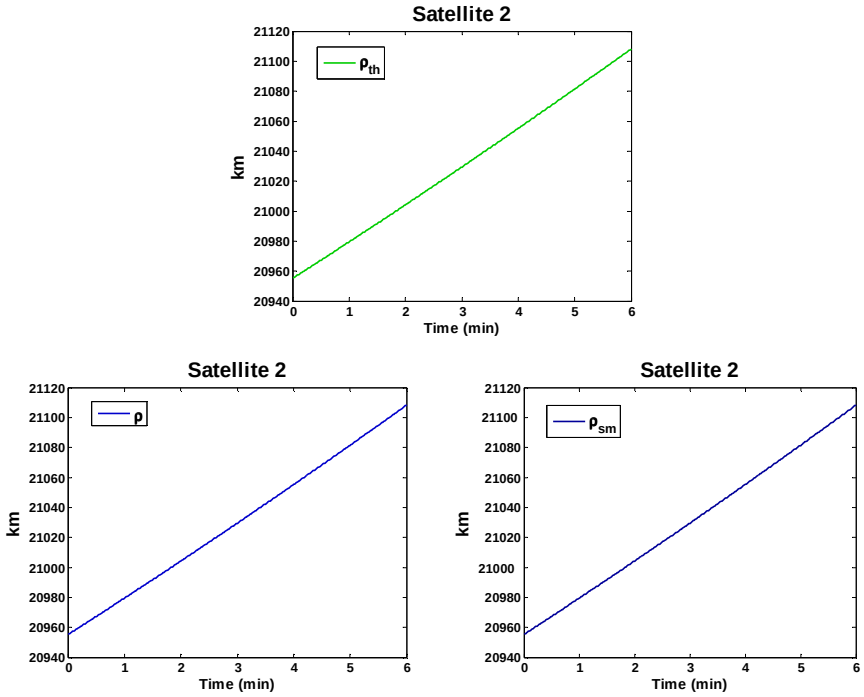


Figure 57 **July 19, 2007 Experiment - Measured (ρ), smoothed ($\rho_{sm}$) and theoretical ($\rho_{th}$) pseudo-ranges.** Relation between these three quantities. Example based on measurements gathered from a satellite that was observed on July 19, 2007 from 9:00 to 9:06.

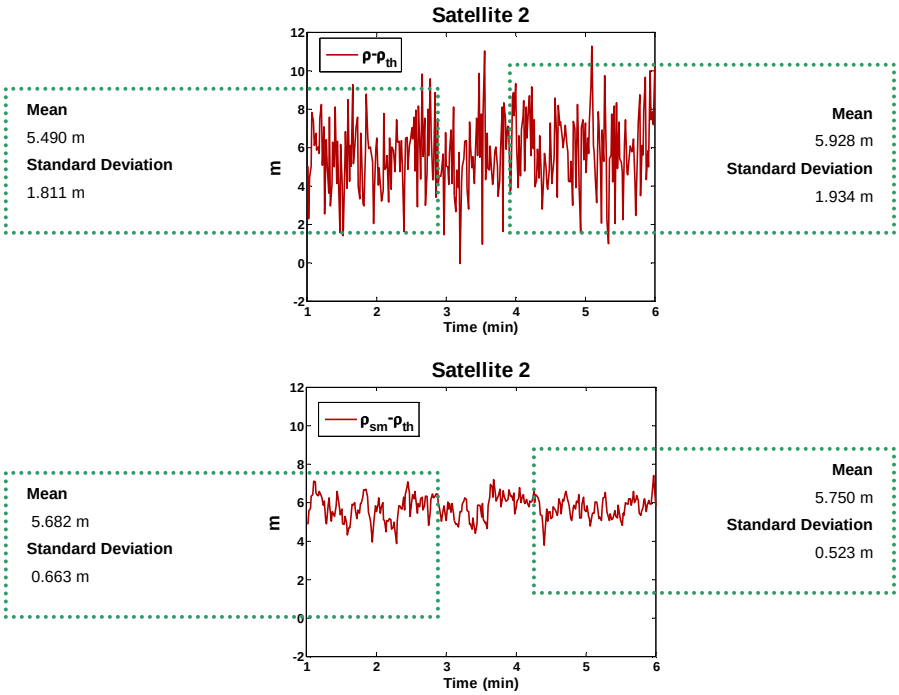


Figure 58 **July 19, 2007 Experiment - Measured (ρ), smoothed ($\rho_{sm}$) and theoretical ($\rho_{th}$) pseudo-ranges –** Differences between these three quantities. Example based on measurements gathered from a satellite that was observed on July 19, 2007 from 9:00 to 9:06.

As expected, the resultant theoretical pseudo-ranges $\rho_{th}$ do not exactly match with the measured and smoothed ones since the differences $\rho$-$\rho_{th}$ $\rho_{tsm}$-$\rho_{th}$ are not exactly zero; these are the consequences of all the inherent biases and noises affecting measurements. The signal $\rho$-$\rho_{th}$ is seemingly mainly conformed by noise and a "bias" component that remains fix around 5-6 metres.

Some aspects must be taken into account. *Firstly*, it has to be considered how accurate are the parameters used to derive the "theoretical" pseudo-ranges (i.e. approximations of the true expected value in the estimation of smoothed pseudo-ranges). In fact, satellite position and their clock errors are estimated by taking into consideration navigation parameters broadcast on satellite signals. These parameters are quite reliable because they are updated by the GPS control segment twice a day. The receiver's clock error is estimated by the navigator processor itself (i.e. the Kalman filter). And the receiver's location is derived from RINEX data. It is obvious that all these quatities are just

approximations to the real values and, therefore, their processing imply a residual error. However, in these studies it was not possible to quantify this residual error.

*Secondly*, the "measured pseudo-ranges" $\rho$ (filtered in the implemented RD CSC scheme defined in (5.2-2) in order to estimate the smoothed pseudo-ranges) are corrupted not only by clock errors but also by atmosphere effects (ionosphere and troposphere) together with multipath and receiver noise. In GPS references, atmosphere effects are considered as "slow variations" (i.e. low frequency components), except in the case of atmosphere scintillations. In contrast, multipath and measurement noise are considered in these studies as time uncorrelated processes, that is, quick variations over time (i.e. high frequency components). The RD CSC Hatch filter defined in (5.2-2) corresponds to a low pass filter, that is, the high frequency "undesirable" components affecting pseudo-ranges will be filtered out with the aid of a "reference signal" that contains lower high frequency noise levels (i.e. the carrier-phases Φ). Therefore, any low-frequency component inherent in pseudo-ranges (i.e. biases like ionosphere and atmosphere effects and clock errors) will not be removed and will remain present on the smoothed pseudo-ranges.

Let's develop the mathematical theory that may define what happened on measurements illustrated in Figure 57 and Figure 58. As mentioned before, the "theoretical" pseudo-ranges were computed as

$$\rho_{th} = \sqrt{(s_x - u_x)^2 + (s_y - u_y)^2 + (s_z - u_z)^2} + c.b_r - c.b_s + \upsilon_{th} \qquad (5.2\text{-}4)$$

where the parameters $(s_x^{(j)}, s_y^{(j)}, s_z^{(j)})$ and $(u_x, u_y, u_z)$ correspond the real satellite position for a certain $j$ satellite and the real receiver's location, respectively. Satellite and receiver clock errors are identified by $c.b_r$ and $c.b_s^{(j)}$. In addition, the term $\upsilon_{th}$ denotes the residual error committed by considering approximation to the real values of these parameters.

In chapter 3 (section 3.2.5), the "measured" pseudo-ranges were defined by a mathematical model stated as

$$\rho = \sqrt{(s_x - u_x)^2 + (s_y - u_y)^2 + (s_z - u_z)^2} + c.(b_r - b_s) + I + T + \rho_{noise} \quad (5.2\text{-}5)$$

where $I$ and $T$ denote the atmosphere errors caused in measurements due to the fact that GPS signals went through the ionosphere and the troposphere. Furthermore, the term $\rho_{noise}$ corresponds to multipath and measurement noise together with other unmodeled error sources.

Hence, the differences $\rho$-$\rho_{th}$ shown in Figure 58 can be mathematically defined by the following equation

$$\rho - \rho_{th} = I + T + \rho_{noise} - \upsilon_{th} \quad (5.2\text{-}6)$$

As mentioned before, atmosphere effects, denoted by $I$ and $T$, are generally considered as low frequency components, as well as the residual error $\upsilon_{th}$ . Therefore, the term that is expected to be suppressed or at least reduced is the one regarding to the noise affecting the measured pseudo-ranges, denoted by $\rho_{noise}$. In fact, this is the term that is normally a hundredth greater than the one affecting carrier phases, as mentioned in chapter 4 (section 4.2). Consequently, the term $\rho_{noise}$ will be the one that suffers the effects of the applied RD CSC schemes

It is worth highlighting that atmosphere models are considered within the routines of the "*GPS Matlab Tool*" used in these studies (see Figure 50) in order to compute some corrections in the pseudo-range measurements before they are processed to derive the navigation solution. For example, the corrections that were applied on pseudo-ranges taken from the satellite 2 (previously mentioned Figure 57 and Figure 58) are illustrated in the following figure.

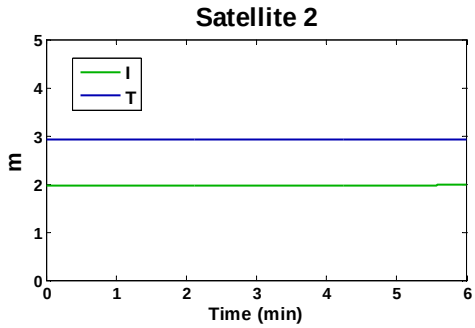


Figure 59 **July 19, 2007 Experiment - Ionosphere (I) and troposphere corrections (T) applied on pseudo-ranges processed to compute the navigation solution.** Example based on measurements gathered from a satellite that was observed on July 19, 2007 from 9:00 to 9:06.

The atmosphere corrections shown in the figure above add up to 5 metres approximately. In these studies, these corrections were considered in the mathematical model (5.2-6) to derive an approximation of the measurement error profile affecting pseudo-ranges that is filtered out when performances are adjusted by the implemented RD CSC approaches. In the following figure, test results derived from the measurements shown in Figure 57 and Figure 58 are displayed.

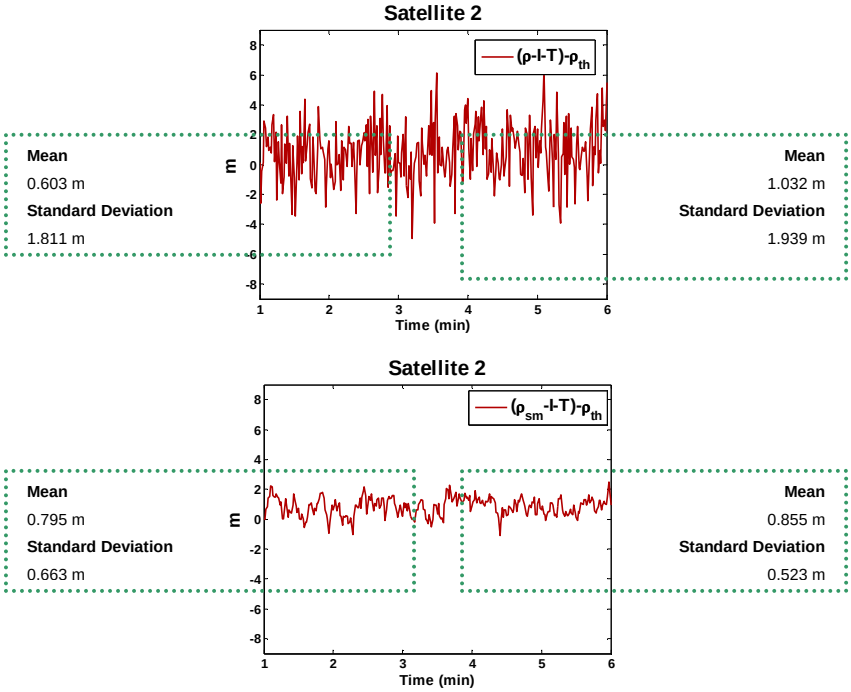


| July 19, 2007 9:00 - 9:06 | Satellite 2: Comparison measured/theoretical pseudo-ranges (ρ-I-T)-$\rho_{th}$ | | | |
|---|---|---|---|---|
| 120 samples | 9:01-9:03 | | 9:04-9:06 | |
| | Mean (m) | Standard Deviation (m) | Mean (m) | Standard Deviation (m) |
| Unsmoothed | 0.603 | 1.811 | 1.032 | 1.939 |
| RDCSC 10 s | 0.664 | 0.731 | 0.978 | 0.652 |
| RDCSC 50 s | 0.748 | 0.671 | 0.874 | 0.522 |
| RDCSC 100 s | 0.795 | 0.663 | 0.855 | 0.523 |
| RDCSC 5 min | 0.802 | 0.664 | 0.861 | 0.526 |

Figure 60 **July 19, 2007 Experiment – Measured/Theoretical pseudo-ranges residuals** obtained by subtracting measured ρ from theoretical $\rho_{th}$ pseudo-ranges and applying atmosphere corrections. Example taken from satellite that was observed on July 19, 2007 from 9:00 to 9:06. Effects while applying a 100s RD CSC scheme are shown by means of graphics and numerical outcomes.

Compare the values of standard deviations shown in the table above. As the maximum smoothing interval is enlarged, standard deviations decrease more and more, i.e. more undesirable high frequency components (or noise) are suppressed. This fact reflects the effects of the performed low-pass CSC filtering schemes. By definition, the filter pass band becomes narrower when the filter's window (i.e. the smoothing interval) expands; hence more high frequency noise components will be suppressed. However, mean values are not zero. In the first minutes of observations, the mean values grow as filter length is enlarged; nevertheless, in the case of the last minutes, they are reduced up to two centimetres.

The test results obtained from the rest of satellites visible in the sky are shown in the Figure 61. The improvement regarding standard deviations of error in measurements (i.e the fluctuations) is up to 65 percent in the first minutes of observations and even 73 percent during the last minutes. In fact, these fluctuations are reduced from almost 2 metres to half metre. However, the mean values are not zero and decrease a few decimetres just during the first minutes of experiments. This effect might be caused by the cumulative effect of ionosphere and troposphere delays.

| **July 19, 2007 9:01 - 9:03** | **Comparison measured/theoretical pseudo-ranges (ρ-I-T)-$\rho_{th}$** | | | | | | | | | |
|---|---|---|---|---|---|---|---|---|---|---|
| | **Means in absolute value (m)** | | | | | | | | | |
| **Satellite** | **2** | **4** | **8** | **10** | **13** | **23** | **25** | **27** | **Average** | |
| **Unsmoothed** | 0.603 | 0.494 | 1.576 | 1.967 | 2.007 | 1.216 | 0.510 | 1.779 | 1.269 | **Improvement regarding unsmoothed** |
| **RDCSC 10 s** | 0.664 | 0.443 | 1.576 | 1.972 | 2.095 | 1.245 | 0.511 | 1.790 | 1.287 | ↑ -1.42 % ☹ |
| **RDCSC 50 s** | 0.748 | 0.355 | 1.428 | 1.916 | 2.168 | 1.113 | 0.372 | 1.880 | 1.248 | ↓ 1.69 % ☺ |
| **RDCSC 100 s** | 0.795 | 0.269 | 1.352 | 1.876 | 2.180 | 1.051 | 0.356 | 1.913 | 1.224 | ↓ 3.54 % ☺ |
| **RDCSC 5 min** | 0.802 | 0.263 | 1.333 | 1.865 | 2.200 | 1.046 | 0.354 | 1.911 | 1.222 | ↓ 3.72 % ☺ |
| | **Standard Deviations (m)** | | | | | | | | | |
| **Unsmoothed** | 1.810 | 1.791 | 1.910 | 2.040 | 1.953 | 2.150 | 1.758 | 2.072 | 1.936 | **Improvement regarding unsmoothed** |
| **RDCSC 10 s** | 0.731 | 0.628 | 0.748 | 0.604 | 0.938 | 0.604 | 0.778 | 0.803 | 0.729 | ↓ 62.33 % ☺ |
| **RDCSC 50 s** | 0.671 | 0,664 | 0.734 | 0.666 | 0.744 | 0.640 | 0.690 | 0.697 | 0.688 | ↓ 64.44 % ☺ |
| **RDCSC 100 s** | 0.663 | 0.666 | 0.710 | 0.668 | 0.704 | 0.648 | 0.679 | 0.678 | 0.677 | ↓ 65.03 % ☺ |
| **RDCSC 5 min** | 0.664 | 0.666 | 0.700 | 0.666 | 0.694 | 0.652 | 0.679 | 0.675 | 0.674 | ↓ 65.16 % ☺ |
| **July 19, 2007 9:04 - 9:06** | **Comparison measured/theoretical pseudo-ranges (ρ-I-T)-$\rho_{th}$** | | | | | | | | | |
| | **Means in absolute value (m)** | | | | | | | | | |
| **Satellite** | **2** | **4** | **8** | **10** | **13** | **23** | **25** | **27** | **Average** | |
| **Unsmoothed** | 1.032 | 0.398 | 1.104 | 1.894 | 1.241 | 0.060 | 0.380 | 2.093 | 1.025 | **Improvement regarding unsmoothed** |
| **RDCSC 10 s** | 0.978 | 0.377 | 1.139 | 1.880 | 1.255 | 0.104 | 0.408 | 2.085 | 1.028 | ↑ -0.26 % ☹ |
| **RDCSC 50 s** | 0.874 | 0.407 | 1.260 | 1.934 | 1.317 | 0.396 | 0.400 | 2.118 | 1.088 | ↑ -6.15 % ☹ |
| **RDCSC 100 s** | 0.855 | 0.423 | 1.380 | 1.986 | 1.443 | 0.612 | 0.342 | 2.157 | 1.150 | ↑ -12.12 % ☹ |
| **RDCSC 5 min** | 0.861 | 0.446 | 1.526 | 2.055 | 1.643 | 0.871 | 0.249 | 2.206 | 1.232 | ↑ -20.15 % ☹ |
| | **Standard Deviations (m)** | | | | | | | | | |
| **Unsmoothed** | 1.938 | 2.022 | 1.740 | 2.002 | 2.310 | 2.052 | 2.019 | 1.989 | 2.009 | **Improvement regarding unsmoothed** |
| **RDCSC 10 s** | 0.652 | 0.459 | 0.581 | 0.438 | 0.636 | 0.477 | 0.773 | 0.757 | 0.597 | ↓ 70.30 % ☺ |
| **RDCSC 50 s** | 0.522 | 0.483 | 0.570 | 0.487 | 0.522 | 0.485 | 0.561 | 0.571 | 0.525 | ↓ 73.87 % ☺ |
| **RDCSC 100 s** | 0.523 | 0.507 | 0.560 | 0.511 | 0.523 | 0.507 | 0.543 | 0.547 | 0.528 | ↓ 73.74 % ☺ |
| **RDCSC 5 min** | 0.526 | 0.523 | 0.545 | 0.527 | 0.526 | 0.518 | 0.534 | 0.535 | 0.529 | ↓ 73.66 % ☺ |

Figure 61 **July 19, 2007 Experiment – Comparison between measured $\rho$ and theoretical $\rho_{th}$ pseudo-ranges when atmosphere corrections are applied –** measurements were taken on July 19, 2007 from 9:00 to 9:06. The considered samples were collected on the time periods 9:01-9:03 and 9:04-9:06. A total of eight satellites were visible in the sky. Different RD CSC schemes were applied on measured pseudo-ranges (10s, 50s, 100s and 5min).

*The considered RD CSC estimator defined in (5.2-2) would be ideal* if the measurement error $\rho - I - T - \rho_{th} = \rho_{noise} - \upsilon_{th}$ is zero, that is, the difference between the estimator's expected pseudo-range (i.e. the theoretical one) and the true achieved quantity (i.e. the smoothed pseudo-range) is zero – considering the applied atmosphere corrections. However, the experimental mean values of this error are not zero (see the tables above) and the implemented RD CSC estimator might not be ideal. This kind of estimators is called *biased estimator* in terms of statistics; in fact, the difference between expected estimates and the true ones is referred to as the *bias.*

### 5.2.3 RD CSC positioning outcomes

Several experiments were performed in order to assess if better positioning results could be obtained when performances are adjusted by the implemented RD CSC approach previously shown in Figure 51.

The processed measurements were collected during the same observation time interval in different days of May and June 2007. In fact, the observation periods lasted 5 minutes (from 9:00 to 9:05 in the morning). As well as experiments shown in sections 5.2.1 and 5.2.2, these measurements were real and the GPS station that gathered them is the same that the one considered in previous studies. The sampling rate was 1 Hz and the first minute of observations was disregarded to avoid possible system instabilities during the initialization of the navigation procedure.

First of all, a qualitative analysis was performed by outlining the error in position estimates and directly observing if better positioning results were obtained when performing the RD CSC approaches. The error in position was evaluated as the geometric distance between the estimated receiver's location and the approximation provided by the processed RINEX files – as illustrated previously in Figure 54 and computed according to the following mathematical equation

$$error = \sqrt{(x_{est} - x_{rinex})^2 + (y_{est} - y_{rinex})^2 + (z_{est} - z_{rinex})^2} \quad (5.2\text{-}7)$$

where the estimation of receiver's position is denoted by $(x_{est}, y_{est}, z_{est})$ and the RINEX reference receiver's location is $(x_{rinex}, y_{rinex}, z_{rinex})$. The resultant experiment outcomes are shown in the following figures. The error in position was rarely above 3.5 metres; even in some cases was up to 1.5 metres. Furthermore, when performances are adjusted by the implemented RD CSC scheme, the fluctuations in positioning error are considerably reduced – specifically in the cases of applying larger smoothing intervals (50s, 100s and 5 min). It seems that the best results are achieved when the maximum smoothing interval was set to 100s or 5 minutes.

Secondly, a quantitative analysis was also performed by evaluating the mean error in position for each minute of observations. The improvements are small; anyway the mean error is generally reduced a few decimetres or centimetres when performances are adjusted by the implemented RD CSC schemes.

In fact, the maximum improvements are achieved when smoothing intervals extended up to 50 or 100 seconds – with respect to 5 minutes, the mean error is slightly increased in four of the eight experiments.

The fluctuations in position error are also “smoothed” with the aid of the RD CSC algorithms. As mentioned before, the fluctuations decreased as the smoothing interval is enlarged. This aspect verifies the time effectiveness of this CSC procedure; however, the slight increases on the mean error limit the considered smoothing intervals. This was the reason why a conservative RD CSC approach was chosen by fixing maximum smoothing interval in 10 seconds, 50 seconds, 100 seconds and 5 minutes.

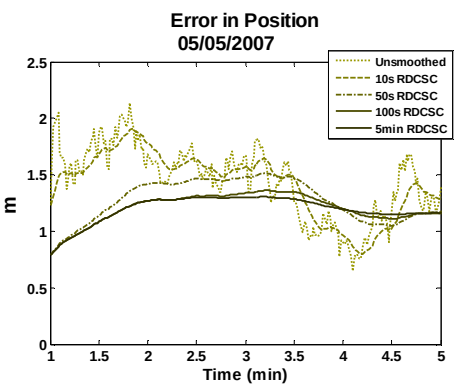


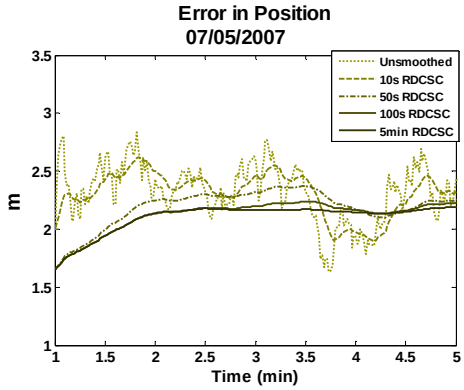


| | Mean Error in Position (m) | | | | |
|---|---|---|---|---|---|
| | Usmt | RD CSC | | | |
| | | 10s | 50s | 100s | 5min |
| **9:01 - 9:02** | 1,919 | 1,217 | 1,030 | 1,030 | 1,030 |
| **9:02 - 9:03** | 1,750 | 1,653 | 1,134 | 1,069 | 1,068 |
| **9:03 - 9:04** | 1,561 | 1,589 | 1,446 | 1,303 | 1,292 |
| **9:04 - 9:05** | 1,293 | 1,344 | 1,412 | 1,316 | 1,271 |
| **Average** | 1,631 | 1,451 | 1,255 | 1,179 | 1,165 |

| | Mean Error in Position (m) | | | | |
|---|---|---|---|---|---|
| | Usmt | RD CSC | | | |
| | | 10s | 50s | 100s | 5min |
| **9:01 - 9:02** | 2,459 | 1,894 | 1,606 | 1,606 | 1,606 |
| **9:02 - 9:03** | 2,457 | 2,391 | 1,986 | 1,929 | 1,929 |
| **9:03 - 9:04** | 2,361 | 2,373 | 2,278 | 2,170 | 2,164 |
| **9:04 - 9:05** | 2,229 | 2,288 | 2,311 | 2,211 | 2,163 |
| **Average** | 2,377 | 2,237 | 2,045 | 1,979 | 1,965 |

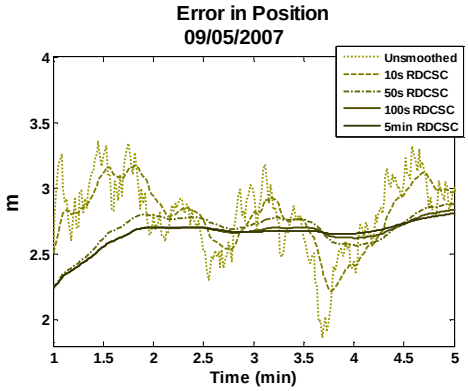


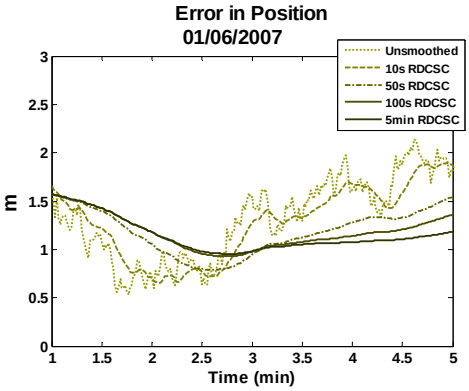


| | Mean Error in Position (m) | | | | |
|---|---|---|---|---|---|
| | Usmt | RD CSC | | | |
| | | 10s | 50s | 100s | 5min |
| **9:01 - 9:02** | 2,858 | 2,495 | 2,289 | 2,289 | 2,289 |
| **9:02 - 9:03** | 3,002 | 2,974 | 2,582 | 2,525 | 2,525 |
| **9:03 - 9:04** | 2,700 | 2,735 | 2,747 | 2,688 | 2,691 |
| **9:04 - 9:05** | 2,575 | 2,628 | 2,703 | 2,676 | 2,668 |
| **Average** | 2,784 | 2,708 | 2,580 | 2,544 | 2,543 |

| | Mean Error in Position (m) | | | | |
|---|---|---|---|---|---|
| | Usmt | RD CSC | | | |
| | | 10s | 50s | 100s | 5min |
| **9:01 - 9:02** | 2,896 | 2,026 | 1,840 | 1,840 | 1,840 |
| **9:02 - 9:03** | 1,007 | 1,164 | 1,361 | 1,406 | 1,406 |
| **9:03 - 9:04** | 0,943 | 0,808 | 0,865 | 1,000 | 1,016 |
| **9:04 - 9:05** | 1,521 | 1,415 | 1,122 | 1,072 | 1,044 |
| **Average** | 1,592 | 1,353 | 1,297 | 1,330 | 1,327 |

Figure 62 **May/June2007 Experiments – Examples of error in position**. Experiments performed with data taken on May/June 2007.

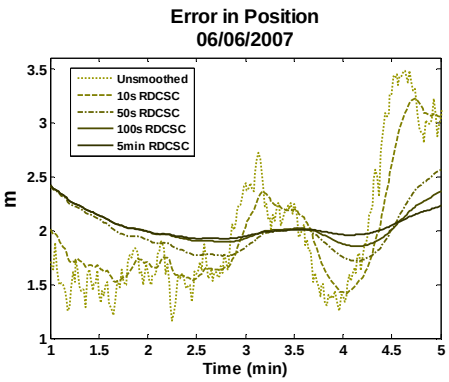


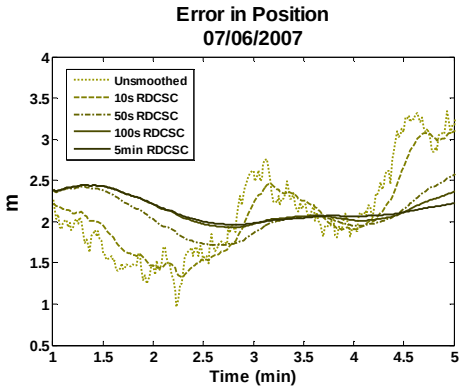


| | Mean Error in Position (m) | | | | |
|---|---|---|---|---|---|
| | Usmt | RD CSC | | | |
| | | 10s | 50s | 100s | 5min |
| **9:01 - 9:02** | 3,372 | 2,971 | 2,898 | 2,899 | 2,899 |
| **9:02 - 9:03** | 1,534 | 1,700 | 2,117 | 2,159 | 2,159 |
| **9:03 - 9:04** | 1,679 | 1,665 | 1,814 | 1,923 | 1,941 |
| **9:04 - 9:05** | 1,962 | 2,021 | 1,941 | 1,978 | 1,987 |
| **Average** | 2,241 | 2,153 | 2,165 | 2,201 | 2,209 |

| | Mean Error in Position (m) | | | | |
|---|---|---|---|---|---|
| | Usmt | RD CSC | | | |
| | | 10s | 50s | 100s | 5min |
| **9:01 - 9:02** | 3,536 | 2,783 | 2,638 | 2,639 | 2,639 |
| **9:02 - 9:03** | 1,696 | 1,883 | 2,310 | 2,377 | 2,378 |
| **9:03 - 9:04** | 1,716 | 1,591 | 1,803 | 2,015 | 2,037 |
| **9:04 - 9:05** | 2,193 | 2,201 | 2,010 | 2,043 | 2,042 |
| **Average** | 2,285 | 2,115 | 2,190 | 2,268 | 2,274 |

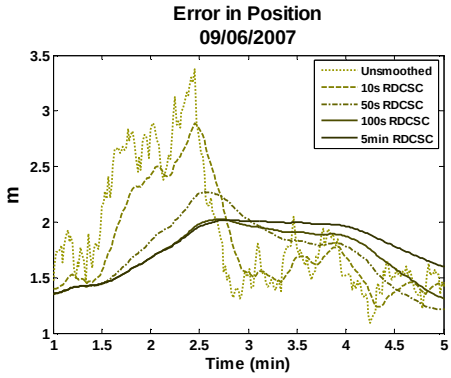


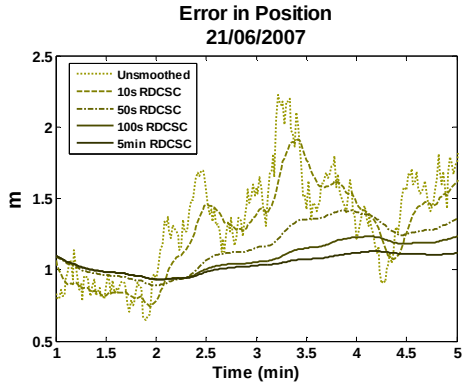


| | Mean Error in Position (m) | | | | |
|---|---|---|---|---|---|
| | Usmt | RD CSC | | | |
| | | 10s | 50s | 100s | 5min |
| **9:01 - 9:02** | 2,429 | 1,873 | 1,824 | 1,824 | 1,824 |
| **9:02 - 9:03** | 2,144 | 1,773 | 1,510 | 1,477 | 1,477 |
| **9:03 - 9:04** | 2,343 | 2,364 | 2,105 | 1,910 | 1,905 |
| **9:04 - 9:05** | 1,658 | 1,614 | 1,857 | 1,913 | 1,992 |
| **Average** | 2,143 | 1,906 | 1,824 | 1,781 | 1,799 |

| | Mean Error in Position (m) | | | | |
|---|---|---|---|---|---|
| | Usmt | RD CSC | | | |
| | | 10s | 50s | 100s | 5min |
| **9:01 - 9:02** | 1,989 | 1,406 | 1,299 | 1,299 | 1,299 |
| **9:02 - 9:03** | 0,862 | 0,852 | 0,973 | 0,996 | 0,996 |
| **9:03 - 9:04** | 1,352 | 1,229 | 1,032 | 0,993 | 0,979 |
| **9:04 - 9:05** | 1,683 | 1,630 | 1,316 | 1,142 | 1,071 |
| **Average** | 1,472 | 1,279 | 1,155 | 1,107 | 1,086 |

Figure 63 **May/June 2007 Experiments – Examples of error in position**. Experiments performed with data taken on May/June 2007.

It can be concluded that a maximum smoothing interval of 50 seconds or 100 seconds provides a good trade-off between the improvements of the mean error in position and fluctuations of this error.

The implemented RD CSC schemes provide improvements in the accuracy of position estimates because they reduce the mean error in position estimation. In that way, the position estimates obtained when performances are adjusted by the implemented RD CSC approach are closer to the actual receiver's position, compared to the outcomes obtained by the conventional unsmoothed method. These improvements are small (at decimetre or centimetre level); anyway, it was possible to reduce the position error under 1.5 metres in some experiments.

It has been observed that some drawbacks were present in the conventional unsmoothed method and have not being overcome by applying the implemented RD CSC approaches. For example, the position estimates derived from these algorithms are sensitive to receiver clock readjustments that affect code measurements but do not have any effect on carrier-phases. As mentioned in chapter 3, the basic quartz crystal oscillators (or clocks) located at receiver site are not so precise as the ones located at the GPS control stations; as a result, these clocks suffer progressive time deviations with respect to the general GPS time frame. The code pseudo-ranges processed in the Kalman filter in order to estimate the receiver's position are time-based measurements and their reliability limits the accuracy of the obtained position estimates. Therefore, receiver manufactures sought solutions to overcome this measurement limitation, one of the strategies that is applied on receivers equipments consists of limiting the time deviations by letting the clock drift until it reaches a certain threshold (typically, 1 ms), and then reset it to return the offset to zero (as mentioned in reference [3.3]). These readjustments generate discontinuities on the derived code measurements, i.e. the pseudo-ranges (1 ms corrections are translated into "length jumps" of 299.79 km). Then, the parallel Hatch filters only "smooth" these discontinuities on pseudo-ranges but do not suppress then. The receiver clock deviations are gradual and will not be eliminated just by applying these low pass filters. In the following figures, an

illustrative example is shown, this was observed while performing the above mentioned experiments.

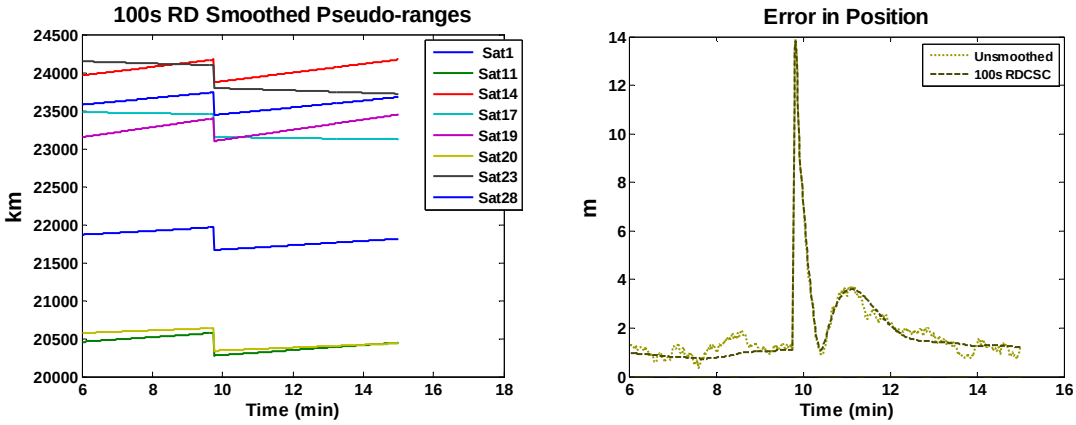


Figure 64 **Effects of receiver clock readjustments in GPS positioning –** experiments performed with data taken on May 5, 2007.

Furthermore, both unsmoothed and RD smoothed algorithms will exhibit problems when the number of visible satellites do not overcome the limit required to solve the navigation equations in the Kalman filter.

## 5.3 PD CSC experimental outcomes

The position domain CSC algorithm implemented in these studies is a Kalman filter posed by Thomas J. Ford in references [4.14], [4.18] and [4.19]; this approach is generally called the *pseudo-range/delta-phase (PDP) Kalman filter*.

The main functions performed by the implemented PDP Kalman filter are illustrated in the following figure (Figure 65). In this approach, carrier-phase measurements are directly incorporated on the Kalman filter that acts as the navigation processor. This modified Kalman algorithm combines the satellite-to-user distance information extracted from both code and carrier-based measurements to obtain a position estimate. To overcome the problems derived from the inherent ambiguities affecting phase measurements, carrier-phases are differenced in time, in that sense, the resultant differenced measurement is treated as a position difference observable between the previous and the current time epochs (as mentioned in section 4.3.2). Therefore, the number of system states in this Kalman filter was enlarged to enclose both current and previous receiver's location to properly process the time differenced carrier-phases as "position difference" observables.

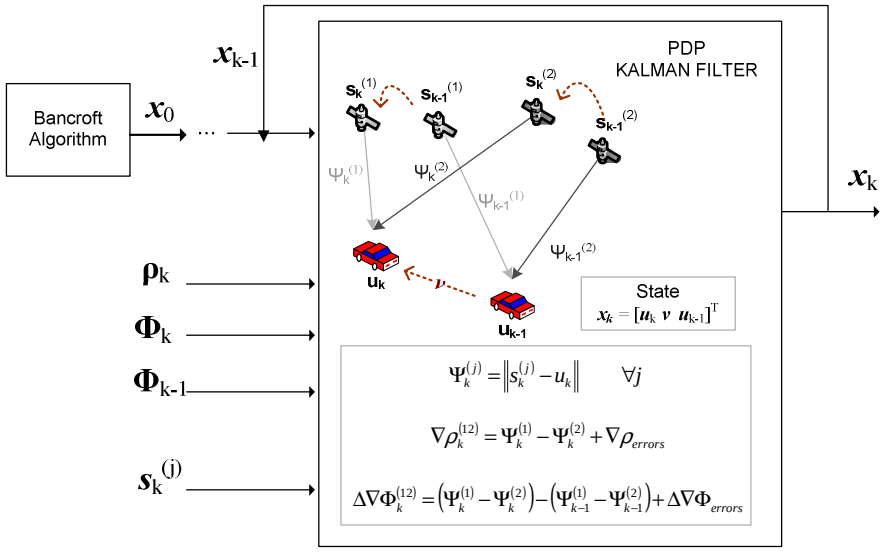


Figure 65 **Block diagram of the implemented PD CSC filtering scheme**. The Pseudo-range/Delta-Phase (PDP) Kalman Filter

In the case of unsmoothed and range domain smoothed algorithms, position errors from a filter that includes clock states would be adversely affected when the system do not have enough observations to generate an instantaneous position and clock estimate by solving the navigation equations. The estimation of clock states is required in order to achieve absolute positioning results; however, as mentioned in section 4.3.2, techniques that construct new positioning observables by differencing the GPS measurements are used in such a way that clock biases are suppressed. In these studies the common error due to receiver's clock deviations was eliminated from measurements by differencing simultaneous measurements gathered from different satellites, i.e. forming "between-satellite" differences, therefore, the modified Kalman filter that processes these differenced measurements does not need to estimate clock states. Hence, the considered system states shown previously in Figure 65 do not enclose the clock states. Furthermore, in some references such as [3.5], it has been mentioned that the impact of several other measurement errors caused by sources such as atmosphere effects and innacuracies in satellite ephemeris parameters is significantly reduced by processing these differenced GPS measurements.

As well as in the case of RD CSC algorithms, several experiments were carried out in order to analyze whether, the position accuracy is enhanced when performances are adjusted by the implemented CSC approach shown in Figure 65. First of all, the July 19, 2007 data set previously used to derive RD CSC test results was considered again to obtain position estimates by performing the implemented PDP Kalman filter. The observation interval was enlarged till it approached 16 minutes (9:00 – 9:16) in order to analyze the sensitivity of position estimates to receiver clock readjustments. As well as in RD CSC experiments, pseudo-range measurements were intentionally corrupted with the same normally distributed random noise of 2-metres standard deviation.

In Figure 66 the satellites layout in the sky is illustrated together with antenna's elevation angles. A total of 8 satellites were monitored during the whole 16-minutes time period.

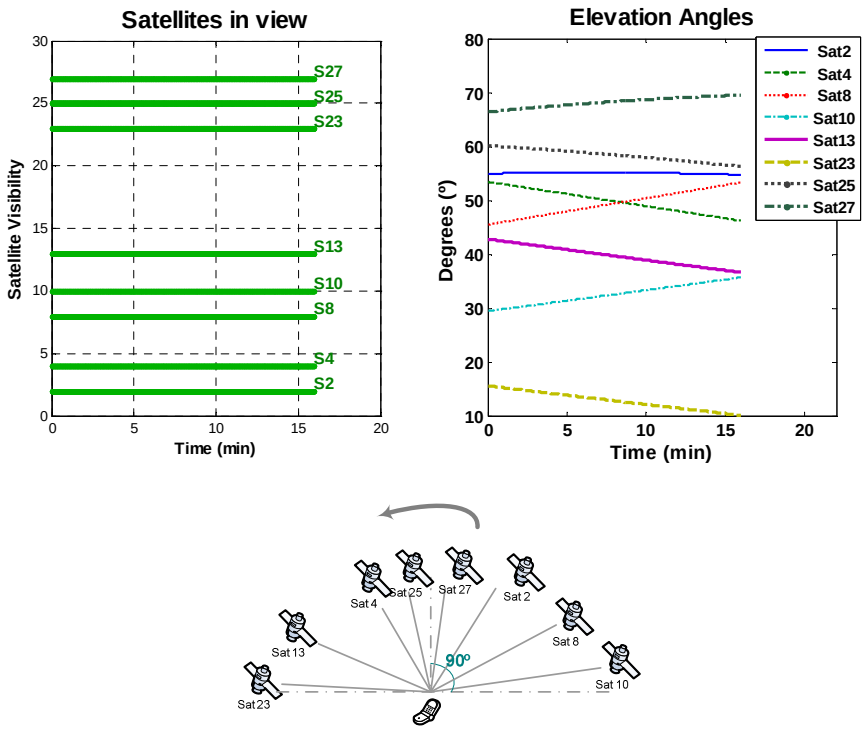


Figure 66 **July 19, 2007 Experiment – Observed satellites and antenna's elevation angles.** GPS measurements were collected in the morning July 19, 2007 (from 9:00 to 9:16 am)

The geometry of this GPS environment, i.e. how satellites are distributed on the sky, is quite homogeneous. Five satellites were moving high and other three rose or set closer to the horizon. It is worth highlighting the importance of satellites location since measurements from high satellites contain smaller errors and noise since the received signal powers are higher and the paths through ionosphere and troposphere are shorter.

The PDP Kalman filter formed the between-satellite measurement differences by considering a reference satellite that is the highest one in order to minimize the measurement error affecting the resultant differenced observables, as mentioned in chapter 4. In this experiment, satellite 27 was chosen to form the measurement differences because it was monitored with the largest antenna's elevation angles – see Figure 66. Hence measurement differences between satellites were computed according to the arrangement shown in the following figure.

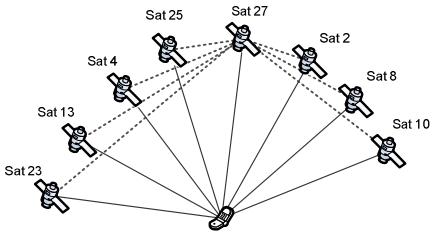


Figure 67 **July 19, 2007 Experiment – Forming between-satellite measurement differences**. Experiment performed with GPS data collected in the morning July 19, 2007 (from 9:00 to 9:16 am)

First of all, the effects on the estimation of the three Cartesian coordinates are analyzed when performances are adjusted by the implemented PDP Kalman filter. In addition, these test results are compared to the ones derived from the conventional Kalman filter that processed either unsmoothed or RD smoothed pseudo-ranges – as shown the following Figure 68. As a second step, a general position error profile was also evaluated by considering the geometric distances between the position estimates and the RINEX reference location as previously defined in the mathematical relation stated in equation (5.2-7). Finally, test results are summarized in order to assess if better positioning outcomes could be obtained when the PDP Kalman filter was applied on performances.

The following figure illustrates the three analyzed procedures. The unsmoothed method and the RD CSC approach used a conventional 8-state position/velocity Kalman filter. In contrast, in the PD CSC approach the modified PDP Kalman filter estimated the position coordinates.

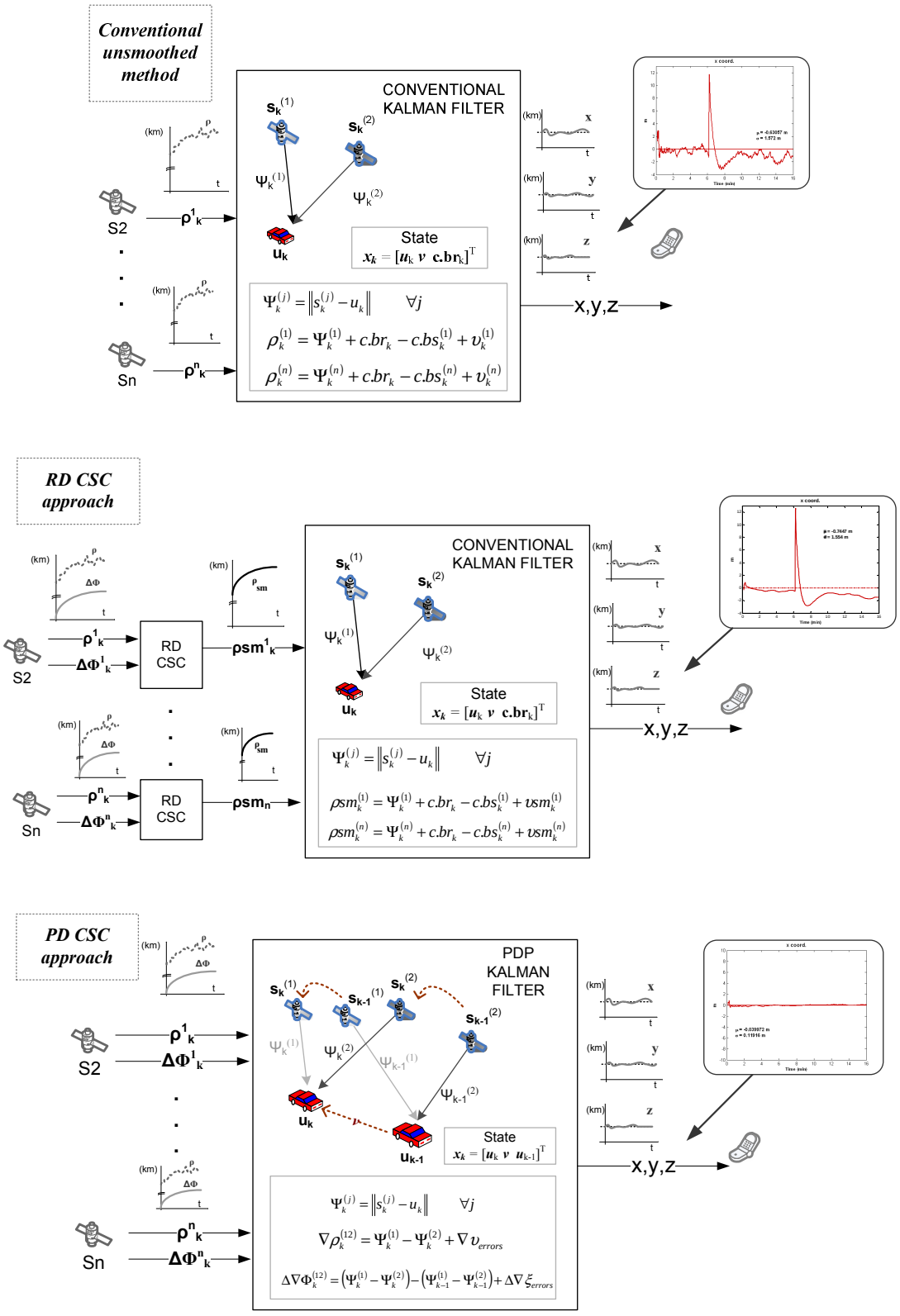


Figure 68 **Analysis performed on the implemented PD CSC scheme –** block diagrams of the conventional "unsmoothed" method (the first sketch) , the RD CSC method and the PD CSC methods.

### 5.3.1 PD CSC effects on positioning

As mentioned before, a qualitative analysis was performed in order to evaluate the error in the estimation of each position coordinate. In this section, the experimental outcomes obtained by processing GPS data collected in July 19, 2007 from 9:00 to 9:16 will be illustrated by means of graphics and numerical outcomes. These error profiles were computed in the same way that test results shown in section 5.2.1.

Observe the following figures (Figure 69, Figure 70 and Figure 71) and compare the outcomes obtained from the conventional unsmoothed approach and the ones derived from applying range domain or position domain smoothing schemes (i.e. the PDP Kalman filter). Charts have been grouped into Cartesian coordinates.

It can be observed that position domain smoothing schemes imply an important improvement in terms of position estimation compared to the unsmoothed and the range domain smoothed methods. In fact, error in position is reduced above 2 metres in the three Cartesian coordinates. In addition, the positon estimates generated by the PDP Kalman filter are not sensitive to receiver clock readjustments affecting code pseudo-ranges because the information contained in the carrier-phase measurements is directly applied while computing the position within this filter.

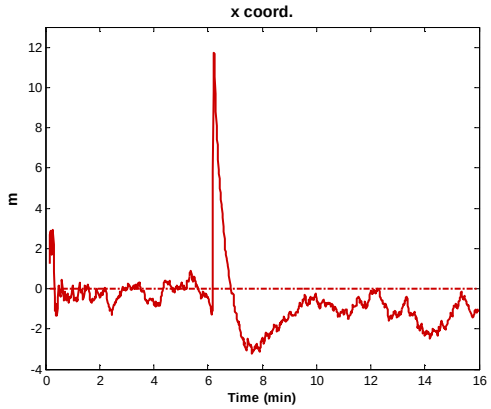


**1**

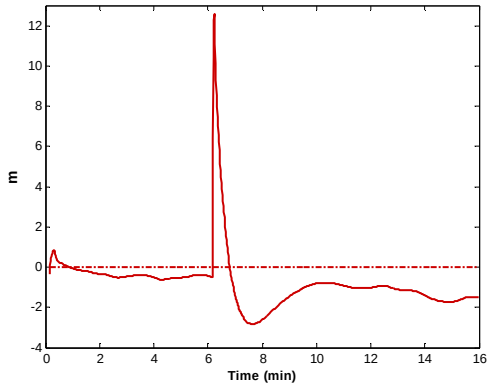


**2**

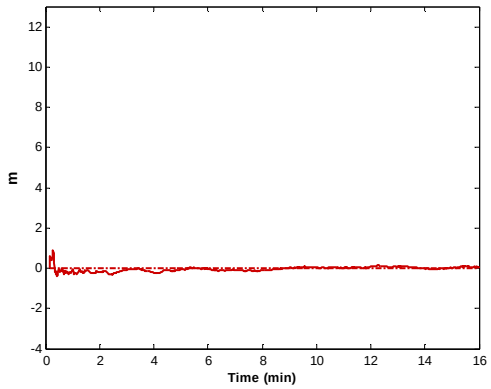


**3**

Figure 69 **July 19, 2007 Experiment - Error in the first coordinate of the 3D stationary positioning solution** derived from measurements taken from 9:01 to 9:16. **1.** Conventional unsmoothed procedure, **2.** Range domain smoothing procedure, **3.** Position domain smoothing procedure (PDP Kalman).

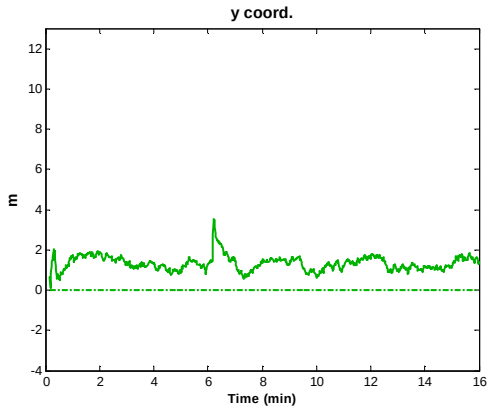


**1**

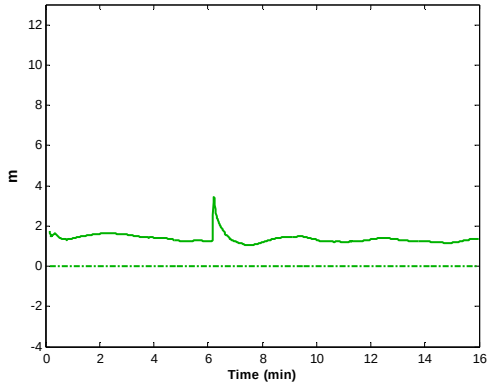


**2**

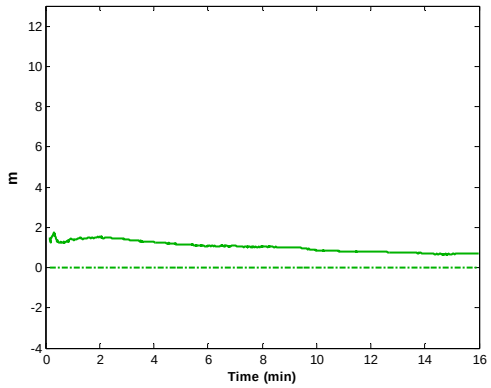


**3**

Figure 70 **July 19, 2007 Experiment - Error in the second coordinate of the 3D stationary positioning solution** derived from measurements taken from 9:01 to 9:16. **1.** Conventional unsmoothed procedure, **2.** Range domain smoothing procedure, **3.** Position domain smoothing procedure (PDP Kalman).

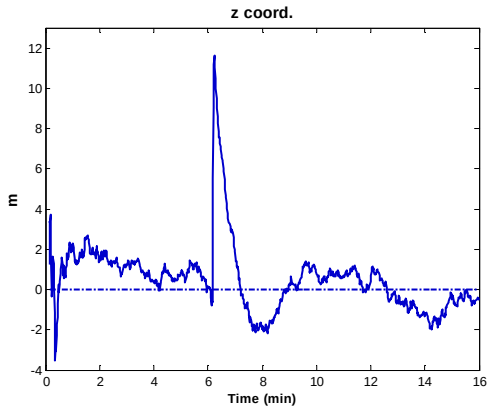


**1**

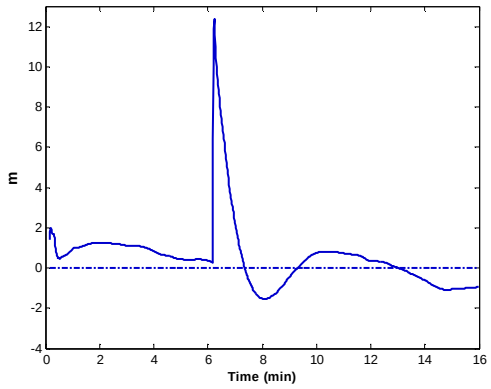


**2**

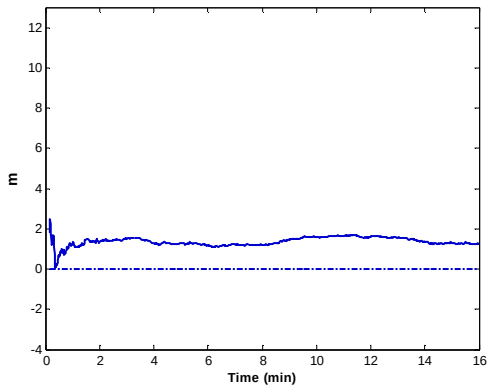


**3**

Figure 71 **July 19, 2007 Experiment - Error in the third coordinate of the 3D stationary positioning solution** derived from measurements taken from 9:01 to 9:16. **1.** Conventional unsmoothed procedure, **2.** Range domain smoothing procedure, **3.** Position domain smoothing procedure (PDP Kalman).

The following figure illustrates the general position error profile estimated by considering the geometric distances between the position estimates and the RINEX reference location. As mentioned before, the PDP Kalman estimates are not affected by the instabilities due to clock readjustments; furthermore, the error in these estimates is not above 2 metres.

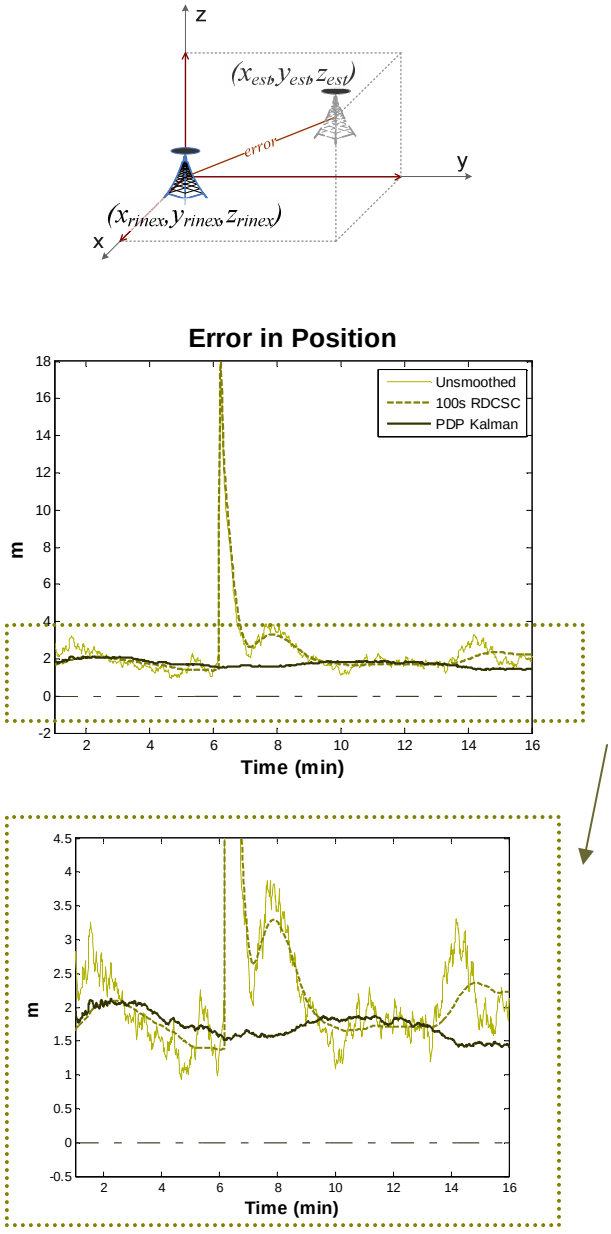


Figure 72 **July 19, 2007 Experiment - Error in position** computed as the geometric distance between the reference RINEX receiver's location and the position estimates. Measurements were taken on July 19, 2007 from 9:01 to 9:16.

In addition, the mean error was computed for each minute of observations. It was observed that the error in position slightly increased in some cases when performances were adjusted by the range domain or position domain smoothing approaches. However, the implemented PDP Kalman filter maintained the error below 2 metres providing robustness to the effects of receiver clock readjustments (as shown in previous figures).

| Mean Error in Position Estimation | | | |
|---|---|---|---|
| | **Unsmoothed** | **RD CSC 100 s** | **PD CSC (PDP Kalman)** |
| **9:01 - 9:02** | 2,597 | 1,882 | 1,962 |
| **9:02 - 9:03** | 2,186 | 2,067 | 2,060 |
| **9:03 - 9:04** | 1,676 | 1,856 | 1,988 |
| **9:04 - 9:05** | 1,294 | 1,600 | 1,764 |
| **9:05 - 9:06** | 1,575 | 1,400 | 1,677 |
| **9:06 - 9:07** | 6,442 | 6,888 | 1,573 |
| **9:07 - 9:08** | 3,072 | 2,996 | 1,588 |
| **9:08 - 9:09** | 2,793 | 2,760 | 1,654 |
| **9:09 - 9:10** | 1,756 | 1,859 | 1,812 |
| **9:10 - 9:11** | 1,564 | 1,671 | 1,828 |
| **9:11 - 9:12** | 1,866 | 1,712 | 1,813 |
| **9:12 - 9:13** | 1,773 | 1,710 | 1,788 |
| **9:13 - 9:14** | 1,961 | 1,767 | 1,648 |
| **9:14 - 9:15** | 2,642 | 2,223 | 1,459 |
| **9:15 - 9:16** | 1,890 | 2,262 | 1,450 |
| **Average Value** | **2,339** | **2,310** | **1,737** |

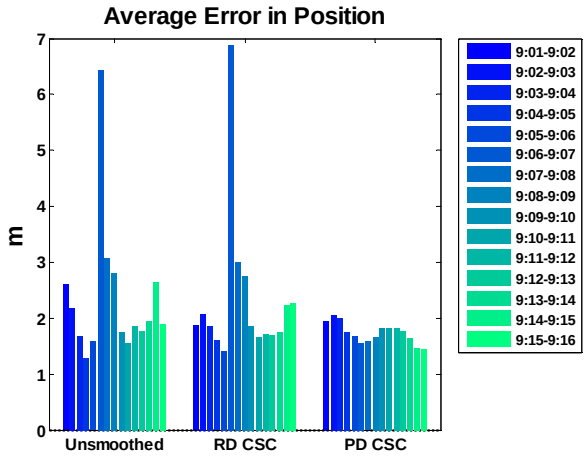


Figure 73 **July 19, 2007 Experiment - Mean error in position** computed for each minute of observations. Measurements were taken on July 19, 2007 from 9:01 to 9:16.

If the "between-satellite" differences would have been considered according to a different satellites arrangement, the error in position would slightly increase, as shown in the following example. These test results were also achieved while performing these experiments.

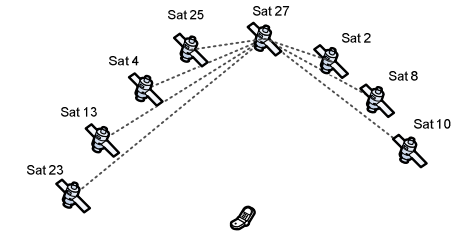


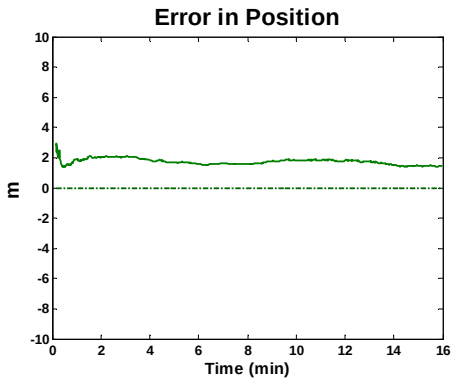


| Mean Error in Position Estimation PD CSC (PDP Kalman) | |
|---|---|
| **9:01 - 9:02** | 1,962 |
| **9:02 - 9:03** | 2,060 |
| **9:03 - 9:04** | 1,988 |
| **9:04 - 9:05** | 1,764 |
| **9:05 - 9:06** | 1,677 |
| **9:06 - 9:07** | 1,573 |
| **9:07 - 9:08** | 1,588 |
| **9:08 - 9:09** | 1,654 |
| **9:09 - 9:10** | 1,812 |
| **9:10 - 9:11** | 1,828 |
| **9:11 - 9:12** | 1,813 |
| **9:12 - 9:13** | 1,788 |
| **9:13 - 9:14** | 1,648 |
| **9:14 - 9:15** | 1,459 |
| **9:15 - 9:16** | 1,450 |
| **Average Value** | **1,737** |

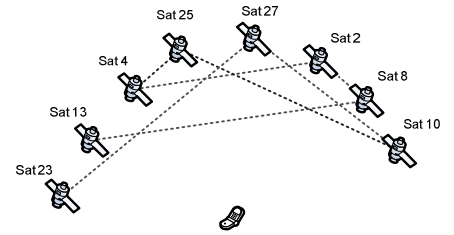


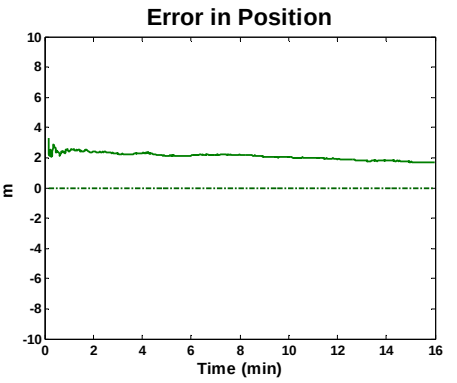


| Mean Error in Position Estimation PD CSC (PDP Kalman) | |
|---|---|
| **9:01 - 9:02** | 2,460 |
| **9:02 - 9:03** | 2,358 |
| **9:03 - 9:04** | 2,253 |
| **9:04 - 9:05** | 2,238 |
| **9:05 - 9:06** | 2,116 |
| **9:06 - 9:07** | 2,188 |
| **9:07 - 9:08** | 2,199 |
| **9:08 - 9:09** | 2,147 |
| **9:09 - 9:10** | 2,058 |
| **9:10 - 9:11** | 2,013 |
| **9:11 - 9:12** | 1,973 |
| **9:12 - 9:13** | 1,866 |
| **9:13 - 9:14** | 1,795 |
| **9:14 - 9:15** | 1,779 |
| **9:15 - 9:16** | 1,699 |
| **Average Value** | **2,076** |

Figure 74 **July 19, 2007 Experiment - Different satellites layout to form between-satellite measurement differences –** Experiment performed with GPS data collected in the morning July 19, 2007 (from 9:00 to 9:16)

If all the visible satellites would have been located low in the sky, the positioning outcomes would be worst because the quality of the gathered measurements would be lower. Therefore, as shown in the above test results, the visibility of at least one satellite placed high in the sky is convenient for the positioning accuracy to be improved (as mentioned in reference [4.19]).

### 5.3.2 PD CSC positioning outcomes

As well as in RD CSC experiments, several performances were carried out in order to assess if better positioning results could be obtained when performances are adjusted by the implemented PDP Kalman filter shown in Figure 65.

The processed measurements were the same GPS data sets considered in the RD CSC experiments. These observations were collected in May and June 2007 and the measurement time periods were enlarged till they approached 16 minutes in order to observe what happened with the effects of receiver clock readjustments on position estimates. The sampling rate was 1 Hz and the first minute of observations was disregarded to avoid possible system instabilities during the initialization of the navigation procedure.

First of all, a qualitative analysis was performed by outlining the error in position estimates and directly observing if better positioning results were obtained when performing the PDP Kalman filter. The error in position was evaluated as the geometric distance between the estimated receiver's location and the approximation provided by the processed RINEX files – as illustrated previously in Figure 54 and computed according to the equation (5.2-7). Secondly, a quantitative analysis was also performed by evaluating the mean error in position in each 2-minutes interval of observations. The improvement in position accuracies is clear when performances were carried out by using the implemented PDP Kalman filter. The mean error in position is not above 2 metres in the case of this position domain smoothing approach and fluctuations in position estimates are considerably reduced.

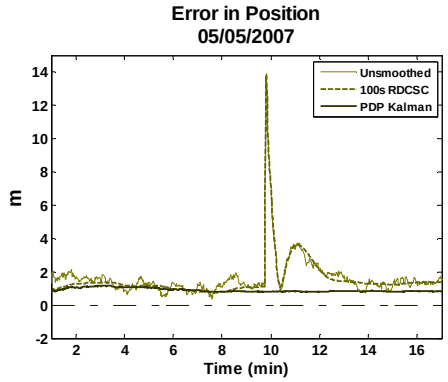


| | Average Error in Position (m) | | |
|---|---|---|---|
| | Unsmoothed | RD CSC 100s | PD CSC PDP Kalman |
| **9:01-9:03** | 0,886 | 0,541 | 0,485 |
| **9:03-9:05** | 1,427 | 1,309 | 1,105 |
| **9:05-9:07** | 1,073 | 1,130 | 1,019 |
| **9:07-9:09** | 0,958 | 0,834 | 0,860 |
| **9:09-9:11** | 2,379 | 2,076 | 0,808 |
| **9:11-9:13** | 2,842 | 2,955 | 0,808 |
| **9:13-9:15** | 1,540 | 1,496 | 0,828 |
| **9:15-9:17** | 1,283 | 1,273 | 0,821 |
| **Average** | 1,549 | 1,452 | 0,842 |

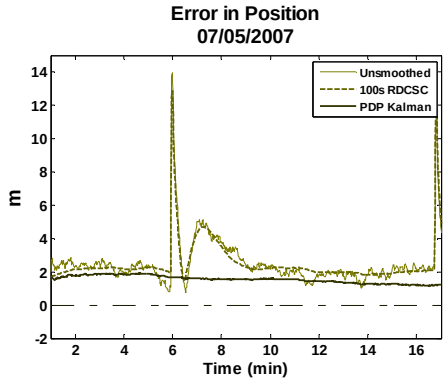


| | Average Error in Position (m) | | |
|---|---|---|---|
| | Unsmoothed | RD CSC 100s | PD CSC PDP Kalman |
| **9:01-9:03** | 1,246 | 0,978 | 0,852 |
| **9:03-9:05** | 2,295 | 2,191 | 1,835 |
| **9:05-9:07** | 2,274 | 2,436 | 1,809 |
| **9:07-9:09** | 4,283 | 4,143 | 1,590 |
| **9:09-9:11** | 2,747 | 2,474 | 1,541 |
| **9:11-9:13** | 1,832 | 2,175 | 1,511 |
| **9:13-9:15** | 1,766 | 1,945 | 1,355 |
| **9:15-9:17** | 2,024 | 1,927 | 1,244 |
| **Average** | 2,309 | 2,284 | 1,467 |

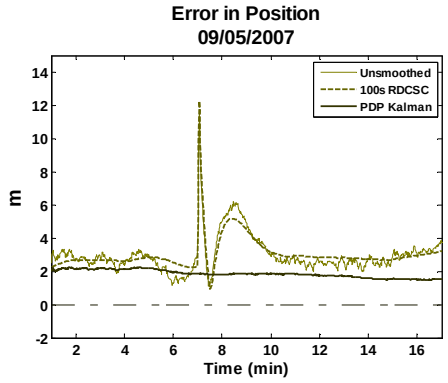


| | Average Error in Position (m) | | |
|---|---|---|---|
| | Unsmoothed | RD CSC 100s | PD CSC PDP Kalman |
| **9:01-9:03** | 1,522 | 1,281 | 1,096 |
| **9:03-9:05** | 2,637 | 2,682 | 2,153 |
| **9:05-9:07** | 2,561 | 2,742 | 2,145 |
| **9:07-9:09** | 2,979 | 3,245 | 1,866 |
| **9:09-9:11** | 4,717 | 4,360 | 1,853 |
| **9:11-9:13** | 2,613 | 2,947 | 1,835 |
| **9:13-9:15** | 2,493 | 2,812 | 1,698 |
| **9:15-9:17** | 2,819 | 2,785 | 1,543 |
| **Average** | 2,793 | 2,857 | 1,774 |

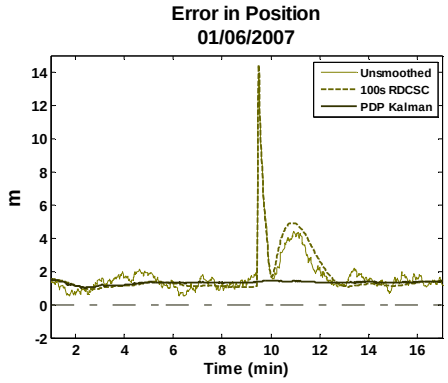


| | Average Error in Position (m) | | |
|---|---|---|---|
| | Unsmoothed | RD CSC 100s | PD CSC PDP Kalman |
| **9:01-9:03** | 0,517 | 0,716 | 0,687 |
| **9:03-9:05** | 1,232 | 1,036 | 1,119 |
| **9:05-9:07** | 1,590 | 1,289 | 1,299 |
| **9:07-9:09** | 1,108 | 1,159 | 1,327 |
| **9:09-9:11** | 2,834 | 2,663 | 1,349 |
| **9:11-9:13** | 3,067 | 3,867 | 1,397 |
| **9:13-9:15** | 1,565 | 1,434 | 1,340 |
| **9:15-9:17** | 1,385 | 1,211 | 1,347 |
| **Average** | 1,662 | 1,672 | 1,233 |

Figure 75 **May/June 2007 Experiments - Error in position.** Experiments performed with data taken on May/June 2007.

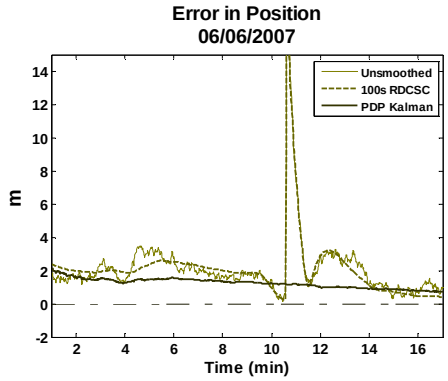


| | Average Error in Position (m) | | |
|---|---|---|---|
| | Unsmoothed | RD CSC 100s | PD CSC PDP Kalman |
| **9:01-9:03** | 0,781 | 1,100 | 0,929 |
| **9:03-9:05** | 1,820 | 1,951 | 1,458 |
| **9:05-9:07** | 2,789 | 2,289 | 1,458 |
| **9:07-9:09** | 1,999 | 2,287 | 1,448 |
| **9:09-9:11** | 1,644 | 1,781 | 1,294 |
| **9:11-9:13** | 4,184 | 4,115 | 1,169 |
| **9:13-9:15** | 2,620 | 2,391 | 0,987 |
| **9:15-9:17** | 0,866 | 0,721 | 0,875 |
| **Average** | 2,088 | 2,079 | 1,202 |

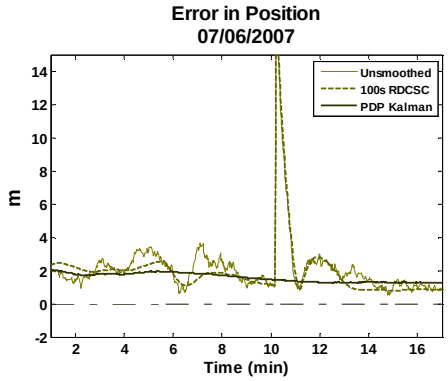


| | Average Error in Position (m) | | |
|---|---|---|---|
| | Unsmoothed | RD CSC 100s | PD CSC PDP Kalman |
| **9:01-9:03** | 0,868 | 1,209 | 0,986 |
| **9:03-9:05** | 1,954 | 2,029 | 1,779 |
| **9:05-9:07** | 2,732 | 2,269 | 1,898 |
| **9:07-9:09** | 2,174 | 1,549 | 1,835 |
| **9:09-9:11** | 1,660 | 1,494 | 1,586 |
| **9:11-9:13** | 4,544 | 4,747 | 1,379 |
| **9:13-9:15** | 1,974 | 1,549 | 1,294 |
| **9:15-9:17** | 1,073 | 0,824 | 1,298 |
| **Average** | 2,122 | 1,959 | 1,507 |

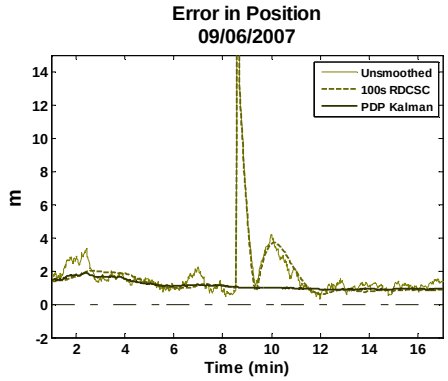


| | Average Error in Position (m) | | |
|---|---|---|---|
| | Unsmoothed | RD CSC 100s | PD CSC PDP Kalman |
| **9:01-9:03** | 1,087 | 0,750 | 0,809 |
| **9:03-9:05** | 2,000 | 1,912 | 1,706 |
| **9:05-9:07** | 1,278 | 1,361 | 1,260 |
| **9:07-9:09** | 1,317 | 1,095 | 1,144 |
| **9:09-9:11** | 4,063 | 3,993 | 1,020 |
| **9:11-9:13** | 1,850 | 2,107 | 0,975 |
| **9:13-9:15** | 1,046 | 0,792 | 0,909 |
| **9:15-9:17** | 1,053 | 0,838 | 0,927 |
| **Average** | 1,712 | 1,606 | 1,094 |

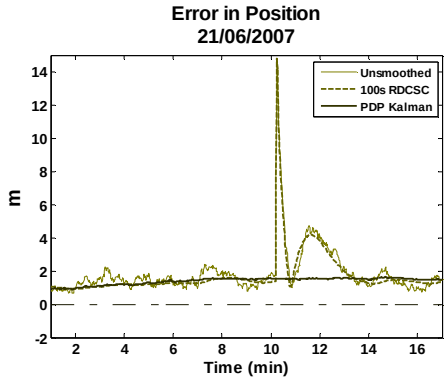


| | Average Error in Position (m) | | |
|---|---|---|---|
| | Unsmoothed | RD CSC 100s | PD CSC PDP Kalman |
| **9:01-9:03** | 0,439 | 0,507 | 0,488 |
| **9:03-9:05** | 1,518 | 1,067 | 1,112 |
| **9:05-9:07** | 1,412 | 1,227 | 1,284 |
| **9:07-9:09** | 1,613 | 1,354 | 1,469 |
| **9:09-9:11** | 1,422 | 1,455 | 1,538 |
| **9:11-9:13** | 4,177 | 4,058 | 1,550 |
| **9:13-9:15** | 2,346 | 2,214 | 1,552 |
| **9:15-9:17** | 1,406 | 1,383 | 1,573 |
| **Average** | 1,792 | 1,658 | 1,321 |

Figure 76 **May/June 2007 Experiments - Error in position**. Experiments performed with data taken on May/June 2007.

In conclusion, the most convenient CSC scheme in terms of position accuracy is the implemented PDP Kalman filter that maintains the error in position estimates less than two metres. However, this error falls below one metre in rare cases.

# Chapter 6

# Conclusions

In this study combination approaches that blend together different types of GPS measurements were analyzed theoretically and some of them were implemented. These algorithms blend together code pseudo-ranges and carrier-phases, derived within a conventional single-frequency GPS receiver, in order to smooth out the noise inherent on pseudo-ranges. This technique is referred to as *carrier smoothing code (CSC)* filtering.

The analyses were aimed at assessing the improvements on position accuracy that can be achieved when performances are adjusted by these CSC approaches. In fact, two different CSC algorithms were chosen to perform simulations.

On the one hand, it was considered the most basic CSC schemes that has been the reference approach for later CSC researchs. This method was first introduced by Ron Hatch in 1982 in a paper entitled "*The synergism of GPS code and carrier measurements*" [4.1]. Hatch's filter basically consists of a recursive scheme that starts with raw pseudo-range measurements to establish an absolute initial smoothed pseudo-range. Progressively, higher weights will be placed on the derived carrier-phase information and less on the one derived from pseudo-ranges. In that way, a smoothed pseudo-range profile is provided as the output of the filter that is directly processed by the navigation processor to obtain a receiver's position estimate. This CSC approach involves the use of a group of parallel Hatch's filters, one for each visible satellite and offers a modest improvement in terms of position estimation. Test results have shown that the mean error in positioning can be reduced as much as a few centimetres (in the range of 2-4 cm) with respect to the conventional unsmoothed methods. However,

fluctuations in the position estimates are considerably smoothed while applying the Hatch's filters on pseudo-range measurements, as shown in the following example derived from an experiment carried out with data collected in May 5, 2007.

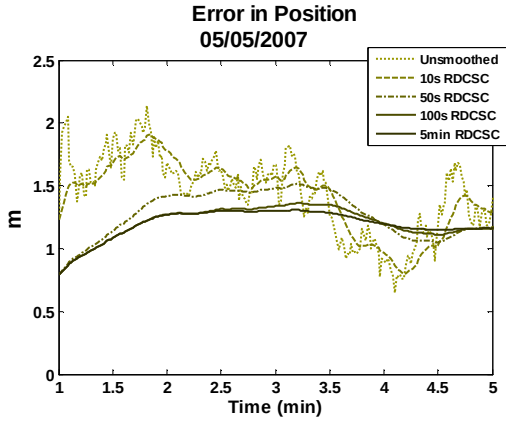


| | Mean Error in Position (m) | | | | |
|---|---|---|---|---|---|
| | Usmt | RD CSC | | | |
| | | 10s | 50s | 100s | 5min |
| **9:01 - 9:02** | 1,919 | 1,217 | 1,030 | 1,030 | 1,030 |
| **9:02 - 9:03** | 1,750 | 1,653 | 1,134 | 1,069 | 1,068 |
| **9:03 - 9:04** | 1,561 | 1,589 | 1,446 | 1,303 | 1,292 |
| **9:04 - 9:05** | 1,293 | 1,344 | 1,412 | 1,316 | 1,271 |
| **Average** | 1,631 | 1,451 | 1,255 | 1,179 | 1,165 |

Figure 77 **Error in position obtained while applying different range domain smoothing approaches.** Experiments performed with data taken on May 5, 2007.

The window's length (i.e. the smoothing interval) of the Hatch's filters is a relevant factor for eliminating the noise on position estimates. In general, the larger the smoothing interval, the more efficient smoothing would be achieved. Hence, this smoothing process is supposed to improve with time but a price is paid for large smoothing intervals in the form of positioning deviations due to changes in atmosphere effects. If it were possible to estimate the rate of ionosphere delay, more effective and efficient use of these Hatch filtering schemes would have been achieved. However, this effect is usually unknown to a single-frequency receiver; therefore, a conservative constant carrier-smoothing time is typically used (these are the different window lengths of 10 seconds, 50 seconds, 100 seconds and 5 minutes, considered while deriving the test results shown in Figure 77).

The second CSC approach that has been considered in these studies is based on Kalman filters. In fact, several references posed the theory of Kalman filters in order to combine carrier-phases and code pseudo-ranges [4.19] [4.18] [4.14] [4.11] and [4.9]. The *pseudo-range/delta-phase (PDP) Kalman filter* posed by Thomas J. Ford in references [4.14], [4.18] and [4.19] has been chosen because of its simplicity and intuitiveness. In this approach, carrier-phase measurements are directly incorporated on the navigation processor that is a modified Kalman filter. This Kalman algorithm combine the positioning information extracted from both code and carrier measurements to derive the position estimates. As a requirement, system states enclose both current and previous receiver's location to properly process carrier-phases as position observables.

This "position domain" smoothing scheme is not so sensitive to receiver clock readjustments as the "range domain" Hatch filter. These readjustments are performed at receiver site to correct the time-deviations caused by the basic quartz crystal oscillators (i.e. the clocks) used in this type of equipments. Some receiver manufacturers attempt to limit these deviations by letting the clock drift until it reaches a certain threshold (typically, 1 ms), and then reset it with a 'jump' to return the bias to zero. As shown in the following figure, these clock readjustments affect pseudo-ranges because they are generated by means of time measurements and therefore, the resultant position estimates are also corrupted.

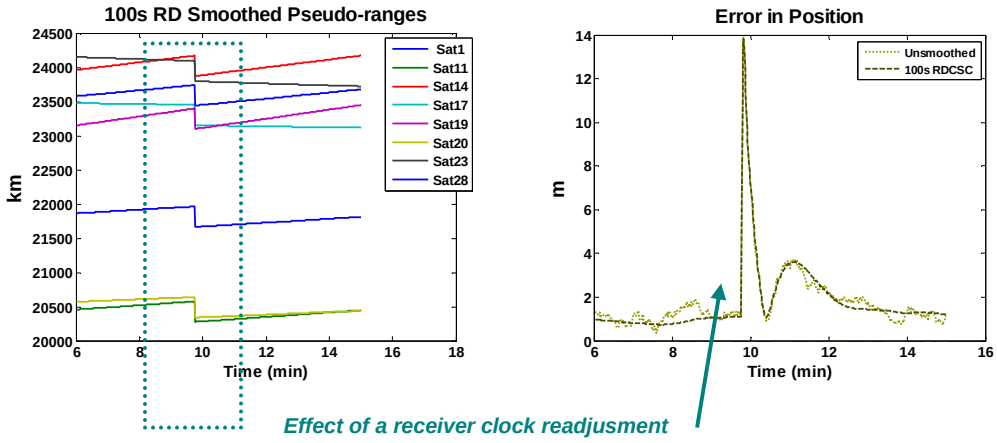


Figure 78 **Effects of receiver clock readjustments in GPS positioning –** experiments performed with data taken on May 5, 2007.

The carrier-phase measurements are not affected by receiver clock readjustments. As a result of incorporanting these GPS measurements in the position estimation within the modified PDP Kalman filter, the position becomes insensitive to these clock readjustments, as shown in the following figure.

In the following figure, effects of clock readjustments on both pseudo-ranges and position estimates are shown. The first coordinate of position, computed while applying the unsmoothed method and the Hatch filter method, i.e. a range domain (RD) smoothing scheme, is compared with the one computed by the PDP Kalman filter. It is observed how positions generated by the PDP Kalman filter are not affected by clock readjustments since phases are applied directly while computing the navigation solution.

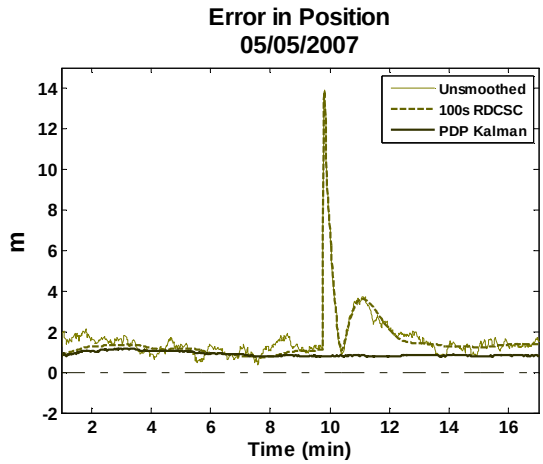


Figure 79 **Example of PDP Kalman positioning robustness to clock readjustments -** Unlike PDP Kalman positioning, position estimates derived from the conventional unsmoothed approach and RD Hatch filter scheme are sensitive to receiver clock readjustments affecting pseudo-range measurements.

Test results have shown that the position domain smoothing scheme implemented by the PDP Kalman filter provide the best outcomes in terms of position accuracies. In fact, the error in PDP Kalman estimates is not above 2 metres and remains stable when a clock readjustmens is carried out within the receiver. However, test results have shown that the remaining error in position is rarely reduced below one metre, even when the PDP Kalman filter is used.

# References

## References cited in Chapter 2

**[2.1]** Kaplan, Elliott D., "Understanding GPS: Principles and Applications", Artech Hous Boston (London)

**[3.1]** P. Misra and P. Enge (2006), "Global Positioning System: Signals, Measurements, and Performance Second Edition", Ganga-Jamuna Press

**[2.2]** The Free Encyclopedia: Wikipedia – en.wikipedia.org

**[2.3]** Electronics: How Stuff Works – www.howstuffworks.com

**[2.4]** RoseIndia – www.roseindia.net

**[2.5]** GPS general public education website created by the U.S. Government – www.gps.gov

**[3.2]** P. Misra, B. Burke and M.M. Pratt (1999), "GPS Performance in Navigation", Proceedings of the IEEE, Vol. 87, No. 1, pages 65-85, January 1999

## References cited in Chapter 3

**[3.3]** P. Misra and P. Enge (2006), "Global Positioning System: Signals, Measurements, and Performance Second Edition", Ganga-Jamuna Press

**[3.4]** G. Lecky Thompson (1999), "Principles and practice of GPS Surveying", University of New South Wales – Sydney (Australia) – www.gmat.unsw.edu.au/snap/gps/about_gps.htm

**[3.5]** C. Rizos (1999), "Principles and practice of GPS surveying", SNAP-UNSW, 1999 www.gmat.unsw.edu.au/snap/gps/gps_survey/principles_gps.htm

**[3.6]** P. Misra, B. Burke and M.M. Pratt (1999), "GPS Performance in Navigation", Proceedings of the IEEE, Vol. 87, No. 1, pages 65-85, January 1999

**[3.7]** R. Hatch (1982), "The Synergism of GPS Code and Carrier Measurements", Proceedings of 3rd Int. Geodetic Symposium on Satellite Doppler Positioning, New Mexico State University, 8±12 February 1982, vol 2, pp 1213±1231.

**[3.8]** B. Hofmann-Wellenhof, H. Lichtenegger and J. Collins (1997), "Global Positioning System. Theory and practice". 4th edition. Springer, Berlin Heiderberg New York.

**[3.9]** B. Hofmann-Wellenhof, H. Lichtenegger and J. Collins (2001), "Global Positioning System. Theory and practice". 5th edition. Springer, Viena, 2001.

# References cited in Chapter 4

**[4.1]** R. Hatch (1982), “The Synergism of GPS Code and Carrier Measurements”, Proceedings of 3rd Int. Geodetic Symposium on Satellite Doppler Positioning, New Mexico State University, 8±12 February 1982, vol 2, pp 1213±1231.

**[4.2]** R. Hatch (1986), “Dynamic Differential GPS at the centimetre level”, Proceedings of 4th Int. Geodetic Symposium on Satellite Positioning, Austing, TX, 28 April±2 May, vol 2, pp 1287±1298.

**[4.3]** B. Hofmann-Wellenhof, H. Lichtenegger and J. Collins (1997), "Global Positioning System. Theory and practice". 4th edition. Springer, Berlin Heidelberg New York.

**[4.4]** B. Hofmann-Wellenhof, H. Lichtenegger and J. Collins (2001), "Global Positioning System. Theory and practice". 5th edition. Springer, Viena, 2001.

**[4.5]** X. X. Jin (1996), “Theory of carrier adjusted DGPS positioning approach and some experimental results”, PhD Diss, Delft University Press, Delft

**[4.6]** G. Lachapelle, J. Hagglund, W. Falkenberg, P. Bellemare, M. Casey and M. Eaton (1986), “GPS land kinematic positioning experiments”. Proceedings of 4th Int. Geodetic Symposium Satellite Positioning, Austin, TX, 28 April±2 May, vol 2, pp 1327±1344

**[4.7]** S.L. Meyerhoff and A.G. Evans (1986), “Demonstration of the combined use of GPS pseudorange and Doppler measurements for improved dynamic positioning”. Proceedings 4th Int. Geodetic Symposium Satellite Positioning, Austin, TX, 28 April±2 May, vol 2, pp 1397±1409

**[4.8]** H.K. Lee and C. Rizos (2003), "Performance analysis of position-domain Hatch filter", submitted to the Royal Institute of Navigation Journal.

**[4.9]** Robert G. Brown and Patrick Y. C. Hwang (1997), “Introduction to Random Signals and applied Kalman filtering” 3rd Edition, John Wiley and Sons, 1997.

**[4.10]** P. Cheng (1998), “Remarks on Doppler-aided smoothing of code ranges”, Chinese Academy of Surveying and Mapping, 16 Beitaiping Road, 100039 Beijing, PRC, 1998.

**[4.11]** P.Y.C. Hwang and R.G. Brown (1990), “GPS navigation: combining pseudorange with continuous carrier phase using a Kalman filter”, NAVIGATION: Journal of The Institute of Navigation Vol. 37, No. 2, pp. 181-196 , Summer 1990, U.S.A

**[4.12]** S.B. Bisnath and R.B. Langley (1999), “Precise, efficient GPS-based geometric tracking of low earth orbiters”, Proceedings of the Institute of Navigation Annual Meeting, Cambridge, Massachusetts, pp. 751-760

**[4.13]** P. Misra and P. Enge (2006), “Global Positioning System: Signals, Measurements, and Performance Second Edition”, Ganga-Jamuna Pres

**[4.14]** Thomas J. Ford (2003), "Position and Velocity Kalman Filter for use with Global Navigation Satellite System receivers" , NovAtel, Inc., Calgary (CA)

**[4.15]** G. Welch and G. Bishop (2006), "An Introduction to the Kalman Filter", Department of Computer Science University of North Carolina at Chapel Hill.

**[4.16]** Kalman Filtering Tutorial (2001): www.innovatia.com/software/papers/kalman.htm

**[4.17]** R. E. Kalman (1960), "A New Approach to Linear Filtering and Prediction Problems," Trans. ASME – J. Basic Engr., 35-45

**[4.18]** Thomas J. Ford and Jason Hamilton (2003), "A New Positioning Filter: Phase Smoothing in the Position Domain" NovAtel Inc., Calgary, Canada.

**[4.19]** Thomas J. Ford and Jason Hamilton, "NovAtel Inc. New Positioning Filter: Phase Smoothing in the Position Domain"

**[4.20]** H. K. Lee, C. Rizos and G. I. Jee (2003), "Design and analysis of DGPS filters with consistent error covariance information",. Proceedings of The 6th International Symposium on Satellite Navigation Technology Including Mobile Positioning & Location Services, Melbourne, Australia, paper no. 47, July 2003

# Index of Figures